# HIGHLY ACCURATE CALCULATIONS OF SPIN-DEPENDENT RELATIVISTIC CORRECTIONS IN SMALL ATOMS WITH ONE AND TWO $p$-ELECTRONS

by

Pavel Rzhevskii

---

A Thesis Submitted to the Faculty of the

DEPARTMENT OF PHYSICS

In Partial Fulfillment of the Requirements
For the Degree of

MASTERS OF SCIENCE

In the School of Sciences and Humanities

NAZARBAYEV UNIVERSITY

2025

NAZARBAYEV UNIVERSITY, SCHOOL OF SCIENCES AND HUMANITIES

As members of the thesis committee, we certify that we have read the thesis prepared by Pavel Rzhevskii entitled

HIGHLY ACCURATE CALCULATIONS OF SPIN-DEPENDENT RELATIVISTIC CORRECTIONS IN SMALL ATOMS WITH ONE AND TWO $p$-ELECTRONS

and recommend that it be accepted as fulfilling the thesis requirement for the degree of Masters of Science.

Final approval and acceptance of this thesis is contingent upon the candidate's submission of the final copies of the thesis to the Department of Physics.

I hereby certify that I have read this thesis prepared under my direction and recommend that it be accepted as fulfilling the thesis requirement.

_____ Date: May 1, 2025

Thesis Director: Sergiy Bubin

## Abstract

I present an algorithm to calculate spin-dependent relativistic corrections using variationally optimized non-relativistic wave functions expanded in terms of explicitly correlated Gaussian basis functions. All matrix elements required for the calculations were derived analytically, with detailed derivations provided. The algorithm can be applied to systems with one and two $p$-electrons, or a single $d$-electron. Using the newly developed algorithm, I studied how the relativistic effects affect the stability of positronic beryllium in the ground singlet $S$ and excited triplet $S$ and $P$ states. I found that the inclusion of relativistic correction changes the binding energies of the considered states only by 2.2% at most. Interestingly, this small change persists even for triplet $P$ states, for which the spin–orbit and spin–spin contributions are not canceled out when the binding energy is computed. In the second application, I investigated the fine-structure of the carbon atom's ground and first excited $^3P^e$ states as well as the lowest $^3D^e$ state. I accounted for the leading-order ($\propto \alpha^2$), electron anomalous magnetic moment ($\propto \alpha^3$), and the dominant part of the second-order perturbation theory ($\propto \alpha^4$) contributions. To my knowledge, these are the first high-precision calculations at the $\alpha^4$ level of theory performed for a system of this size. The computed values of the fine-structure splittings represent the most accurate calculations of the carbon atom reported to date and are in agreement with experiment at the level of 0.0001-0.01 cm$^{-1}$. In addition, I report the isotopic shifts in the fine-structure levels of $^{13}$C, $^{14}$C, and $^{\infty}$C relative to $^{12}$C.

# TABLE OF CONTENTS

# 1 Introduction

Accurate atomic calculations are essential for both fundamental and applied research. From the fundamental perspective, the comparison between high-precision spectroscopic measurements and theoretical predictions of atomic properties serves as a tool to test quantum electrodynamics (QED), determine fundamental physics constants and nuclear properties, and even search for new physics beyond the Standard Model [1–8]. In the applied context, theoretical calculations may provide the values of atomic quantities that are more accurate than the existing experimental measurements, especially when the latter are technically challenging or impossible [9, 10]. In these cases, theoretical predictions may stimulate experimentalists to conduct more accurate measurements and guide them in the design of the experimental setup or procedures.

Depending on the size of the atomic system and the desired level of accuracy, various computational methods have been developed. For small atomic systems, up to 6-7 particles, the highest accuracy is provided by the variational methods in which the exact wave function of a system is approximated by minimizing the energy functional $E(\Psi)$ in the Hilbert space of trial wave functions $\Psi$:

$$E(\Psi) = \frac{\langle \Psi | \mathcal{H} | \Psi \rangle}{\langle \Psi | \Psi \rangle} \to \min, \tag{1.1}$$

where $\mathcal{H}$ is the Hamiltonian of a system. These methods are based on a variational principle which states that the functional $E(\Psi)$ is always greater or equal than the exact ground-state energy $E_0$, $E(\Psi) \geq E_0$, with the equality attained for the exact wave function. The most common choices of the basis functions that are used to expand the trial wave function are explicitly correlated Gaussian functions [11] and Hyllerass-type exponential functions [12]. Another form of variational approach is called quantum Monte Carlo [13], in which the basis functions can be arbitrary, but the integrals required for energy minimization are evaluated using stochastic Monte Carlo techniques.

If the wave function is represented as a sum of electronic configurations (i.e. antisymmetrized product of one-electron spin-orbitals), we arrive at the configuration interaction (CI) approach [14]. In this method, only the linear coefficients in front of the electronic configurations are optimized, while the spin-orbitals are kept fixed. An extension of the CI method, in which both the spin-orbitals and configuration coefficients are variationally optimized, is known as the multiconfiguration Hartree–Fock (MCHF) method [15].

The application of variational methods to systems containing more than ten particles is problematic due to an exponential scaling of computational cost. Among the non-variational methods, the most well-known are many-body perturbation theory (MBPT) [16] and coupled-cluster (CC) method [17]. These techniques have lower accuracy, but do not suffer from rapid exponential scaling of the computational cost, and thus can be applied to larger systems containing tens of electrons.

Atomic and molecular systems with hundreds of electrons are most efficiently treated using the Density Functional Theory (DFT) [18], which employs the electron density, rather than the wave function, as the fundamental quantity. Naturally, the electron density conveys significantly less information than the wave function, making this approach a trade-off between accuracy and computational cost.

In the current work, we adopt the variational ECG approach [19], which provides the highest accuracy for the atoms with three to six electrons as compared to all the other existing methods. Explicitly correlated Gaussian basis sets have a remarkable property that all the quantities required for variational minimization (Hamiltonian matrix elements and energy gradients) can be obtained analytically, enabling efficient and extensive parameter optimization. On the other hand, the Gaussian wave functions are not natural for Coulomb-interacting systems in the sense that they do not have correct decaying behavior at large distances and do not satisfy the Kato cusp condition [20]. These disadvantages lead to the necessity of employing very large basis expansions of the wave function, consisting of thousands of Gaussians, to reproduce the correct behavior of the wave function and achieve spectroscopic accuracy.

To obtain accurate values of atomic quantities (e.g. transition frequencies between energy levels), one needs to account for the relativistic corrections. The inclusion of these corrections is usually done perturbatively, as a series in fine-structure constant $\alpha \approx 1/137$. In this work, we focus on spin-dependent relativistic corrections, which manifest themselves in the fine-structure splitting of atomic energy levels. The most accurate fine-structure calculations have been done for helium and lithium, up to the orders of $\alpha^5$ and $\alpha^5 \ln \alpha$, respectively [21, 22]. Obtaining the same order of accuracy for larger, four- and five-electron systems, is a challenging task — e.g. fine-structure calculations for beryllium and boron are currently limited to the $\alpha^3$ contributions, while the $\alpha^4$ effects are either completely neglected or estimated crudely [10, 23–25].

Accurate fine-structure calculations for the systems with the dominant configuration containing two $p$-electrons have not been performed so far. Moreover, no successful attempts to accurately account for relativistic contributions beyond the order of $\alpha^3$ have been done for the systems with more than three electrons. In this work, I fill these gaps by developing a formalism for spin-dependent calculations in atomic systems whose dominant configurations contain one or two $p$-electrons, building upon the methodology introduced by our former group member D. Tumakov. The proposed method is validated through the calculations of spin-dependent relativistic corrections in positronic beryllium [26], and fine-structure calculations in the lowest triplet states of neutral carbon. For carbon, the reported fine-structure splittings partially include $\alpha^4$ contribution and are the most accurate results obtained so far. Moreover, the carbon calculations presented here are the most accurate ones ever done for a six-electron system. This work demonstrates that the capabilities of the variational ECG approach are now sufficiently advanced to accurately describe the properties of a six-electron system.

## 2 Notations

The mathematical formalism of variational ECG calculations relies on matrix differential calculus [27] which requires dealing with matrices and vectors of different dimensions. To ensure consistent notation throughout the manuscript and prevent any confusion, below we introduce some conventions and explain our notations:

- $\nu$ — the number of spatial degrees of freedom per particle. For example, for $3D$-motion, $\nu$ is equal to three.
- $N$ — the number of particles in the system.
- $n = N - 1$ — the number of pseudoparticles. Since the center-of-mass motion can be factored out in the total wave function, one may make a change of coordinates to eliminate three degrees of freedom (e.g. transform to the center-of-mass frame, or choose one of the particles to be the origin of a new coordinate frame). The particles associated with the new coordinates may appear in the Hamiltonian with different masses or other modified properties, so we refer to them as pseudoparticles.
- $\mathcal{N}$ — the number of basis functions in the expansion of a trial wave function.

For operators, scalars, matrices, and vectors, we adopt the following conventions:

- $\mathcal{H}, \mathcal{O}, \mathcal{S}$ — Calligraphic Greek characters denote quantum mechanical operators.
- $\alpha, \beta, \gamma$ — Lower-case Greek characters denote scalars.
- $\boldsymbol{\alpha}, \boldsymbol{\beta}, \boldsymbol{\gamma}$ — Bold lower-case Greek characters denote $\nu$-component vectors.
- $a, b, c$ — Lower-case Latin characters denote $n$-component vectors.
- $\boldsymbol{a}, \boldsymbol{b}, \boldsymbol{c}$ — Bold lower-case Latin characters denote $\nu n$-component vectors.
- $\mathrm{a}, \mathrm{b}, \mathrm{c}$ — Serif font with lower-case Latin characters denotes $N$-component vectors.
- $\mathbf{a}, \mathbf{b}, \mathbf{c}$ — Bold Serif font with lower-case Latin characters denotes $\nu N$-component vectors.
- $\mathtt{a}, \mathtt{b}, \mathtt{c}$ — Typewriter font with lower-case Latin characters denotes $\mathcal{N}$-component vectors.
- $A, B, C$ — Upper-case Latin characters denote $n \times n$ matrices.
- $\boldsymbol{\Lambda}$, $\boldsymbol{\Xi}$, $\boldsymbol{\Omega}$ – Bold upper-case Greek characters denote $\nu \times \nu$ matrices.
- $\boldsymbol{A}, \boldsymbol{B}, \boldsymbol{C}$ — Bold upper-case Latin characters denote $\nu n \times \nu n$ matrices.
- $\mathrm{A}, \mathrm{B}, \mathrm{C}$ — Serif font with upper-case Latin characters denotes for $N \times N$ matrices.

- $\mathtt{A}, \mathtt{B}, \mathtt{C}$ — Typewriter font with upper-case Latin characters denotes $\mathcal{N} \times \mathcal{N}$ matrices.

For the matrix and vector operations, we use the following conventions:

- Vector and matrix transposition is denoted by the prime symbol, e.g. if $\boldsymbol{v}$ is a column vector, then $\boldsymbol{v}'$ is a row vector.
- The complex conjugation of a matrix $\boldsymbol{M}$ is denoted as $\boldsymbol{M}^*$. The hermitian conjugation is denoted as $\boldsymbol{M}^\dagger$. For the complex/hermitian conjugation of an operator or a vector, we use the same notation.
- The determinant of a matrix $A$ is denoted as $|A|$.
- The Kronecker product of matrices $A$ and $B$ (or, respectively, vectors $v$ and $w$) is denoted as $A \otimes B$ (respectively, $v \otimes w$).
- The gradient w.r.t. particle $i$, whose position is given by the radius-vector $\boldsymbol{R}_i$, is denoted as $\boldsymbol{\nabla}_{\boldsymbol{R}_i}$ or just $\boldsymbol{\nabla}_i$. The first option ($\boldsymbol{\nabla}_{\boldsymbol{R}_i}$) is usually used when we need to emphasize in which coordinate system we take the gradient.

Note that there will be some exceptions to the above notation scheme. However, they will be obvious and should not cause any confusion.

# 3 Theory of variational atomic calculations

## 3.1 The variational principle

As noted earlier, variational atomic calculations are based on the minimization of an energy functional $E(\Psi)$ (1.1). A systematic way to carry out this procedure is provided by the Rayleigh–Ritz variational method [28]. In this method, the trial wave function $\Psi$ is represented as a sum of $\mathcal{N}$ basis functions $\{\phi_i\}_{i=1}^{\mathcal{N}}$ as follows:

$$\Psi = \sum_{i=1}^{\mathcal{N}} c_i \phi_i, \tag{3.1}$$

where $c_i$ are linear coefficients, complex-valued in general. Coefficients $\{c_i\}_{i=1}^{\mathcal{N}}$ can be easily obtained by requiring the functional $E(\Psi)$ to be minimal under the condition that basis functions $\{\phi_i\}_{i=1}^{\mathcal{N}}$ are fixed. Varying w.r.t. linear parameters $c_i$ gives the eigenvalue problem:

$$\mathtt{Hc} = \epsilon \mathtt{Sc}, \tag{3.2}$$

where $\mathtt{H}$ and $\mathtt{S}$ are $\mathcal{N} \times \mathcal{N}$ Hamiltonian and overlap matrices, with the matrix elements given by:

$$\mathtt{H}_{ij} = \langle \phi_i | \mathcal{H} | \phi_j \rangle \,, \tag{3.3}$$

$$\mathtt{S}_{ij} = \langle \phi_i | \phi_j \rangle \,, \quad i, j = 1, \ldots, \mathcal{N}. \tag{3.4}$$

Here $\mathsf{c}$ is an $\mathcal{N}$-vector of linear parameters, $\mathsf{c} = (c_1, c_2, \ldots c_n)'$, and $\epsilon$ is an energy eigenvalue. If we now arrange the eigenvalues $\{\epsilon_n\}_{n=1}^{\mathcal{N}}$ in an ascending order, the first eigenvalue and the corresponding eigenvector will give the approximate energy and wave function for the ground state, the next eigenvalue-eigenvector pair — for the first excited state, and so on.

The Rayleigh–Ritz variational method described above allows one to obtain approximate wave function and energy for a particular state given the basis functions $\{\phi_i\}_{i=1}^{\mathcal{N}}$. However, the main strength of the variational method, which allows one to obtain very accurate wave functions and energies, lies in the extensive optimization of basis functions. Typically, each basis function $\phi_i$ depends on the set of $K$ non-linear parameters $\alpha_j$ $(j = 1, \ldots, K)$, which are heavily optimized to deliver the minimum to the functional $E(\Psi)$. In particular, in our calculations with the ECG basis functions, each increment of the basis set is accompanied by a step-by-step non-linear optimization of all basis functions appearing in the expansion (3.1).

### 3.2 Basis functions

A natural choice for the basis functions $\phi_i$ is exponential functions that explicitly depend on interparticle distances. Such basis functions were first introduced by Hylleraas in his pioneering work on the ground and first excited states of helium [29]. The general form of the trial wave function expanded in Hylleraas basis set is:

$$\Psi = e^{-\xi s} \sum_{i=1}^{\mathcal{N}} c_i s^{n_i} t^{2l_i} u^{m_i} \tag{3.5}$$

with the Hylleraas coordinates defined as:

$$s = r_1 + r_2, \quad t = -r_1 + r_2, \quad u = r_{12}, \tag{3.6}$$

where $r_i$ are nucleus–electron distances, and $r_{12}$ is the interelectron distance. The variational parameters here are $\xi$ and $c_i$. Note that one can build different expansions depending on the choice of the non-negative integer triples $(n_i,\, l_i,\, 2m_i)$ [12].

The expansion (3.5) contains the correlation terms (in the form of powers of interelectronic distances) only in the preexponential factor, but not in the argument of exponent. An alternative is to consider Slater-type wave functions [30] in which the correlation effects are taken into account by introducing the interelectronic distance in the exponent. Both approaches allowed to perform the most accurate calculations of helium [31, 32] and lithium-like atoms [33–35] as compared to other methods.

Despite the remarkable performance of Hylleraas-type and Slater-type wave functions for two- and three-electron system, the method is not applicable to larger systems due to analytical difficulty in evaluating four-electron integrals with this type of basis functions. For four- to six-electron systems, the best choice of basis functions is explicitly correlated

Gaussians that were first introduced for atomic calculations by Boys [11] and Singer [36]. For an atom consisting of $n$ electrons, their general form is:

$$\phi_i(\boldsymbol{r}_1, \boldsymbol{r}_2, \ldots, \boldsymbol{r}_n) = Y_{lm}(\boldsymbol{r}_1, \boldsymbol{r}_2, \ldots, \boldsymbol{r}_n) \exp\left[ -\sum_{i=1}^{n} \alpha_i^2 \boldsymbol{r}_i^2 - \sum_{i>j}^{n} \alpha_{ij} \boldsymbol{r}_i' \boldsymbol{r}_j \right], \tag{3.7}$$

where $\boldsymbol{r}_i$ is a vector pointing from a nucleus to the $i$-th electron, $\alpha_i$, $\alpha_{ij}$ are non-linear variational parameters, and $Y_{lm}(\boldsymbol{r}_1, \boldsymbol{r}_2, \ldots, \boldsymbol{r}_n)$ is an angular prefactor corresponding to an atom carrying orbital angular momentum $l$ with projection $m$.

Unlike Hylleraas-type or Slater-type wave functions, the argument of ECG exponent is a quadratic form of a $3n$-dimensional all-electron vector $\boldsymbol{r} = (\boldsymbol{r}_1, \ldots, \boldsymbol{r}_n)'$. This feature gives rise to the key advantage of the method — the possibility to obtain the matrix elements of non-relativistic Hamiltonian, as well as energy gradient w.r.t. non-linear variational parameters, analytically. Moreover, the analytic complexity of these formulas does not depend on the system size. This property allows for a very efficient optimization of a trial wave function. On the other hand, Gaussian basis functions do not have proper short- and long-range behavior. Specifically, they do not satisfy the Kato cusp condition [20] – the requirement on the discontinuity of a first derivative when one or more interparticle distances are zero. Also, they decay too rapidly for large interparticle distances. In contrast, Hylleraas- and Slater-type bases do not suffer from these limitations. To mitigate these drawbacks, one needs to use very large expansions of highly optimized Gaussians for a trial wave function.

### 3.3 Non-relativistic Hamiltonian and center-of-mass reduction

Due to translational invariance in the absence of external fields, the center-of-mass motion can be factored out in the total wave function. Therefore, we may eliminate three coordinates and come to internal coordinates describing only the relative motion of particles. It is often convenient to choose the heaviest particle (in atomic systems, it is a nucleus) to be the reference one and place the origin of a new coordinate system at the position of that particle. Further, we briefly outline this procedure.

Consider the Coulomb-interacting system of $N$ particles with charges $Q_i$ and masses $M_i$. The positions of the particles in the laboratory frame are given by the radius-vectors $\boldsymbol{R}_i$, as Fig. 1 shows.

The non-relativistic Hamiltonian $\mathcal{H}_{\text{NR}}$ in laboratory frame reads:

$$\mathcal{H}_{\text{NR}} = \sum_{i=1}^{N} \frac{\boldsymbol{P}_i^2}{2M_i} + \sum_{i>j}^{N} \frac{Q_i Q_j}{2R_{ij}}, \tag{3.8}$$

where $R_{ij} = |\boldsymbol{R}_j - \boldsymbol{R}_i|$, $\boldsymbol{P}_i = -i\boldsymbol{\nabla}_{\boldsymbol{R}_i} = -i\frac{\partial}{\partial \boldsymbol{R}_i}$.

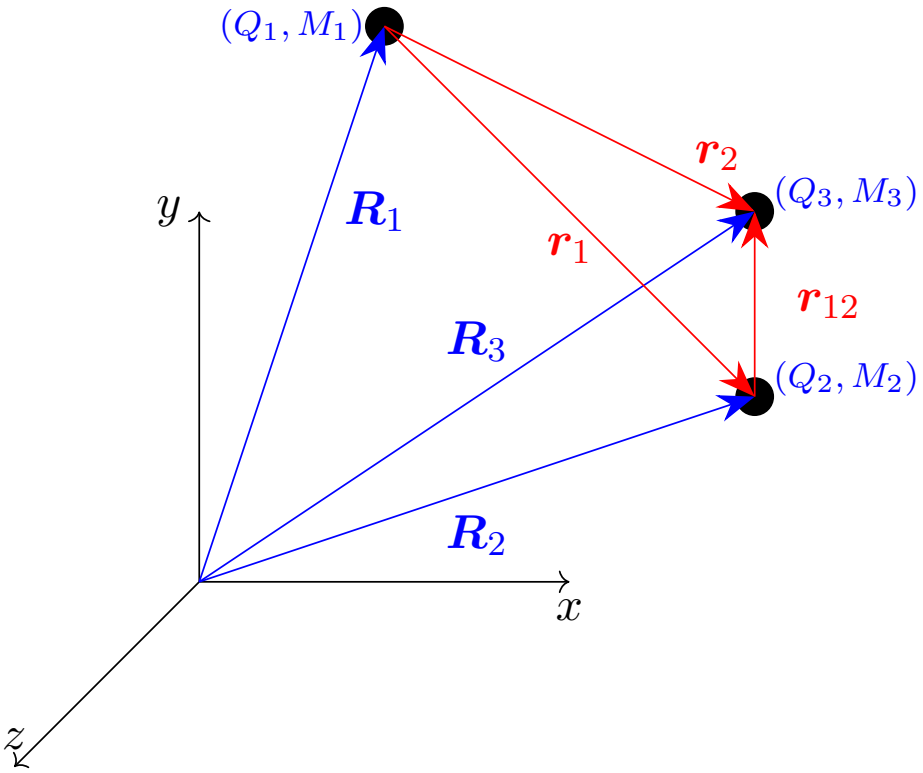


**Figure 1:** The transformation from laboratory frame coordinates $\boldsymbol{R}_i$ (blue color) to internal coordinates $\boldsymbol{r}_i$ (red color)

Now, we introduce the new set of coordinates $\{\boldsymbol{r}_i\}_{i=1}^N$ according to the rule:

$$\boldsymbol{r}_i = \boldsymbol{R}_{i+1} - \boldsymbol{R}_1, \; i = 1, \ldots, N-1, \tag{3.9}$$

$$\boldsymbol{r}_N \equiv \boldsymbol{r}_{\rm cm} = \frac{\sum\limits_{i=1}^{n} M_i \boldsymbol{R}_i}{M}, \tag{3.10}$$

where $M$ is the total mass of all particles, $M = \sum\limits_{i=1}^{N} M_i$. In other words, we has transformed from laboratory coordinates to the center-of-mass coordinate $\boldsymbol{r}_N$ and $n = N-1$ coordinates $\{\boldsymbol{r}_i\}_{i=1}^n$ relative to the reference particle 1. For convenience, we introduce the notations with shifted indices $m_i = M_{i+1}$, $q_i = Q_{i+1} (i = 0, \ldots, N-1)$. According to this convention, the reference particle has mass $m_0 \equiv M_1$ and charge $q_0 \equiv Q_1$. Using the chain rule for differentiation, we express the momentum operators in laboratory coordinates $\boldsymbol{P}_i = -i\boldsymbol{\nabla}_{\boldsymbol{R}_i}$ through the momentum in new coordinates $\boldsymbol{p}_i = -i\boldsymbol{\nabla}_{\boldsymbol{r}_i}$, and obtain for the Hamiltonian $\mathcal{H}'_{\rm NR}$ in new coordinates:

$$\mathcal{H}'_{\rm NR} = \sum_{i=1}^{n} \frac{p_i^2}{2\mu_i} + \frac{1}{2m_0} \sum_{i \neq j}^{n} \boldsymbol{p}'_i \boldsymbol{p}_j + \frac{1}{2} \sum_{i>j}^{n} \frac{q_i q_j}{r_{ij}} + \sum_{i=1}^{n} \frac{q_0 q_i}{r_i} + \frac{\boldsymbol{p}_N^2}{2M}, \tag{3.11}$$

where $\mu_i = m_0 m_i / (m_0 + m_i)$ is the reduced mass of particle $i+1$.

As one can see, our initial Hamiltonian decoupled into the part depending on internal coordinates $\{\boldsymbol{r}_i\}_{i=1}^n$ and the one depending on the center-of-mass motion. The latter does not represent any interest and we will work only with internal Hamiltonian $\mathcal{H}_{\mathrm{NR}}^{\mathrm{int}'}$:

$$\mathcal{H}_{\mathrm{NR}}^{\mathrm{int}'} = \sum_{i=1}^{n} \frac{p_i^2}{2\mu_i} + \frac{1}{2m_0} \sum_{i \neq j}^{n} \boldsymbol{p}_i' \boldsymbol{p}_j + \frac{1}{2} \sum_{i>j}^{n} \frac{q_i q_j}{r_{ij}} + \sum_{i=1}^{n} \frac{q_0 q_i}{r_i}. \tag{3.12}$$

The particles associated with coordinates $\{\boldsymbol{r}_i\}_{i=1}^n$ are referred to as pseudoparticles. As seen from (3.12), at the non-relativistic level, they interact via Coulomb forces like particles with masses $\mu_i$ and charges $q_i$ in the field of reference particles $q_0$. Note that the motion of these pseudoparticles is also coupled through the mass-polarization term $\frac{1}{2m_0} \sum_{i \neq j}^{n} \boldsymbol{p}_i' \boldsymbol{p}_j$.

For the sake of simplicity, in this thesis we will denote Hamiltonian (3.12) by $\mathcal{H}_{\mathrm{NR}}$. Also, we will use the terms 'pseudoparticle' and 'particle' interchangeably, when the meaning is clear from the context or not essential.

### 3.4 Spin-free formalism

The total wave function $\Phi$ of an atom containing $n$ electrons is an antisymmetrized product of spin part $\Theta$ and spatial part $\Psi$:

$$\Phi(\boldsymbol{\sigma}, \boldsymbol{r}) = \mathcal{A}\left[\Theta(\boldsymbol{\sigma})\Psi(\boldsymbol{r})\right], \tag{3.13}$$

where $\boldsymbol{\sigma}$ and $\boldsymbol{r}$ are all-electron spin and position vectors, respectively:

$$\boldsymbol{\sigma} = (\sigma_1, \ldots, \sigma_n), \tag{3.14}$$

$$\boldsymbol{r} = (\boldsymbol{r}_1, \ldots, \boldsymbol{r}_n). \tag{3.15}$$

Antisymmetrization operator $\mathcal{A}$ is defined as:

$$\mathcal{A} = \frac{1}{\sqrt{n!}} \sum_{\mathcal{P}_i \in S_n} \varepsilon_{\mathcal{P}_i} \mathcal{P}_i, \tag{3.16}$$

where $\varepsilon_{\mathcal{P}_i}$ is the parity of permutation $\mathcal{P}_i$ and the summation runs over all possible permutations of $n$ identical particles. $S_n$ denotes the symmetric group of permutations of $n$ particles. The antisymmetrizer $\mathcal{A}$ ensures that the total wave function $\Phi(\boldsymbol{\sigma}, \boldsymbol{r})$ is totally antisymmetric under the exchange of any two particles, as required by the Fermi–Dirac statistics for a system of identical fermions:

$$\mathcal{P}_{ij}\Phi(\boldsymbol{\sigma}, \boldsymbol{r}) = -\Phi(\boldsymbol{\sigma}, \boldsymbol{r}), \tag{3.17}$$

where operator $\mathcal{P}_{ij}$ permutes spin and spatial variables of particles $i$ and $j$.

If we aim to find the expectation value of a spin-independent operator $\mathcal{O}$, we may

exclude spin from the consideration. To do this, we need to project basis functions $\phi_i(\boldsymbol{r})$ onto the irreducible representation corresponding to the total spin $S$ via spatial Young operator $\mathcal{Y}^r$ [37, 38]. Thus, to find the desired matrix element, we consider the spin-free Young-projected wave function $\mathcal{Y}^r\Psi(\boldsymbol{r})$:

$$\mathcal{Y}^r\Psi(\boldsymbol{r}) = \sum_{i=1}^{\mathcal{N}} c_i \mathcal{Y}^r \phi_i(\boldsymbol{r}), \tag{3.18}$$

and the corresponding expectation value is then written as:

$$\langle \mathcal{O} \rangle = \frac{\langle \mathcal{Y}^r\Psi | \mathcal{O} | \mathcal{Y}^r\Psi \rangle}{\langle \mathcal{Y}^r\Psi | \mathcal{Y}^r\Psi \rangle} = \frac{\langle \Psi | \mathcal{O}\mathcal{Y}^{r\dagger}\mathcal{Y}^r | \Psi \rangle}{\langle \Psi | \mathcal{Y}^{r\dagger}\mathcal{Y}^r\Psi \rangle}, \tag{3.19}$$

where we assumed that the operator $\mathcal{O}$ commutes with any permutation $\mathcal{P}$ from the group $S_n$. Computing the matrix element with such spin-free basis functions is equivalent to using the full wave functions and summing over spin variables.

Finally, we show how one can construct spatial Young operator $\mathcal{Y}^r$ for a system of $n$ identical fermions with spin 1/2 and total spin $S$. We will follow Ref. [39] to describe the construction of Young table — a scheme to write the Young operator. To begin, we determine the number $p$ of two-cell rows in the Young table, given by $p = n/2 - S$. The number of one-cell rows is then $n - 2p$, and the corresponding partition of the table is $\mu = [2^p, 1^{n-2p}]$. For example, for a five-particle system ($n = 5$) with spin $S = 1/2$, the partition is $[2^2, 1]$, meaning the table consists of two two-cell rows and one single-cell row. Next, we enumerate the particles and place their labels in the table, starting from the upper-left corner. The labels can be arranged either left to right, row by row, or top to bottom, column by column. In our example, we choose to place the labels from top to bottom which results in the following Young table:

| | |
|---|---|
| 1 | 4 |
| 2 | 5 |
| 3 | |

(3.20)

To write the spatial Young operator $\mathcal{Y}^r$, we should symmetrize over indices in rows, and antisymmetrize over indices in columns:

$$\mathcal{Y}^r = \mathcal{S}_{14}\mathcal{S}_{25}\mathcal{A}_{123}\mathcal{A}_{45}, \tag{3.21}$$

where $\mathcal{S}$ and $\mathcal{A}$ are symmetrization and antisymmetrization operators, respectively, and

the indices in the subscript denote the particles on which the operators act. In our case,

$$\mathcal{S}_{14} = (\mathcal{I} + \mathcal{P}_{14}), \tag{3.22}$$

$$\mathcal{S}_{25} = (\mathcal{I} + \mathcal{P}_{25}), \tag{3.23}$$

$$\mathcal{A}_{123} = (\mathcal{I} - \mathcal{P}_{12})(\mathcal{I} - \mathcal{P}_{12} - \mathcal{P}_{13}), \tag{3.24}$$

$$\mathcal{A}_{45} = (\mathcal{I} - \mathcal{P}_{45}), \tag{3.25}$$

where $\mathcal{I}$ is the identity operator.

### 3.5 Spin-dependent formalism

To evaluate spin-dependent relativistic energy corrections, the full wave function must be used. Let us assume that we constructed the non-relativistic trial wave function $\Psi(\boldsymbol{r})$:

$$\Psi(\boldsymbol{r}) = \sum_{i=1}^{\mathcal{N}} c_i \phi_i(\boldsymbol{r}) \tag{3.26}$$

by minimizing the expectation value of the Schrödinger Hamiltonian (3.12) with the spatial Young-projected wave function $\mathcal{Y}^{\boldsymbol{r}}\Psi(\boldsymbol{r})$ (see Eq. (3.19)).

We can now construct the spin wave function $\Theta(\boldsymbol{r})$ by using the spin Young operator $\mathcal{Y}^{\boldsymbol{\sigma}}$. The spin Young table is the spatial one transposed. In our example, the table takes the form:

| | | |
|---|---|---|
| 1 | 2 | 3 |
| 4 | 5 | |

(3.27)

with the spin Young operator $\mathcal{Y}^{\boldsymbol{\sigma}}$ given by:

$$\mathcal{Y}^{\boldsymbol{\sigma}} = \mathcal{S}_{123}\mathcal{S}_{45}\mathcal{A}_{14}\mathcal{A}_{25}. \tag{3.28}$$

To construct spin wave function, we will now use a "primitive" spin function which is a simple product of one-electron spinors. Let us now take a primitive spin function which is an eigenfunction of the total spin operator $\mathcal{S}^2$ and spin projection operator $\mathcal{S}_z$ with eigenvalue $S_z = S$. For example, in our case, we may choose:

$$\theta = |\uparrow\rangle_1 |\uparrow\rangle_2 |\uparrow\rangle_3 |\downarrow\rangle_4 |\downarrow\rangle_5 , \tag{3.29}$$

where $|\uparrow\rangle_i$ and $|\downarrow\rangle_i$ denote the spin up and spin down state of the $i$-th particle, respectively. Then we act with the spin Young operator $\mathcal{Y}^{\boldsymbol{\sigma}}$ on the primitive $\theta$ to obtain a properly symmetrized spin wave function $\Theta$:

$$\Theta = \mathcal{Y}^{\boldsymbol{\sigma}}\theta. \tag{3.30}$$

It may happen that $\mathcal{Y}^{\boldsymbol{\sigma}}\theta$ is identically zero. Then we should try another primitive function

$\tilde{\theta}$ (e.g. by permuting some of the particles) and act on it with $\mathcal{Y}^{\boldsymbol{\sigma}}$. This process must be continued unless we find the primitive that does not vanish under the action of $\mathcal{Y}^{\boldsymbol{\sigma}}$.

Thus, the algorithm to obtain the full wave function of atomic system can be summarized as follows:

1. We obtain the variational trial spatial wave function $\Psi(\boldsymbol{r})$ by minimizing the expectation value of a Hamiltonian with a spatial Young-projected wave function $\mathcal{Y}^{r}\Psi(\boldsymbol{r})$.

2. We construct the spin wave function $\Theta(\boldsymbol{\sigma})$ from the primitive spin function $\theta(\boldsymbol{\sigma})$ which is an *any* eigenfunction of operators $\mathcal{S}^2$ and $\mathcal{S}_z$ with the maximum projection $S_z = S$ and that does not vanish under the action of spin Young operator $\mathcal{Y}^{\boldsymbol{\sigma}}$:

$$\Theta(\boldsymbol{\sigma}) = \mathcal{Y}^{\boldsymbol{\sigma}}\theta(\boldsymbol{\sigma}). \tag{3.31}$$

3. The total wave function $\Phi(\boldsymbol{\sigma}, \boldsymbol{r})$ is an antisymmetrized product of spin and spatial parts:

$$\Phi(\boldsymbol{\sigma}, \boldsymbol{r}) = \mathcal{A}\left[\Theta(\boldsymbol{\sigma})\Psi(\boldsymbol{r})\right]. \tag{3.32}$$

Finally, let us consider the spin-dependent operator $\mathcal{O}$ that commutes with any permutations $\mathcal{P} \in S_n$ and can be factorized into the product of spin and spatial parts: $\mathcal{O} = \mathcal{O}^{\boldsymbol{\sigma}}\mathcal{O}^{\boldsymbol{r}}$. Similarly, we express the permutation operator $\mathcal{P}$ as the product of its spin and spatial components: $\mathcal{P} = \mathcal{P}^{\boldsymbol{\sigma}}\mathcal{P}^{\boldsymbol{r}}$. In this case, the expectation value $\langle\mathcal{O}\rangle$ can be written as follows:

$$\langle\mathcal{O}\rangle = \sum_{\mathcal{P}_i \in S_n} \varepsilon_{\mathcal{P}_i} \langle\Theta|\mathcal{O}^{\boldsymbol{\sigma}}\mathcal{P}^{\boldsymbol{\sigma}}|\Theta\rangle \langle\Psi|\mathcal{O}^{\boldsymbol{r}}\mathcal{P}^{\boldsymbol{r}}|\Psi\rangle. \tag{3.33}$$

# 4 Theory of atomic fine structure

## 4.1 Physical picture

The state of an atom is conventionally described via atomic term symbol $n\,^{2S+1}L^p_J$, where $L$ is the orbital angular momentum quantum number, $S$ — spin quantum number, and $J = L \oplus S$ — total angular momentum quantum number. The principal quantum number $n$ labels the terms of the same $L$ and $S$ according to their energy ordering. The character $p = \{e, o\}$ in the superscript denotes the parity of a state, where $e$ represents an even-parity state, and $o$ — odd-parity state. The non-relativistic Schrödinger Hamiltonian (3.12) assigns particular energy for each atomic term. However, atomic levels with the same $L$ and $S$ quantum numbers, but different $J$, are degenerate. The inclusion of non-scalar spin-dependent relativistic contributions, namely, the spin–orbit and spin–spin interactions, removes the degeneracy. Certainly, the new levels remain degenerate with respect to the projection of total angular momentum $M_J$.

The spin–orbit interaction describes the coupling between the electrons' magnetic moments, associated with their spins, and the atomic magnetic field, while the spin–spin

interaction accounts for the dipole–dipole interaction between the electrons' magnetic moments. As a result, the previously degenerate states with different $J$ values split into distinct energy levels, which can be observed in atomic spectra. This phenomenon is called fine-structure splitting — the name reflects small intervals between the levels with different $J$ values, as compared to the energy separation between atomic terms corresponding to non-relativistic Hamiltonian (the so-called gross structure).

The total angular momentum quantum number $J$ may take the values from $J = |L-S|$ to $J = L+S$, according to the usual rules of angular momentum algebra [40]. A schematic representation of fine-structure splitting for an atomic term ${}^{2S+1}L$ is given in Fig. 2.

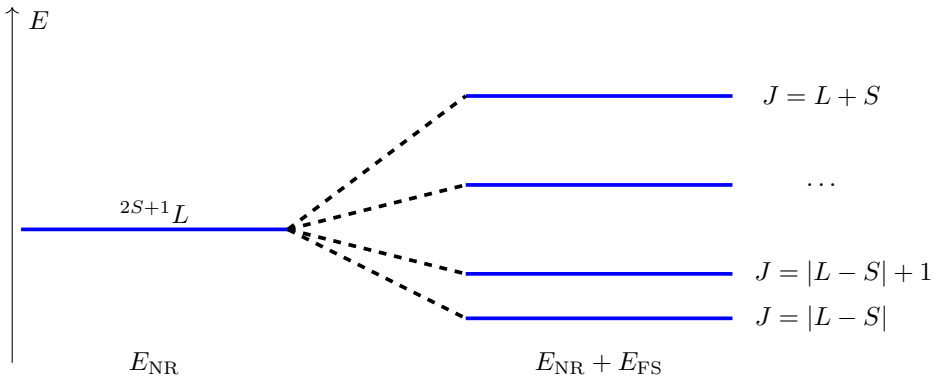


**Figure 2:** Fine-structure splitting of an atomic term ${}^{2S+1}L$. $E_{\rm NR}$ denotes the non-relativistic energy, $E_{\rm FS}$ — higher-order contributions.

### 4.2 Dirac–Breit Hamiltonian

The inclusion of relativistic and QED corrections for light atoms can be carried out systematically in the framework of non-relativistic quantum electrodynamics (NRQED) [41] by expanding the energy in powers of fine-structure constant $\alpha$:

$$E = E^{(0)}_{\rm NR} + E^{(2)} + E^{(3)} + E^{(4)} + \ldots, \tag{4.1}$$

where $E^{(0)}_{\rm NR}$ represents the energy corresponding to the Schrödinger Hamiltonian (3.12), $E^{(2)}$ is the expectation value of relativistic corrections from the effective Dirac–Breit Hamiltonian [42, 43], etc.

At the leading-order ($\propto \alpha^2$), we can separate the contributions that result in an overall shift of atomic term from those that cause fine-structure splitting by writing the Dirac–Breit Hamiltonian $\mathcal{H}^{(0)}_{\rm R}$ as $\mathcal{H}^{(0)}_{\rm R} = \mathcal{H}^{(0)}_{\rm NR} + \mathcal{H}^{(2)}_{\rm SR} + \mathcal{H}^{(2)}_{\rm FS}$, where $\mathcal{H}^{(2)}_{\rm SR}$ represents all leading-order scalar relativistic effects and $\mathcal{H}^{(2)}_{\rm FS}$ describes the leading-order fine-structure splittings.

The scalar relativistic part contains the following terms:

$$\mathcal{H}^{(2)}_{\rm SR} = \mathcal{H}^{(2)}_{\rm MV} + \mathcal{H}^{(2)}_{\rm D} + \mathcal{H}^{(2)}_{\rm OO} + \mathcal{H}^{(2)}_{\rm SSF}, \tag{4.2}$$

which are commonly known as mass-velocity, Darwin, orbit–orbit, and contact spin–spin Fermi interactions. Their explicit expressions in internal coordinates can be found in [26]. Although the spin–spin contact Fermi interaction depends on the electrons' spins, it does not lead to energy level splitting because it is a scalar interaction — i.e. corresponds to a spin tensor of rank zero.

The leading-order fine-structure Hamiltonian consists of two terms, $\mathcal{H}^{(2)}_{\rm FS} = \mathcal{H}^{(2)}_{\rm SO} + \mathcal{H}^{(2)}_{\rm SSNC}$, where $\mathcal{H}^{(2)}_{\rm SO}$ and $\mathcal{H}^{(2)}_{\rm SSNC}$ are the spin–orbit and the electron part of the non-contact (dipolar) spin–spin interactions, respectively. The spin–orbit Hamiltonian is usually written as $\mathcal{H}^{(2)}_{\rm SO} = \mathcal{H}^{(2)}_{\rm SO1} + \mathcal{H}^{(2)}_{\rm SO2}$, where $\mathcal{H}^{(2)}_{\rm SO1}$ and $\mathcal{H}^{(2)}_{\rm SO2}$ are commonly referred to as spin–same–orbit and spin–other–orbit contributions. In internal coordinates, these operators are written as follows [44]:

$$\mathcal{H}^{(2)}_{\rm SO1} = -\alpha^2 \sum_{i=1}^{n} \frac{q_0 q_i}{2m_i} \left( \frac{1+2a_{\rm e}}{m_i} + \frac{2(1+a_{\rm e})}{m_0} \right) \frac{\boldsymbol{s}'_i}{r_i^3} \left[ \boldsymbol{r}_i \times \boldsymbol{p}_i \right], \tag{4.3}$$

$$\begin{aligned} \mathcal{H}^{(2)}_{\rm SO2} = -\alpha^2 \sum_{j\neq i}^{n} \Bigg\{ & (1+a_{\rm e}) \frac{q_0 q_i}{m_0 m_i} \frac{\boldsymbol{s}'_i}{r_i^3} \left[ \boldsymbol{r}_i \times \boldsymbol{p}_j \right] + \\ & + \frac{q_i q_j}{2m_i} \frac{\boldsymbol{s}'_i}{r_{ij}^3} \left[ \boldsymbol{r}_{ji} \times \left( \frac{1+2a_{\rm e}}{m_i} \boldsymbol{p}_i - \frac{2(1+a_{\rm e})}{m_j} \boldsymbol{p}_j \right) \right] \Bigg\}, \end{aligned} \tag{4.4}$$

$$\mathcal{H}^{(2)}_{\rm SSNC} = \alpha^2 \sum_{j>i}^{n} (1+a_{\rm e})^2 \frac{q_i q_j}{m_i m_j} \left[ \frac{(\boldsymbol{s}'_i \boldsymbol{s}_j)}{r_{ij}^3} - 3 \frac{(\boldsymbol{s}'_i \boldsymbol{r}_{ij})(\boldsymbol{s}'_j \boldsymbol{r}_{ij})}{r_{ij}^5} \right], \tag{4.5}$$

where $\boldsymbol{s}_i$ is the spin of the $i$-th electron, $\boldsymbol{r}_{ij} = \boldsymbol{r}_j - \boldsymbol{r}_i$, are interparticle separation vectors, and $a_{\rm e} = \alpha/2\pi + \ldots \approx 1.159\,652\,180\,46 \times 10^{-3}$, is the electron anomalous magnetic moment [45]. Note that $\mathcal{H}^{(2)}_{\rm FS}$ effectively contains terms $\propto \alpha^3$ and higher through the electron magnetic moment anomaly.

### 4.3 Perturbation series approach

Up to the fourth power of $\alpha$, the fine-structure energy levels can be expressed as the sum of the first-order and second-order perturbation theory contributions. The corresponding expression for the total $J$-dependent part of the energy in state $|\psi\rangle \equiv |nJM_J LS\rangle$ is:

$$E_{nJ} = \langle\psi|\mathcal{H}^{(2)}_{\rm FS}|\psi\rangle + \sum_{\phi\neq\psi} \frac{\left|\langle\phi|\mathcal{H}^{(2)}_{\rm FS}|\psi\rangle\right|^2}{E_\psi - E_\phi} + 2\sum_{\phi\neq\psi} \frac{\langle\psi|\mathcal{H}^{(2)}_{\rm SR}|\phi\rangle\langle\phi|\mathcal{H}^{(2)}_{\rm FS}|\psi\rangle}{E_\psi - E_\phi} + \langle\psi|\mathcal{H}^{(4)}_{\rm FS}|\psi\rangle. \tag{4.6}$$

The first term in Eq. (4.6) contains the leading-order contribution of the order of $\alpha^2$ and anomalous magnetic moment correction of the order of $\alpha^3$ and higher. The second and third terms come from the second-order perturbation theory. The summation involves all eigenstates $|\phi\rangle$ of the non-relativistic Hamiltonian (3.12). The last term comes from the higher-order effective Hamiltonian obtained by the Foldy–Wouthuysen transformation of

the Dirac equation. The explicit expression for $\mathcal{H}^{(4)}_{\rm FS}$ can be found in Refs. [22, 46].

### 4.4 Hyperfine structure

The magnetic dipole hyperfine interaction arises from the coupling between the nuclear magnetic moment and the magnetic field generated by the electrons. As a result, the total electronic angular momentum $J$ is no longer conserved. Instead, the conserved quantity is the total angular momentum $F$, defined as the sum of the nuclear spin $I$ and the electronic angular momentum $J$: $F = I \oplus J$. The hyperfine structure (HFS) splitting is much smaller than that of a fine-structure, approximately by the order of the ratio of proton to electron mass.

Hyperfine structure interaction has the following Hamiltonian [47]:

$$\mathcal{H}^{(2)}_{\rm HFS} = \mathcal{H}^{\rm SSF}_{\rm HFS} + \mathcal{H}^{\rm SO}_{\rm HFS} + \mathcal{H}^{\rm SSNC}_{\rm HFS}, \tag{4.7}$$

which is a sum of contact Fermi, spin–orbit and spin–dipolar interactions. In internal coordinates, they are written as follows [24]:

$$\mathcal{H}^{\rm SSF}_{\rm HFS} = g_{\rm e} g_N \mu_{\rm B} \mu_{\rm N} \boldsymbol{I}' \sum_{i=1}^{n} \frac{8\pi}{3} \delta(\boldsymbol{r}_i) \boldsymbol{s}_i, \tag{4.8}$$

$$\mathcal{H}^{\rm SO}_{\rm HFS} = \boldsymbol{I}' \left\{ \sum_{i=1}^{n} \left( \frac{g_N}{2 m_i m_{\rm p}} + \frac{g_N}{2 m_{\rm N} m_{\rm p}} - \frac{Z}{2 m_{\rm N}^2} \right) \frac{1}{r_i^3} [\boldsymbol{r}_i \times \boldsymbol{p}_i] + \sum_{\substack{i,j=1 \\ i \neq j}}^{n} \left( \frac{g_N}{2 m_{\rm N} m_{\rm p}} - \frac{Z}{2 m_{\rm N}^2} \right) \frac{1}{r_i^3} [\boldsymbol{r}_i \times \boldsymbol{p}_j] \right\}, \tag{4.9}$$

$$\mathcal{H}^{\rm SSNC}_{\rm HFS} = g_{\rm e} g_N \mu_{\rm B} \mu_{\rm N} \boldsymbol{I}' \sum_{i=1}^{n} \left( \frac{3 \boldsymbol{r_i} (\boldsymbol{s}_i' \boldsymbol{r}_i)}{r_i^5} - \frac{\boldsymbol{s}_i}{r_i^3} \right). \tag{4.10}$$

Here $m_{\rm N}$ and $m_{\rm p}$ are nuclear and proton masses, $\mu_{\rm B} = \frac{e\hbar}{2 m_{\rm e} c}$ and $\mu_{\rm N} = \frac{e\hbar}{2 m_{\rm p} c}$ are Bohr and nuclear magnetons, $g_{\rm e} \approx 2 + \frac{\alpha}{\pi}$ is the electron spin $g$-factor, and $g_N$ is the nucleuar $g$-factor that is related to the nuclear magnetic moment $\boldsymbol{\mu}$ as: $\boldsymbol{\mu} = g_N \mu_{\rm N} \boldsymbol{I}$.

Note that analogously to the case of fine-structure, spin–orbit hyperfine structure contribution (4.9) consists of tho sums. However, the second sum over $i \neq j$ comes solely from the transformation to internal coordinates. Another point to note is that in Eq. (4.9), the terms proportional to $Z$ originate from the so-called Thomas precession [48] — a purely kinematic contribution to the Hamiltonian that takes place for a fermion moving with acceleration.

The leading-order contribution to the HFS splitting for the case of nuclear spin $I = 1/2$

can be expressed in terms of the hyperfine parameter $A_J$:

$$E_J = A_J(\boldsymbol{I}'\boldsymbol{J}) = \frac{1}{2}A_J K, \tag{4.11}$$

where $K = F(F+1) - I(I+1) - J(J+1)$. This form predicts the HFS splitting ratio and has the form analogous to the Lande interval rule for the fine-structure. The form (4.11) originates from the fact that the HFS Hamiltonian can be represented as a scalar product of rank-one tensors [47].

# 5 Evaluation of diagonal spin-dependent matrix elements

## 5.1 Operator factorization technique

To evaluate the matrix elements of spin-dependent operators, it is convenient to factorize them into the product of spin and spatial components, and then use formula (3.33) to compute them in the ECG basis set. The general formalism for evaluating matrix elements of such separable operators is given in Ref. [49], and explicit expressions for spin–orbit and spin–spin interactions can be found in Ref. [44]. Here we briefly introduce this formalism.

First, we define the scalar product of two tensor operators $\boldsymbol{T}^{(k)}$ and $\boldsymbol{U}^{(k)}$ of rank $k$:

$$\boldsymbol{T}^{(k)} \cdot \boldsymbol{U}^{(k)} = \sum_{q=-k}^{k} (-1)^q T^{(k)}_{-q} U^{(k)}_q. \tag{5.1}$$

The tensorial component $T^{(k)}_{-q}$ is defined to transform under rotations in the same way as the spherical harmonic $Y^{(k)}_q$. For example, for a $3D$ vector $\boldsymbol{V} = (V_x, V_y, V_z)$, the tensorial components of a corresponding rank-one tensor are defined as:

$$\begin{aligned} V_1 &= -\frac{V_x + iV_y}{\sqrt{2}}, \\ V_0 &= V_z, \\ V_{-1} &= \frac{V_x - iV_y}{\sqrt{2}}. \end{aligned} \tag{5.2}$$

Notice that with this definition, the usual Euclidean scalar product of two $3D$-vectors $\boldsymbol{V}$ and $\boldsymbol{W}$ can be expressed through its tensorial components as:

$$\boldsymbol{V}'\boldsymbol{W} = V_x W_x + V_y W_y + V_z W_z = -V_{-1}W_1 + V_0 W_0 - V_1 W_{-1}. \tag{5.3}$$

Next, the cross-product of tensors $\boldsymbol{T}^{(K)}$ and $\boldsymbol{U}^{(P)}$ of ranks $K$ and $P$, forming the

tensor of rank $Q$, is defined component-wise as:

$$[\boldsymbol{T}^{(K)} \times \boldsymbol{U}^{(P)}]^{(Q)}_q = \sum_{\substack{m,n \\ m+n=q}} C^{Qq}_{Km,Pn} T^{(K)}_m U^{(P)}_n, \tag{5.4}$$

where $C^{Qq}_{Km,Pn}$ are Clebsch–Gordan coefficients.

As we will see later, spin–orbit and spin–spin Hamiltonians can be represented in a form (5.1), namely, as a sum of tensor scalar products of spin $\boldsymbol{T}^{(k)}$ and spatial $\boldsymbol{U}^{(k)}$ operators of rank $k$. Let us now derive the formulas to evaluate the expectation value of such operator $\mathcal{O}$:

$$\mathcal{O} = \sum_{\{j\}} \boldsymbol{T}^{(k)}_j \cdot \boldsymbol{U}^{(k)}_j, \tag{5.5}$$

where index $j$ runs over all particles. The expectation value $\langle \mathcal{O} \rangle_J$ in a state with a definite $J$ value is:

$$\langle \mathcal{O} \rangle_J = \langle \gamma S L J M_J | \mathcal{O} | \gamma S L J M_J \rangle \,, \tag{5.6}$$

where $M_J$ is the projection of total angular momentum, and $\gamma$ denotes all additional quantum numbers required to uniquely specify the state. Notice, that the matrix element (5.6) is independent of the projection $M_J$, since $\mathcal{O}$ does not carry angular momentum.

To further simplify (5.6), it is convenient to come from a coupled basis $|SLJM_J\rangle$ to an uncoupled representation $|SM_SLM_L\rangle$ (here $M_S$ and $M_L$ are projections of spin and orbital angular momentum). This can be routinely done using Clebsch–Gordan coefficients:

$$|\gamma S L J M_J\rangle = \sum_{M_S+M_L=M_J} C^{JM_J}_{SM_SLM_L} \, |\gamma S M_S L M_L\rangle \,. \tag{5.7}$$

Using the angular momentum algebra [49] to handle Clebsch–Gordan coefficients, we can express $\mathcal{O}_J$ for different $J$ using a single matrix element for the case of a maximum projection of total angular momentum $M_J = J$ (corresponding to $M_L = L$ and $M_S = S$) [44]:

$$\langle \mathcal{O} \rangle_J = C_J \sum_{\mathcal{P}_i \in S_n} \varepsilon_{\mathcal{P}_i} \sum_{\{j\}} \left\langle SS \left| T^{(k)}_{j,0} \mathcal{P}^{\boldsymbol{\sigma}}_i \right| SS \right\rangle \left\langle \gamma LL \left| U^{(k)}_{j,0} \mathcal{P}^{\boldsymbol{r}}_i \right| \gamma LL \right\rangle, \tag{5.8}$$

where the coefficient $C_J$ accounts for the symmetry properties of the matrix elements and is expressed through 6-$j$ symbol as:

$$C_J = (-1)^{S+L+J} \frac{\sqrt{(2S-k)!\,(2S+k+1)!\,(2L-k)!\,(2L+k+1)!}}{(2S)!\,(2L)!} \begin{Bmatrix} S & S & k \\ L & L & J \end{Bmatrix}. \tag{5.9}$$

Below, we present the matrix elements of the non-scalar spin-dependent operators of the Dirac—Breit Hamiltonian, evaluated in the ECG basis set. In the code, we separately compute the leading-order contributions ($\propto \alpha^2$) from the spin–orbit and non-contact spin–spin interactions, as well as the $\alpha^3$ correction arising from the electron magnetic

moment anomaly. This separation allows us to assess the relative significance of each term. Accordingly, in the following derivations, we set $a_e = 0$ to isolate the leading-order effects. If one wants to restore full formulas with $a_e \neq 0$, this can be easily done using complete expressions given in (4.3), (4.4), and (4.5).

*Spin–orbit interaction*

The spin–orbit (SO) operator $\mathcal{H}_{\rm SO}$ already has the form (5.1) of a scalar product of rank-one spin and spatial tensors with $T^{(1)}_{j,0}$ and $U^{(1)}_{j,0}$ given by [44]:

$$\begin{aligned} T^{(1)}_{j,0} &= \boldsymbol{s}_{j,z}, \\ U^{(1)}_{j,0} &= i\frac{q_0 q_j}{2m_j}\left(\frac{1}{m_j}+\frac{2}{m_0}\right)\frac{1}{r_j^3}\left[\boldsymbol{r}_j\times\boldsymbol{\nabla}_j\right]_z + i\sum_{\substack{k=1\\k\neq j}}^{n}\left\{\frac{q_0 q_j}{m_0 m_j}\frac{1}{r_j^3}\left[\boldsymbol{r}_j\times\boldsymbol{\nabla}_k\right]_z - \right. \\ &\quad \left. -\frac{q_j q_k}{2m_j}\frac{1}{r_{jk}^3}\left[\boldsymbol{r}_{jk}\times\left(\frac{2}{m_k}\boldsymbol{\nabla}_k-\frac{1}{m_j}\boldsymbol{\nabla}_j\right)\right]_z\right\}. \end{aligned} \tag{5.10}$$

The evaluation of spin part is trivial since $\boldsymbol{s}_{j,z}$ just returns a spin projection of particle $j$ when applied to a primitive spin function.

*Spin–spin non-contact interaction*

The electron part of spin–spin non-contact (SSNC) interaction can be factorized into a scalar product of rank-two tensors:

$$\mathcal{H}_{\rm SSNC} = \sum_{\substack{i,j=1,\\ i>j}}^{n}\frac{q_i q_j}{m_i m_j}\left\{\left(\left[\boldsymbol{s}_i^{(1)}\times\boldsymbol{s}_j^{(1)}\right]^{(2)}\cdot\left[\boldsymbol{\nabla}_i^{(1)}\times\boldsymbol{\nabla}_j^{(1)}\right]^{(2)}\right)\frac{1}{r_{ij}}\right\}, \tag{5.11}$$

which leads to the following expressions for $T^{(2)}_{ij,0}$ and $U^{(2)}_{ij,0}$ [44]:

$$T^{(2)}_{ij,0} = \frac{1}{\sqrt{6}}(3s_{i,z}s_{j,z} - \boldsymbol{s}_i'\boldsymbol{s}_j), \tag{5.12}$$

$$U^{(2)}_{ij,0} = \frac{q_i q_j}{m_i m_j}\frac{1}{\sqrt{6}}\left[\left(3\left(\boldsymbol{\nabla}_i\right)_z\left(\boldsymbol{\nabla}_j\right)_z - \boldsymbol{\nabla}_i'\boldsymbol{\nabla}_j\right)\frac{1}{r_{ij}}\right], \tag{5.13}$$

where the gradients act only on $1/r_{ij}$.

For the spin part, we may use the Dirac identity for the scalar product of spins $\boldsymbol{s}_i'\boldsymbol{s}_j$:

$$\boldsymbol{s}_i'\boldsymbol{s}_j = -\frac{1}{4}+\frac{1}{2}\mathcal{P}^{\sigma}_{ij}, \tag{5.14}$$

to obtain:

$$T^{(2)}_{ij,0} = \frac{1}{\sqrt{6}} \left( 3 s_{i,z} s_{j,z} - \frac{1}{2} \mathcal{P}^{\sigma}_{ij} + \frac{1}{4} \right), \tag{5.15}$$

and we can evaluate the corresponding matrix element straightforwardly.

In what follows, we will focus on the spatial parts of spin–spin and spin–orbit operators.

## 5.2 Matrix elements for the systems with one $p$-electron

We will now briefly review the general formalism of evaluating spatial matrix elements in the ECG basis set corresponding to a single electron in a $p$-state. A detailed description can be found in Ref. [50].

### 5.2.1 Basis functions

We choose the origin of internal coordinates to coincide with the position of a nucleus and express the Gaussian basis function $|l\rangle$ of an $n$-(pseudo)particle system as:

$$|l\rangle = \boldsymbol{v}_l' \boldsymbol{r} \exp(-\boldsymbol{r}' \boldsymbol{C}_l \boldsymbol{r}). \tag{5.16}$$

Here, the $3n$-dimensional vector $\boldsymbol{r}$ represents the positions of all particles:

$$\boldsymbol{r} = (\boldsymbol{r}_1, \boldsymbol{r}_2, \ldots, \boldsymbol{r}_n)', \tag{5.17}$$

$3n$-dimensional vector $\boldsymbol{v}_l$ specifies which particle carries angular momentum $l = 1$ and can be written as the Kronecker product of two vectors:

$$\boldsymbol{v}_l = v_l \otimes \boldsymbol{\epsilon}_+, \tag{5.18}$$

where the $n$-dimensional vector $v_l$ has a single non-zero component corresponding to particle $n_l$ in a $p$-state: $v_q = \delta_{qn_l}$, and a $3D$-vector $\boldsymbol{\epsilon}_+ = \frac{1}{\sqrt{2}}(1, i, 0)$ specifies the angular momentum projection with magnetic quantum number $m_l = 1$.

A symmetric positive-definite matrix $\boldsymbol{C}_l$ is a $3n \times 3n$ matrix of non-linear variational parameters to be optimized. The rotational invariance of the non-relativistic Hamiltonian allows one to factorize $\boldsymbol{C}_l$ as follows:

$$\boldsymbol{C}_l = C_l \otimes \boldsymbol{I}_3, \tag{5.19}$$

where $\boldsymbol{I}_3$ is a $3D$ identity matrix.

The matrix $\boldsymbol{C}_l$ contains $n(n+1)/2$ non-linear variational parameters. In principle, these parameters may be complex, and we consider this general case in the following derivations. However, in the ECG code being developed in our group, we use real Gaussians for atoms in a $P$-state.

Note that during the minimization procedure, not only the non-linear parameters of

matrix $C_l$ are optimized, but also the integer $n_l$ defining the particle carrying angular momentum $l = 1$. Thus, in total for $\mathcal{N}$ basis functions, we have $\mathcal{N}\frac{n(n+1)}{2}$ real parameters and $\mathcal{N}$ integer parameters to be optimized.

Next, to analytically evaluate matrix elements, it is convenient to introduce generating functions $\varphi_l$ with an auxiliary real variable $\alpha_l$:

$$\varphi_l = \exp\left[\alpha_l \boldsymbol{v}_l' \boldsymbol{r} - \boldsymbol{r}' \boldsymbol{C}_l \boldsymbol{r}\right] \tag{5.20}$$

such that

$$|l\rangle = \partial_{\alpha_l} \varphi_l|_{\alpha_l=0}. \tag{5.21}$$

Therefore, the matrix element of operator $\mathcal{O}$ taken between two basis functions can be expressed through the matrix element with the generating functions as follows:

$$\langle k|\mathcal{O}|l\rangle = \partial_{\alpha_k}\partial_{\alpha_l} \langle \varphi_k|\mathcal{O}|\varphi_l\rangle . \tag{5.22}$$

We also need to know how to act on a basis function $|l\rangle$ with the permutation operator $\mathcal{P}$ with the corresponding matrix $\boldsymbol{P}$ (see Eq. (3.33)). Substituting $\boldsymbol{r} \to \boldsymbol{P}\boldsymbol{r}$ into (5.16), we obtain:

$$\mathcal{P}\,|l\rangle = \boldsymbol{v}_l' \boldsymbol{P}\boldsymbol{r} \exp(-\boldsymbol{r}'\boldsymbol{P}'\boldsymbol{C}_l\boldsymbol{P}\boldsymbol{r}) \equiv \tilde{\boldsymbol{v}}_l' \boldsymbol{r} \exp\left(-\boldsymbol{r}'\tilde{\boldsymbol{C}}_l\boldsymbol{r}\right) \equiv \left|\tilde{l}\right\rangle , \tag{5.23}$$

where

$$\tilde{\boldsymbol{v}}_l = \boldsymbol{P}'\boldsymbol{v}_l, \tag{5.24}$$

$$\tilde{\boldsymbol{C}}_l = \boldsymbol{P}'\boldsymbol{C}_l\boldsymbol{P}. \tag{5.25}$$

Thus, the action of the permutation operator $\mathcal{P}$ on a wave function $|l\rangle$ or $\varphi_l$ reduces to a transformation of the matrix $\boldsymbol{C}_l$ and vector $\boldsymbol{v}_l$. In the following, to avoid introducing excessive notation, we will omit tilde symbols and implicitly assume that the matrix $\boldsymbol{C}_l$ and vector $\boldsymbol{v}_l$ have been transformed by the permutation operator.

### 5.2.2 Overlap matrix element

The overlap matrix element between two basis functions $|k\rangle$ and $|l\rangle$ reads:

$$S_{kl} = \langle k|l\rangle = \partial_{\alpha_k}\partial_{\alpha_l} \langle \varphi_k|\varphi_l\rangle \,|_{\boldsymbol{\alpha}=0} = \partial_{\alpha_k}\partial_{\alpha_l} \int d\boldsymbol{r} \exp\left[\alpha_k \boldsymbol{v}_k^\dagger \boldsymbol{r} + \alpha_l \boldsymbol{v}_l' \boldsymbol{r} - \boldsymbol{r}'(\boldsymbol{C}_k^* + \boldsymbol{C}_l)\boldsymbol{r}\right]\Big|_{\boldsymbol{\alpha}=0} \tag{5.26}$$

Here for brevity we introduced notation $\boldsymbol{\alpha} = (\alpha_k, \alpha_l)$.

To find the overlap matrix element, we introduce matrix $\boldsymbol{C}_{kl} = \boldsymbol{C}_k^* + \boldsymbol{C}_l$ and use the

value of $n$-dimensional Gaussian integral:

$$\int dx \exp\left[-x'Ax + y'x\right] = \frac{\pi^{n/2}}{|A|^{1/2}} \exp\left[\frac{1}{4} y' A^{-1} y\right], \tag{5.27}$$

where $A$ is $n \times n$ positive definite symmetric matrix, and $x, y$ are $n$-dimensional vectors.

Thus, for the overlap matrix element, we have:

$$S_{kl} = \partial_{\alpha_k}\partial_{\alpha_l} \frac{\pi^{3n/2}}{|C_{kl}|^{3/2}} \exp\left[\frac{1}{4}(\alpha_k \boldsymbol{v}_k^* + \alpha_l \boldsymbol{v}_l)' \boldsymbol{C}_{kl}^{-1} (\alpha_k \boldsymbol{v}_k^* + \alpha_l \boldsymbol{v}_l)\right]\Big|_{\boldsymbol{\alpha}=0} = \\ = \frac{\pi^{3n/2}}{2|C_{kl}|^{3/2}} [\boldsymbol{v}_k^\dagger \boldsymbol{C}_{kl}^{-1} \boldsymbol{v}_l]. \tag{5.28}$$

Note that we used $|\boldsymbol{C}_{kl}|^{1/2} = |C_{kl}|^{3/2}$ due to factorizability of matrix $\boldsymbol{C}_{kl}$ (see Eq. (5.19)).

### 5.2.3 Matrix element of spin–orbit operator

The matrix element of the spin–orbit operator for atoms and atom–positron complexes with one particle in a $p$-state was previously derived and implemented in the ECG code by our former group member D. Tumakov. For the sake of completeness and to provide a clear description of the methodology, I provide this derivation below.

First, we introduce the quantity $f$:

$$f \equiv f[ij, ij] \equiv \left\langle k \left| \frac{1}{r_{ji}^3} \boldsymbol{\epsilon}_z \cdot [\boldsymbol{r}_{ij} \times \boldsymbol{\nabla}_j] \right| l \right\rangle = -\left\langle k \left| \boldsymbol{\epsilon}_z \cdot \left[\boldsymbol{\nabla}_i \left(\frac{1}{r_{ij}}\right) \times \boldsymbol{\nabla}_j\right] \right| l \right\rangle, \tag{5.29}$$

where $\boldsymbol{\epsilon}_z$ is a unit vector in $z$-direction and

$$\boldsymbol{r}_{ij} \equiv \boldsymbol{r}_j - \boldsymbol{r}_i, \tag{5.30}$$

$$\boldsymbol{r}_{ii} \equiv \boldsymbol{r}_i. \tag{5.31}$$

The expectation value of the spatial tensor $U_{i,z}$ is then written as:

$$\langle \gamma LL | U_{i,z} | \gamma LL \rangle_r = -i\Big\{ -\frac{q_0 q_i}{2m_i}\left(\frac{1}{m_i} + \frac{2}{m_0}\right) f[ii, ii] - \frac{q_0 q_i}{m_0 m_i} \sum_{\substack{j=1 \\ j\neq i}}^{n} f[ii, ij] - \\ - \frac{q_i}{m_i} \sum_{\substack{j=1 \\ j\neq i}}^{n} \frac{q_j}{m_j} f[ji, jj] - \frac{q_i}{2m_i^2} \sum_{\substack{j=1 \\ j\neq i}}^{n} q_j f[ij, ii]\Big\}. \tag{5.32}$$

Rearranging the operators and integrating by parts in the matrix element (5.29) (so that all differential operators act on a bra-, or ket-vector), we obtain for the quantity $f$

the following expression:

$$f = \boldsymbol{\epsilon}_z \cdot \left\langle k \left| \frac{1}{r_{ij}} \right| [\boldsymbol{\nabla}_i \times \boldsymbol{\nabla}_j]\, l \right\rangle + \boldsymbol{\epsilon}_z \cdot \left\langle \boldsymbol{\nabla}_i k \left| \frac{1}{r_{ij}} \times \right| \boldsymbol{\nabla}_j l \right\rangle = \\ = \left\langle k \left| \frac{1}{r_{ij}} \boldsymbol{\nabla}' \boldsymbol{F}_{ij} \boldsymbol{\nabla} \right| l \right\rangle + \left\langle \boldsymbol{\nabla}' k \left| \frac{1}{r_{ij}} \boldsymbol{G}_{ij} \right| \boldsymbol{\nabla} l \right\rangle, \quad (5.33)$$

where matrices $\boldsymbol{F}_{ij}$ and $\boldsymbol{G}_{ij}$ are defined as:

$$\boldsymbol{F}_{ij} \equiv (E_{ij} - E_{ji}) \otimes \boldsymbol{\epsilon}_x \boldsymbol{\epsilon}'_y, \quad (5.34)$$

$$\boldsymbol{G}_{ij} \equiv E_{ij} \otimes (\boldsymbol{\epsilon}_x \boldsymbol{\epsilon}'_y - \boldsymbol{\epsilon}_y \boldsymbol{\epsilon}'_x), \quad (5.35)$$

$$\boldsymbol{\nabla} \equiv \sum_{m=1}^{n} j^m \otimes \boldsymbol{\nabla}_m. \quad (5.36)$$

Here $\boldsymbol{\epsilon}_\alpha$ are unit vectors in $\alpha$-direction ($\alpha = x, y, z$), $n \times n$ matrix $E_{ij}$ and $n$-dimensional vector $j^i$ are defined component-wise as:

$$(E_{ij})_{mk} = \delta_{im}\delta_{jk}, \quad (5.37)$$

$$(j^i)_m = \delta_{im}. \quad (5.38)$$

Notice how we represent matrices and vectors as the Kronecker product of parts corresponding to $n$-dimensional pseudoparticle space, and $3D$ Cartesian space. This separation allows us to treat these spaces independently, simplifying and generalizing the analysis.

We further rewrite (5.33) using the generating functions:

$$f = \frac{\partial^2}{\partial \alpha_k \partial \alpha_l} \left[ \left\langle \varphi_k \left| \frac{1}{r_{ij}} \boldsymbol{\nabla}' \boldsymbol{F}_{ij} \boldsymbol{\nabla} \right| \varphi_l \right\rangle + \left\langle \boldsymbol{\nabla}' \varphi_k \left| \frac{1}{r_{ij}} \boldsymbol{G}_{ij} \right| \boldsymbol{\nabla} \varphi_l \right\rangle \right]_{\boldsymbol{\alpha}=0} \quad (5.39)$$

and act on generating functions with differential operators:

$$\boldsymbol{\nabla}' \boldsymbol{F}_{ij} \boldsymbol{\nabla} \varphi_l = \left[ -2\mathrm{tr}[\boldsymbol{C}_l \boldsymbol{F}_{ij}] + 4\boldsymbol{r}' \boldsymbol{C}_l \boldsymbol{F}_{ij} \boldsymbol{C}_l \boldsymbol{r} - 2\alpha_l \boldsymbol{v}'_l \left( \boldsymbol{F}_{ij} + \boldsymbol{F}'_{ij} \right) \boldsymbol{C}_l \boldsymbol{r} + O(\alpha_l^2) \right] \varphi_l, \quad (5.40)$$

$$\boldsymbol{\nabla}' \varphi^*_k \boldsymbol{G}_{ij} \boldsymbol{\nabla} \varphi_l = \left[ 4\boldsymbol{r}' \boldsymbol{C}^*_k \boldsymbol{G}_{ij} \boldsymbol{C}_l \boldsymbol{r} - 2\alpha_l \boldsymbol{r}' \boldsymbol{C}^*_k \boldsymbol{G}_{ij} \boldsymbol{v}_l - 2\alpha_k \boldsymbol{v}^\dagger_k \boldsymbol{G}_{ij} \boldsymbol{C}_l + \alpha_k \alpha_l \boldsymbol{v}^\dagger_k \boldsymbol{G}_{ij} \boldsymbol{v}_l \right] \varphi^*_k \varphi_l. \quad (5.41)$$

Note that in (5.40) the first term $\mathrm{tr}[\boldsymbol{C}_l \boldsymbol{F}_{ij}]$ is zero, and the last term $\propto \alpha_l^2$ will vanish after taking derivative w.r.t. $\alpha_l$ and setting $\alpha_l = 0$. Thus, the matrix elements in (5.39) become:

$$\left\langle k \left| \frac{1}{r_{ij}} \boldsymbol{\nabla}' \boldsymbol{F}_{ij} \boldsymbol{\nabla} \right| l \right\rangle = 4 \left\langle k \left| \frac{1}{r_{ij}} \boldsymbol{r}' (\boldsymbol{C}_l \boldsymbol{F}_{ij} \boldsymbol{C}_l) \boldsymbol{r} \right| l \right\rangle - 2 \left\langle k \left| \frac{1}{r_{ij}} \right| l \right\rangle_{\boldsymbol{v}_l \to \boldsymbol{C}_l \left( \boldsymbol{F}_{ij} + \boldsymbol{F}'_{ij} \right) \boldsymbol{v}_l}, \quad (5.42)$$

$$\left\langle \boldsymbol{\nabla}' k \left| \frac{1}{r_{ij}} \boldsymbol{G}_{ij} \right| \boldsymbol{\nabla} l \right\rangle = 4 \left\langle k \left| \frac{1}{r_{ij}} \boldsymbol{r}' (\boldsymbol{C}_k^* \boldsymbol{G}_{ij} \boldsymbol{C}_l) \boldsymbol{r} \right| l \right\rangle - 2 \left\langle k \left| \frac{1}{r_{ij}} \right| l \right\rangle_{\boldsymbol{v}_l \to \boldsymbol{C}_k^* \boldsymbol{G}_{ij} \boldsymbol{v}_l} - 2 \left\langle k \left| \frac{1}{r_{ij}} \right| l \right\rangle_{\boldsymbol{v}_k \to \boldsymbol{C}_l^* \boldsymbol{G}_{ij}^\dagger \boldsymbol{v}_k} + \boldsymbol{v}_k^\dagger \boldsymbol{G}_{ij} \boldsymbol{v}_l \left\langle \varphi_k \left| \frac{1}{r_{ij}} \right| \varphi_l \right\rangle_{\alpha_k, \alpha_l = 0} . \quad (5.43)$$

To proceed further, we need to introduce several auxiliary matrix elements that appear in the rhs of (5.42) and (5.43). We start with the matrix element of inverse interparticle distance taken between the generating functions $\varphi_k$ and $\varphi_l$:

$$\left\langle \varphi_k \left| \frac{1}{r_{ij}} \right| \varphi_l \right\rangle_{\alpha_k, \alpha_l = 0} . \quad (5.44)$$

For convenience, we express the square of interparticle distance $r_{ij}^2$ as a vector-matrix-vector product $r_{ij}^2 = \boldsymbol{r}' \boldsymbol{J}_{ij} \boldsymbol{r}$, where $J_{ij} = (j^i - j^j)(j^i - j^j)'$, $\boldsymbol{J}_{ij} = J_{ij} \otimes \boldsymbol{I}_3$, and by definition $r_{ii} \equiv r_i$, $J_{ii} \equiv E_{ii}$. Next, we rewrite the desired matrix element as an integral over an auxiliary parameter $\beta$ and use a reference Gaussian integral (5.27):

$$\left\langle \varphi_k \left| \frac{1}{r_{ij}} \right| \varphi_l \right\rangle_{\alpha_k, \alpha_l = 0} = \frac{2}{\sqrt{\pi}} \int_0^\infty d\beta \left\langle \varphi_k \left| e^{-\beta^2 \boldsymbol{r}' \boldsymbol{J}_{ij} \boldsymbol{r}} \right| \varphi_l \right\rangle_{\alpha_k, \alpha_l = 0} = \pi^{(3n-1)/2} \int_0^\infty d\beta \frac{1}{|C_{kl} + \beta^2 J_{ij}|^{3/2}} . \quad (5.45)$$

Since $J_{ij}$ is a rank-one matrix, we can factor out the $\beta$ dependence from the determinant:

$$\left| C_{kl} + \beta^2 J_{ij} \right|^{3/2} = |C_{kl}|^{3/2} \left| 1 + \beta^2 C_{kl}^{-1} J_{ij} \right|^{3/2} = |C_{kl}|^{3/2} \left( 1 + \beta^2 \mathrm{tr} \left[ C_{kl}^{-1} J_{ij} \right] \right)^{3/2} . \quad (5.46)$$

Then, the integration of (5.45) over $\beta$ yields:

$$\left\langle \varphi_k \left| \frac{1}{r_{ij}} \right| \varphi_l \right\rangle_{\alpha_k, \alpha_l = 0} = \frac{\pi^{(3n-1)/2}}{|C_{kl}|^{3/2}} \gamma_{ij}, \quad (5.47)$$

where $\gamma_{ij} = \mathrm{tr}[C_{kl}^{-1} J_{ij}]^{-1/2}$.

Now, we evaluate the same operator with the basis functions $|k\rangle$ and $|l\rangle$:

$$\left\langle k \left| \frac{1}{r_{ij}} \right| l \right\rangle . \quad (5.48)$$

We use the same trick as before by putting the operator $1/r_{ij}$ in the exponent at the cost of additional integration:

$$\left\langle k \left| \frac{1}{r_{ij}} \right| l \right\rangle = \frac{2}{\sqrt{\pi}} \int_0^\infty d\beta \left\langle k \left| e^{-\beta^2 \boldsymbol{r}' \boldsymbol{J}_{ij} \boldsymbol{r}} \right| l \right\rangle = \pi^{(3n-1)/2} \int_0^\infty d\beta \frac{\boldsymbol{v}_k^\dagger (\boldsymbol{C}_{kl} + \beta^2 \boldsymbol{J}_{ij})^{-1} \boldsymbol{v}_l}{|\boldsymbol{C}_{kl} + \beta^2 \boldsymbol{J}_{ij}|^{1/2}} . \quad (5.49)$$

We use the Sherman–Morrison formula to simplify the matrix inverse:

$$\left(C_{kl}+\beta^2 J_{ij}\right)^{-1}=C_{kl}^{-1}-\frac{\beta^2 C_{kl}^{-1}J_{ij}C_{kl}^{-1}}{1+\beta^2\mathrm{tr}\left[C_{kl}^{-1}J_{ij}\right]}. \tag{5.50}$$

Substituting this expression into the integral, we obtain::

$$\left\langle k\left|\frac{1}{r_{ij}}\right|l\right\rangle=\frac{\pi^{(3n-1)/2}}{|C_{kl}|^{3/2}}\int d\beta\frac{1}{1+\beta^2\mathrm{tr}[C_{kl}^{-1}J_{ij}]}\boldsymbol{v}_k^\dagger\left(\boldsymbol{C}_{kl}-\frac{\beta^2\boldsymbol{C}_{kl}^{-1}\boldsymbol{J}_{ij}\boldsymbol{C}_{kl}^{-1}}{1+\beta^2\mathrm{tr}[C_{kl}^{-1}J_{ij}]}\right)\boldsymbol{v}_l=$$
$$=\frac{\pi^{(3n-1)/2}}{|C_{kl}|^{3/2}}\left(\gamma_{ij}[\boldsymbol{v}_k^\dagger\boldsymbol{C}_{kl}^{-1}\boldsymbol{v}_l]-\frac{1}{3}\gamma_{ij}^3[\boldsymbol{v}_k^\dagger\boldsymbol{C}_{kl}^{-1}\boldsymbol{J}_{ij}\boldsymbol{C}_{kl}^{-1}\boldsymbol{v}_l]\right). \tag{5.51}$$

Finally, we consider the symmetric matrix $\boldsymbol{A}=A\otimes\boldsymbol{K}$ and $\mathrm{tr}\boldsymbol{A}=0$ (note that matrices $\boldsymbol{F}_{ij}$ and $\boldsymbol{G}_{ij}$ have this form), and evaluate the following matrix element:

$$\left\langle k\left|\frac{1}{r_{ij}}\boldsymbol{r}'\boldsymbol{A}\boldsymbol{r}\right|l\right\rangle. \tag{5.52}$$

Here we may raise the quadratic form $\boldsymbol{r}'\boldsymbol{A}\boldsymbol{r}$ to the exponent at the cost of derivative w.r.t. real variable $\gamma$, and then use the matrix element of inverse interparticle distance found above, with the substitution $\boldsymbol{C}_l\to\boldsymbol{C}_l+\gamma\boldsymbol{A}$:

$$\left\langle k\left|\frac{1}{r_{ij}}\boldsymbol{r}'\boldsymbol{A}\boldsymbol{r}\right|l\right\rangle=-\frac{\partial}{\partial\gamma}\left[\left\langle k\left|\frac{1}{r_{ij}}\right|l\right\rangle_{\boldsymbol{C}_l\to\boldsymbol{C}_l+\gamma\boldsymbol{A}}\right]_{\gamma=0}=$$
$$=\pi^{(3n-1)/2}\int_0^\infty\frac{\boldsymbol{v}_k^\dagger(\boldsymbol{C_{kl}}+\beta^2\boldsymbol{J}_{ij})^{-1}\boldsymbol{A}(\boldsymbol{C_{kl}}+\beta^2\boldsymbol{J}_{ij})^{-1}\boldsymbol{v}_l}{|\boldsymbol{C_{kl}}+\beta^2\boldsymbol{J}_{ij}|^{1/2}}d\beta=$$
$$=\pi^{(3n-1)/2}\int_0^\infty\frac{v_k^\dagger(C_{kl}+\beta^2J_{ij})^{-1}A(C_{kl}+\beta^2J_{ij})^{-1}v_l}{|C_{kl}+\beta^2J_{ij}|^{3/2}}d\beta\cdot\boldsymbol{\epsilon}_+^\dagger\boldsymbol{K}\boldsymbol{\epsilon}_+, \tag{5.53}$$

where we used the formula for the differential of an inverse matrix:

$$dA^{-1}=-A^{-1}dAA^{-1}, \tag{5.54}$$

and the Jacobi's formula for the differential of a determinant:

$$d|A|=|A|\mathrm{tr}[A^{-1}dA]. \tag{5.55}$$

Note that if the condition $\mathrm{tr}[\boldsymbol{A}]=0$ was not satisfied, we would have an additional term $\propto\mathrm{tr}[\boldsymbol{C}_{kl}^{-1}\boldsymbol{A}]$ in (5.53). Finally, we separate out $\beta$ in the determinant and inverse matrix,

and write an answer:

$$\left\langle k\left|\frac{1}{r_{ij}}\boldsymbol{r}'\boldsymbol{A}\boldsymbol{r}\right|l\right\rangle = \frac{\pi^{(3n-1)/2}}{|C_{kl}|^{3/2}}\Big(\gamma_{ij}\mathrm{tr}\left[C_{kl}^{-1}AC_{kl}^{-1}v_l v_k'\right] - \frac{1}{3}\gamma_{ij}^3\mathrm{tr}\left[C_{kl}^{-1}AC_{kl}^{-1}J_{ij}C_{kl}^{-1}v_l v_k'\right] - \frac{1}{3}\gamma_{ij}^3\mathrm{tr}\left[C_{kl}^{-1}J_{ij}C_{kl}^{-1}AC_{kl}^{-1}v_l v_k'\right] + \frac{1}{5}\gamma_{ij}^5\mathrm{tr}\left[C_{kl}^{-1}J_{ij}C_{kl}^{-1}AC_{kl}^{-1}J_{ij}C_{kl}^{-1}v_l v_k'\right]\Big)[\boldsymbol{\epsilon}_+^\dagger\boldsymbol{K}\boldsymbol{\epsilon}_+]. \quad (5.56)$$

Now, we have everything to evaluate the matrix elements in the rhs of (5.42) and (5.43). For illustration, we demonstrate one example of using auxiliary matrix element (5.52) to evaluate the following matrix element:

$$\left\langle k\left|\frac{1}{r_{ij}}\boldsymbol{r}'(\boldsymbol{C}_l\boldsymbol{F}_{ij}\boldsymbol{C}_l)\boldsymbol{r}\right|l\right\rangle \quad (5.57)$$

For this case, we set

$$\boldsymbol{A} = \mathrm{Symm}[\boldsymbol{C}_l\boldsymbol{F}_{ij}\boldsymbol{C}_l] = \frac{1}{2}C_l(E_{ij}-E_{ji})C_l\otimes\boldsymbol{K}, \quad (5.58)$$

where $3\times 3$ matrix $\boldsymbol{K}$ is defined as $\boldsymbol{K} = (\boldsymbol{\epsilon}_x\boldsymbol{\epsilon}_y' - \boldsymbol{\epsilon}_y\boldsymbol{\epsilon}_x')$. Note that $\mathrm{tr}[\boldsymbol{K}] = 0$ so that $\mathrm{tr}[\boldsymbol{A}] = 0$ and we may use formula (5.56) with $\boldsymbol{\epsilon}_+^\dagger\boldsymbol{K}\boldsymbol{\epsilon}_+ = i$.

Analogously, using matrix elements (5.44), (5.48) and (5.52), we obtain all parts of the spin–orbit matrix element. For example, in the matrix element $\left\langle k\left|\frac{1}{r_{ij}}\right|l\right\rangle_{\boldsymbol{v}_l\to\boldsymbol{C}_l\left(\boldsymbol{F}_{ij}+\boldsymbol{F}_{ij}'\right)\boldsymbol{v}_l}$, we use formula (5.51) with $\boldsymbol{v}_l$ substituted by $\boldsymbol{C}_l\left(\boldsymbol{F}_{ij}+\boldsymbol{F}_{ij}'\right)\boldsymbol{v}_l$. After some simplifications, we get for the four possible combinations $f[ii,ii]$, $f[ii,ij]$, $f[ij,jj]$, $f[ij,ii]$ that appear in the SO operator (5.32) the following compact expressions written in terms of vector-matrix-vector products:

$$f[ii,ii] = \frac{2i}{3}\frac{\pi^{(3n-1)/2}}{|C_{kl}|^{3/2}}\gamma_{ii}^3(j^{i\prime}v_l\cdot j^{i\prime}C_{kl}^{-1}v_k + j^{i\prime}C_lC_{kl}^{-1}v_k\cdot j^{i\prime}C_{kl}^{-1}v_l - j^{i\prime}C_{kl}^{-1}v_k\cdot j^{i\prime}C_lC_{kl}^{-1}v_l), \quad (5.59)$$

$$f[ii,ij] = \frac{2i}{3}\frac{\pi^{(3n-1)/2}}{|C_{kl}|^{3/2}}\gamma_{ii}^3\left(j^{j\prime}v_l\cdot j^{i\prime}C_{kl}^{-1}v_k + j^{j\prime}C_lC_{kl}^{-1}v_k\cdot j^{i\prime}C_{kl}^{-1}v_l - j^{i\prime}C_{kl}^{-1}v_k\cdot j^{j\prime}C_lC_{kl}^{-1}v_l\right), \quad (5.60)$$

$$f[ij,ii] = \frac{2i}{3}\frac{\pi^{(3n-1)/2}}{|C_{kl}|^{3/2}}\gamma_{ij}^3(j^{i\prime}v_l\cdot(j^{i\prime}C_{kl}^{-1}v_k - j^{j\prime}C_{kl}^{-1}v_k) + j^{i\prime}C_lC_{kl}^{-1}v_k\cdot(j^{i\prime}C_{kl}^{-1}v_l - j^{j\prime}C_{kl}^{-1}v_l) + j^{i\prime}C_lC_{kl}^{-1}v_l\cdot(j^{j\prime}C_{kl}^{-1}v_k - j^{i\prime}C_{kl}^{-1}v_k)), \quad (5.61)$$

$$f[ij,jj] = \frac{2i}{3}\frac{\pi^{(3n-1)/2}}{|C_{kl}|^{3/2}}\gamma_{ij}^3(j^{j\prime}v_l\cdot(j^{i\prime}C_{kl}^{-1}v_k - j^{i\prime}C_{kl}^{-1}v_k) + j^{j\prime}C_lC_{kl}^{-1}v_k\cdot(j^{j\prime}C_{kl}^{-1}v_l - j^{i\prime}C_{kl}^{-1}v_l) + j^{j\prime}C_lC_{kl}^{-1}v_l\cdot(j^{i\prime}C_{kl}^{-1}v_k - j^{j\prime}C_{kl}^{-1}v_k)). \quad (5.62)$$

### 5.2.4 Matrix element of non-contact spin–spin operator

Similarly to the case of spin–orbit operator, we begin by introducing the base matrix element $g_{ij}$:

$$g_{ij} = \left\langle k \middle| \left( \left[ \boldsymbol{\nabla}_i^{(1)} \times \boldsymbol{\nabla}_j^{(1)} \right]_0^{(2)} \frac{1}{r_{ij}} \right) \middle| l \right\rangle = \left\langle k \middle| \left( \frac{1}{\sqrt{6}} \left( 3 \left( \boldsymbol{\nabla}_i \right)_z \left( \boldsymbol{\nabla}_j \right)_z - \boldsymbol{\nabla}_i' \boldsymbol{\nabla}_j \right) \frac{1}{r_{ij}} \right) \middle| l \right\rangle, \tag{5.63}$$

where the gradients act only on $1/r_{ij}$. Then, the spatial part $U_{ij,0}^{(2)}$ of the spin–spin non-contact operator is rewritten as (see Eqs. (5.11) and (5.13)):

$$U_{ij,0}^{(2)} = \frac{q_i q_j}{m_i m_j} g_{ij}. \tag{5.64}$$

Rearranging the gradients and integrating by parts so that all derivatives act on either the bra or ket wave functions, we obtain for $g_{ij}$:

$$g_{ij} = \left\langle k \middle| \left( \left[ \boldsymbol{\nabla}_i^{(1)} \times \boldsymbol{\nabla}_j^{(1)} \right]_0^{(2)} \frac{1}{r_{ij}} \right) \middle| l \right\rangle = -\frac{1}{\sqrt{6}} \left( \left\langle \boldsymbol{\nabla}' \boldsymbol{D_{ij}} \boldsymbol{\nabla} k \middle| \frac{1}{r_{ij}} \middle| l \right\rangle + \left\langle k \middle| \frac{1}{r_{ij}} \middle| \boldsymbol{\nabla}' \boldsymbol{D_{ij}} \boldsymbol{\nabla} l \right\rangle + \right.$$
$$\left. + 2 \left\langle \boldsymbol{\nabla}' k \middle| \frac{1}{r_{ij}} \boldsymbol{D_{ij}} \middle| \boldsymbol{\nabla} l \right\rangle \right) = -\frac{1}{\sqrt{6}} \left( g_{ij}^{(2,0)} + g_{ij}^{(0,2)} + 2 g_{ij}^{(1,1)} \right), \tag{5.65}$$

where matrix $\boldsymbol{D_{ij}} = D_{ij} \otimes \boldsymbol{\Upsilon} = \frac{1}{2}(E_{ij} + E_{ji}) \otimes \boldsymbol{\Upsilon}$ and $\boldsymbol{\Upsilon}$ is a $3 \times 3$ diagonal matrix that selects particular Cartesian coordinates of the gradients: $\boldsymbol{\Upsilon} = \mathrm{diag}\{1, 1, -2\}$. Note that both $D_{ij}$ and $\boldsymbol{\Upsilon}$ are symmetric and traceless matrices, and $\boldsymbol{\varepsilon}_+^\dagger \boldsymbol{\Upsilon} \boldsymbol{\varepsilon}_+ = 1$. The notation $g_{ij}^{(p,q)}$ refers to individual terms in Eq. (5.65), where the first superscript $p$ indicates the number of gradients acting on the bra-vector, and the second one $q$ indicates those acting on the ket-vector. Later, for brevity, we will not write subscripts $i, j$ in $g_{ij}^{(p,q)}$, implicitly assuming them.

First, we find how the operators in (5.65) act on the generating wave functions:

$$\left( \boldsymbol{\nabla}' \varphi_k^* \right) \boldsymbol{D_{ij}} \boldsymbol{\nabla} \varphi_l = \Big( 4 \boldsymbol{r}' (\boldsymbol{C}_k^* \boldsymbol{D}_{ij} \boldsymbol{C}_l) \boldsymbol{r} - 2\alpha_l \boldsymbol{r}' (\boldsymbol{C}_k^* \boldsymbol{D}_{ij}) \boldsymbol{v}_l - 2\alpha_k \boldsymbol{v}_k^\dagger (\boldsymbol{D}_{ij} \boldsymbol{C}_l) \boldsymbol{r} +$$
$$+ \alpha_k \alpha_l \boldsymbol{v}_k^\dagger \boldsymbol{D}_{ij} \boldsymbol{v}_l \Big) \varphi_k^* \varphi_l. \tag{5.66}$$

$$\boldsymbol{\nabla}' \boldsymbol{D_{ij}} \boldsymbol{\nabla} \varphi_l = \left( 4 \boldsymbol{r}' (\boldsymbol{C}_l \boldsymbol{D}_{ij} \boldsymbol{C}_l) \boldsymbol{r} - 4\alpha_l \boldsymbol{v}_l' (\boldsymbol{D}_{ij} \boldsymbol{C}_l) \boldsymbol{r} + O(\alpha_l^2) \right) \varphi_l, \tag{5.67}$$

$$\boldsymbol{\nabla}' \boldsymbol{D_{ij}} \boldsymbol{\nabla} \varphi_k^* = \left( 4 \boldsymbol{r}' (\boldsymbol{C}_k^* \boldsymbol{D}_{ij} \boldsymbol{C}_k^*) \boldsymbol{r} - 4\alpha_k \boldsymbol{v}_k^\dagger (\boldsymbol{D}_{ij} \boldsymbol{C}_k^*) \boldsymbol{r} + O(\alpha_k^2) \right) \varphi_k^*, \tag{5.68}$$

Thus, for $g^{(p,q)}$ we get:

$$g^{(0,2)} = \left\langle k \middle| \frac{1}{r_{ij}} \middle| \boldsymbol{\nabla}' \boldsymbol{D_{ij}} \boldsymbol{\nabla} l \right\rangle = 4 \left\langle k \middle| \frac{1}{r_{ij}} \boldsymbol{r}' (\boldsymbol{C}_l \boldsymbol{D}_{ij} \boldsymbol{C}_l) \boldsymbol{r} \middle| l \right\rangle - 4 \left\langle k \middle| \frac{1}{r_{ij}} \middle| l \right\rangle_{\boldsymbol{v}_l \to \boldsymbol{C}_l \boldsymbol{D}_{ij} \boldsymbol{v}_l}, \tag{5.69}$$

$$g^{(2,0)} = \left\langle \boldsymbol{\nabla}' \boldsymbol{D_{ij}} \boldsymbol{\nabla} k \left| \frac{1}{r_{ij}} \right| l \right\rangle = 4 \left\langle k \left| \frac{1}{r_{ij}} \boldsymbol{r}' (\boldsymbol{C}_k^* \boldsymbol{D}_{ij} \boldsymbol{C}_k^*) \boldsymbol{r} \right| l \right\rangle - 4 \left\langle k \left| \frac{1}{r_{ij}} \right| l \right\rangle_{\boldsymbol{v}_k \to \boldsymbol{C}_k \boldsymbol{D}_{ij} \boldsymbol{v}_k}, \tag{5.70}$$

$$g^{(1,1)} = \left\langle \boldsymbol{\nabla}' k \left| \frac{1}{r_{ij}} \boldsymbol{D_{ij}} \right| \boldsymbol{\nabla} l \right\rangle = 4 \left\langle k \left| \frac{1}{r_{ij}} \boldsymbol{r}' (\boldsymbol{C}_k^* \boldsymbol{D}_{ij} \boldsymbol{C}_l) \boldsymbol{r} \right| l \right\rangle - 2 \left\langle k \left| \frac{1}{r_{ij}} \right| l \right\rangle_{\boldsymbol{v}_k \to \boldsymbol{C}_l^* \boldsymbol{D}_{ij} \boldsymbol{v}_k} -$$
$$- 2 \left\langle k \left| \frac{1}{r_{ij}} \right| l \right\rangle_{\boldsymbol{v}_l \to \boldsymbol{C}_k^* \boldsymbol{D}_{ij} \boldsymbol{v}_l} + \boldsymbol{v}_k^\dagger \boldsymbol{D}_{ij} \boldsymbol{v}_l \left\langle \varphi_k \left| \frac{1}{r_{ij}} \right| \varphi_l \right\rangle_{\alpha_k = \alpha_l = 0}. \tag{5.71}$$

All of the above matrix elements have the form of auxiliary integrals calculated previously (Eqs. (5.44), (5.48) and (5.52)) and can be readily evaluated. Skipping the intermediate stage involving the evaluation of each $g^{(p,q)}$, we write the final answer for $g$:

$$g = (2g^{(1,1)} + g^{(2,0)} + g^{(0,2)}) = \frac{4\pi^{(3n-1)/2}}{5\sqrt{6}} \frac{1}{|C_{kl}|^{3/2}} \gamma_{ij}^5 (j^{i\prime} C_{kl}^{-1} v_k \cdot j^{i\prime} C_{kl}^{-1} v_l + j^{j\prime} C_{kl}^{-1} v_k \cdot j^{j\prime} C_{kl}^{-1} v_l -$$
$$- j^{j\prime} C_{kl}^{-1} v_k \cdot j^{i\prime} C_{kl}^{-1} \tilde{v}_l - j^{i\prime} C_{kl}^{-1} v_k \cdot j^{j\prime} C_{kl}^{-1} v_l). \tag{5.72}$$

This is truly remarkable that the sum of matrix elements $g^{(p,q)}$ in $g$ reduced to such a compact and elegant expression (5.72).

## 5.3 Matrix elements for the systems with two $p$-electrons

### 5.3.1 Basis functions

Atoms with configurations that contain two electrons occupying $p$-orbitals can have total orbital angular momentum $L = 0, 1, 2$ (corresponding to $S$-, $P$-, and $D$-states, respectively). The matrix elements of spin–orbit and spin–spin operators for $S$-states vanish due to rotational properties of the matrix element: both the initial and final states have angular momentum $L = 0$, while the spatial parts of spin–orbit and spin–spin operators transform as tensors with $L = 1$ and $L = 2$, respectively. Therefore, the matrix element vanishes due to the Wigner-Eckart theorem [49].

We choose the maximum projection $M_L = 1$ for the wave function of a $P$-state:

$$|l\rangle_{L=1} = \frac{1}{\sqrt{2}} \left( (x_{i_l} + i y_{i_l}) z_{j_l} - z_{i_l} (x_{j_l} + i y_{j_l}) \right) \exp(-\boldsymbol{r}' \boldsymbol{C}_l \boldsymbol{r}), \tag{5.73}$$

where integer indices $i_l, j_l$ refer to particles carrying angular momentum $l = 1$.

Similarly, the wave function of a $D$-state with the maximum projection is given by:

$$|l\rangle_{L=2} = \frac{1}{2} (x_{i_l} + i y_{i_l})(x_{j_l} + i y_{j_l}) \exp(-\boldsymbol{r}' \boldsymbol{C}_l \boldsymbol{r}). \tag{5.74}$$

It is convenient to represent the wave functions (5.73) and (5.74) as a linear combina-

tion of more general "elementary" functions:

$$|l\rangle = (\boldsymbol{v}_l'\boldsymbol{r})(\boldsymbol{w}_l'\boldsymbol{r})\exp(-\boldsymbol{r}'\boldsymbol{C}_l\boldsymbol{r}), \tag{5.75}$$

where, analogously to the case of a single $p$-electron (see Eq. (5.16)), vectors $\boldsymbol{v}_l$ and $\boldsymbol{w}_l$ specify which particles are in a $p$-state and determine the projection of orbital momentum:

$$\boldsymbol{v}_l = v_l \otimes \boldsymbol{\eta}_v^l, \tag{5.76}$$

$$\boldsymbol{w}_l = w_l \otimes \boldsymbol{\eta}_w^l. \tag{5.77}$$

If the particles $i_l$, $j_l$ are in a $p$-state, the components of vectors $v_l$ and $w_l$ are given by: $(v_l)_q = \delta_{i_l q}$, $(w_l)_q = \delta_{j_l q}$. The $3D$-vectors $\boldsymbol{\eta}_v^l$, $\boldsymbol{\eta}_w^l$ define the orbital momentum projection of a particle. For example, in case of a $D$-state, we have:

$$\boldsymbol{\eta}_w^l = \boldsymbol{\eta}_v^l = \boldsymbol{\epsilon}_+ = \frac{1}{\sqrt{2}}(1, i, 0). \tag{5.78}$$

Note, that the case $i_l = j_l$ corresponds to a particle $i_l$ being in a $d$-state. Therefore, the elementary basis functions in (5.75) can be used to describe not only atomic systems with dominant configurations involving two particles in $p$-states, but also those containing a single particle in a $d$-state.

The basis function $|l\rangle$ (5.75) can be expressed through the mixed second derivative of the generating function $\varphi_l(\boldsymbol{r})$ (cf. Eq. (5.21)):

$$\varphi_l(\boldsymbol{r}) = \exp(-\boldsymbol{r}'\boldsymbol{C}_l\boldsymbol{r} + \alpha_l\boldsymbol{v}_l'\boldsymbol{r} + \beta_l\boldsymbol{w}_l'\boldsymbol{r}), \tag{5.79}$$

$$|l\rangle = \partial_{\alpha_l}\partial_{\beta_l}\varphi_l(\boldsymbol{r})|_{\alpha_l=\beta_l=0}. \tag{5.80}$$

Since all parts of spin–orbit and non-contact spin–spin matrix elements can be expressed through the overlap matrix element $S_{kl}$ by making substitutions or applying extra operations, like differentiation or integration w.r.t. some auxiliary variables, here we also provide the expression for $S_{kl}$:

$$S_{kl} = \langle k|l\rangle = \frac{\partial}{\partial\beta_k}\frac{\partial}{\partial\beta_l}\frac{\partial}{\partial\alpha_k}\frac{\partial}{\partial\alpha_l}\langle\varphi_k|\varphi_l\rangle_0 = \frac{1}{4}\frac{\pi^{3n/2}}{|C_{kl}|^{3/2}}\Big([\boldsymbol{v}_k^\dagger\boldsymbol{C}_{kl}^{-1}\boldsymbol{v}_l][\boldsymbol{w}_k^\dagger\boldsymbol{C}_{kl}^{-1}\boldsymbol{w}_l] + \\ + [\boldsymbol{v}_k^\dagger\boldsymbol{C}_{kl}^{-1}\boldsymbol{w}_k^*][\boldsymbol{v}_l'\boldsymbol{C}_{kl}^{-1}\boldsymbol{w}_l] + [\boldsymbol{v}_k^\dagger\boldsymbol{C}_{kl}^{-1}\boldsymbol{w}_l][\boldsymbol{w}_k^\dagger\boldsymbol{C}_{kl}^{-1}\boldsymbol{v}_l]\Big). \tag{5.81}$$

From now on, we will use subscript "0" in the matrix element to indicate that after all operators have been applied, the parameters $\alpha_l, \beta_l, \alpha_k, \beta_k$ should be set to zero.

A detailed formalism and evaluation of scalar matrix elements in the ECG basis set corresponding to two electrons in a $p$-state can be found in Ref. [39]. It should be noted that there are alternative ways to represent the basis wave function (5.75) — for example, one can use the vector-matrix-vector product $\boldsymbol{r}'\boldsymbol{W}\boldsymbol{r}$ as an angular prefactor instead of two

scalar products $(\boldsymbol{v}'\boldsymbol{r})(\boldsymbol{w}'\boldsymbol{r})$. The algorithm corresponding to this representation is introduced in Ref. [51]. However, this approach is much less efficient in terms of computational cost, as discussed in Ref. [39].

### 5.3.2 Matrix element of spin–orbit operator

The expression for the base quantity $f$ is given in Eq. (5.33).

We first find how the differential operators act on generating wave functions:

$$\boldsymbol{\nabla}'\boldsymbol{F}_{ij}\boldsymbol{\nabla}\varphi_l = \big(4\boldsymbol{r}'(\boldsymbol{C}_l\boldsymbol{F}_{ij}\boldsymbol{C}_l)\boldsymbol{r} - 2\alpha_l\boldsymbol{v}_l'(\boldsymbol{F}_{ij}+\boldsymbol{F}_{ij}')\boldsymbol{C}_l\boldsymbol{r} - 2\beta_l\boldsymbol{w}_l'(\boldsymbol{F}_{ij}+\boldsymbol{F}_{ij}')\boldsymbol{C}_l\boldsymbol{r} + \\ +\alpha_l\beta_l\boldsymbol{v}_l'(\boldsymbol{F}_{ij}+\boldsymbol{F}_{ij}')\boldsymbol{w}_l + O(\alpha_l^2) + O(\beta_l^2)\big)\,\varphi_l, \quad (5.82)$$

$$(\boldsymbol{\nabla}'\varphi_k^*)\boldsymbol{G}_{ij}(\boldsymbol{\nabla}\varphi_l) = \Big(4\boldsymbol{r}'(\boldsymbol{C}_k^*\boldsymbol{G}_{ij}\boldsymbol{C}_l)\boldsymbol{r} - 2\alpha_l\boldsymbol{r}'\boldsymbol{C}_k^*\boldsymbol{G}_{ij}\boldsymbol{v}_l - 2\alpha_k\boldsymbol{v}_k^\dagger\boldsymbol{G}_{ij}\boldsymbol{C}_l\boldsymbol{r} - 2\beta_l\boldsymbol{r}'\boldsymbol{C}_k^*\boldsymbol{G}_{ij}\boldsymbol{w}_l - \\ -2\beta_k\boldsymbol{w}_k^\dagger\boldsymbol{G}_{ij}\boldsymbol{C}_l\boldsymbol{r} + \alpha_k\alpha_l\boldsymbol{v}_k^\dagger\boldsymbol{G}_{ij}\boldsymbol{v}_l + \beta_k\beta_l\boldsymbol{w}_k^\dagger\boldsymbol{G}_{ij}\boldsymbol{w}_l + \alpha_k\beta_l\boldsymbol{v}_k^\dagger\boldsymbol{G}_{ij}\boldsymbol{w}_l + \beta_k\alpha_l\boldsymbol{w}_k^\dagger\boldsymbol{G}_{ij}\boldsymbol{v}_l\Big)\,\varphi_k^*\varphi_l. \quad (5.83)$$

The corresponding matrix elements are then written as follows:

$$\left\langle k\left|\frac{1}{r_{ij}}\boldsymbol{\nabla}'\boldsymbol{F}_{ij}\boldsymbol{\nabla}\right|l\right\rangle = 4\left\langle k\left|\frac{1}{r_{ij}}\boldsymbol{r}'(\boldsymbol{C}_l\boldsymbol{F}_{ij}\boldsymbol{C}_l)\boldsymbol{r}\right|l\right\rangle - 2\left\langle k\left|\frac{1}{r_{ij}}\right|l\right\rangle_{\boldsymbol{v}_l\to\boldsymbol{C}_l(\boldsymbol{F}_{ij}+\boldsymbol{F}_{ij}')\boldsymbol{v}_l} - \\ - 2\left\langle k\left|\frac{1}{r_{ij}}\right|l\right\rangle_{\boldsymbol{w}_l\to\boldsymbol{C}_l(\boldsymbol{F}_{ij}+\boldsymbol{F}_{ij}')\boldsymbol{w}_l} + \boldsymbol{v}_l'(\boldsymbol{F}_{ij}+\boldsymbol{F}_{ij}')\boldsymbol{w}_l\frac{\partial}{\partial\alpha_k}\frac{\partial}{\partial\beta_k}\left\langle\varphi_k\left|\frac{1}{r_{ij}}\right|\varphi_l\right\rangle_0, \quad (5.84)$$

$$\left\langle\boldsymbol{\nabla}'k\left|\frac{1}{r_{ij}}\boldsymbol{G}_{ij}\right|\boldsymbol{\nabla}l\right\rangle = 4\left\langle k\left|\frac{1}{r_{ij}}\boldsymbol{r}'(\boldsymbol{C}_k^*\boldsymbol{G}_{ij}\boldsymbol{C}_l)\boldsymbol{r}\right|l\right\rangle - 2\left\langle k\left|\frac{1}{r_{ij}}\right|l\right\rangle_{\boldsymbol{v}_l\to\boldsymbol{C}_k^*\boldsymbol{G}_{ij}\boldsymbol{v}_l} - \\ - 2\left\langle k\left|\frac{1}{r_{ij}}\right|l\right\rangle_{\boldsymbol{v}_k\to\boldsymbol{C}_l^*\boldsymbol{G}_{ij}^\dagger\boldsymbol{v}_k} - 2\left\langle k\left|\frac{1}{r_{ij}}\right|l\right\rangle_{\boldsymbol{w}_l\to\boldsymbol{C}_k^*\boldsymbol{G}_{ij}\boldsymbol{w}_l} - 2\left\langle k\left|\frac{1}{r_{ij}}\right|l\right\rangle_{\boldsymbol{w}_k\to\boldsymbol{C}_l^*\boldsymbol{G}_{ij}^\dagger\boldsymbol{w}_k} + \\ + \boldsymbol{v}_k^\dagger\boldsymbol{G}_{ij}\boldsymbol{v}_l\frac{\partial}{\partial\beta_k}\frac{\partial}{\partial\beta_l}\left\langle\varphi_k\left|\frac{1}{r_{ij}}\right|\varphi_l\right\rangle_0 + \boldsymbol{w}_k^\dagger\boldsymbol{G}_{ij}\boldsymbol{w}_l\frac{\partial}{\partial\alpha_k}\frac{\partial}{\partial\alpha_l}\left\langle\varphi_k\left|\frac{1}{r_{ij}}\right|\varphi_l\right\rangle_0 + \\ + \boldsymbol{v}_k^\dagger\boldsymbol{G}_{ij}\boldsymbol{w}_l\frac{\partial}{\partial\alpha_l}\frac{\partial}{\partial\beta_k}\left\langle\varphi_k\left|\frac{1}{r_{ij}}\right|\varphi_l\right\rangle_0 + \boldsymbol{w}_k^\dagger\boldsymbol{G}_{ij}\boldsymbol{v}_l\frac{\partial}{\partial\beta_l}\frac{\partial}{\partial\alpha_k}\left\langle\varphi_k\left|\frac{1}{r_{ij}}\right|\varphi_l\right\rangle_0. \quad (5.85)$$

Before proceeding to the specific cases of $P$- and $D$-states, we give some useful identities for matrices $\boldsymbol{F}_{ij}$ and $\boldsymbol{G}_{ij}$:

$$\boldsymbol{F}_{ij}+\boldsymbol{F}_{ij}' = (E_{ij}-E_{ji})\otimes K, \quad (5.86)$$

$$\boldsymbol{G}_{ij}+\boldsymbol{G}_{ij}' = (E_{ij}-E_{ji})\otimes K, \quad (5.87)$$

$$\boldsymbol{K} = \boldsymbol{\epsilon}_x\boldsymbol{\epsilon}_y' - \boldsymbol{\epsilon}_y\boldsymbol{\epsilon}_x', \quad (5.88)$$

and for the vector-matrix-vector products of $3D$-vectors:

$$\boldsymbol{\epsilon}_+^\dagger \boldsymbol{K} \boldsymbol{\epsilon}_+ = i, \tag{5.89}$$

$$\boldsymbol{\epsilon}_z^\dagger \boldsymbol{K} \boldsymbol{\epsilon}_z = 0. \tag{5.90}$$

We first start with the matrix elements of $P$-states.

*$P$-state*

The matrix element with the basis function corresponding to $L = 1$ (5.74) is expanded into the sum of four matrix elements with the "elementary" functions of the form (5.75). However, we need to evaluate the matrix elements for only one combinations of prefactors — for example, $\langle (x_{i_k} + iy_{i_k}) z_{j_k} | (x_{i_l} + iy_{i_l}) z_{j_l} \rangle$ (in this notation we left only angular prefactors corresponding to basis functions $|k\rangle$, $|l\rangle$, omitting any constant factors in front of them and the Gaussian exponents themselves). All the other combinations can be obtained from that by simple substitutions of $n$-vectors $v_k$, $w_k$, $v_l$, $w_l$ in the final expressions. For the quantity $f$ that corresponds to electrons $i_k$, $j_k$, $i_l$, $j_l$ with the projections of orbital momentum $m_{i_k}$, $m_{j_k}$, $m_{i_l}$, $m_{j_l}$ we use the following notation: $f^{m_{i_k} m_{j_k} / m_{i_l} m_{j_l}}$. Thus, for the $L = 1$ state with $M_L = 1$ we have:

$$f = f^{10/10} - f^{10/01} - f^{01/10} + f^{01/01}. \tag{5.91}$$

Further, we provide a detailed derivation for $f^{10/10}$:

$$f^{10/10}(\text{case } \langle (x_{i_k} + iy_{i_k}) z_{j_k} | (x_{i_l} + iy_{i_l}) z_{j_l} \rangle). \tag{5.92}$$

We choose $\boldsymbol{\eta}_v^k = \boldsymbol{\eta}_v^l = \boldsymbol{\epsilon}_+$ and $\boldsymbol{\eta}_w^k = \boldsymbol{\eta}_w^l = \boldsymbol{\epsilon}_z$.

Similarly to the case of one electron in a $p$-state, we have three types of matrix elements that appear in Eqs. (5.84) and (5.85). Let us write them in order:

$$\frac{\partial}{\partial \alpha_k} \frac{\partial}{\partial \alpha_l} \left\langle \varphi_k \left| \frac{1}{r_{ij}} \right| \varphi_l \right\rangle_0 = \pi^{(3n-1)/2} \int_0^\infty \frac{d\beta}{|C_{kl} + \beta^2 J_{ij}|^{3/2}} [\boldsymbol{v}_k^\dagger (\boldsymbol{C}_{kl} + \beta^2 \boldsymbol{J}_{ij})^{-1} \boldsymbol{v}_l], \tag{5.93}$$

$$\left\langle k \left| \frac{1}{r_{ij}} \right| l \right\rangle = \frac{\pi^{(3n-1)/2}}{2} \int_0^\infty \frac{d\beta}{|C_{kl} + \beta^2 J_{ij}|^{3/2}} [\boldsymbol{v}_k^\dagger (\boldsymbol{C}_{kl} + \beta^2 \boldsymbol{J}_{ij})^{-1} \boldsymbol{v}_l] \, [\boldsymbol{w}_k^\dagger (\boldsymbol{C}_{kl} + \beta^2 \boldsymbol{J}_{ij})^{-1} \boldsymbol{w}_l], \tag{5.94}$$

$$\left\langle k\left|\frac{1}{r_{ij}}\boldsymbol{r}'\boldsymbol{A}\boldsymbol{r}\right|l\right\rangle = -\frac{\partial}{\partial\gamma}\left\langle k\left|\frac{2}{\sqrt{\pi}}\int_0^\infty d\beta\exp\{\left[-\boldsymbol{r}'\left(\gamma\boldsymbol{A}+\beta^2\boldsymbol{J}_{ij}\right)\boldsymbol{r}\right]\}\right|l\right\rangle =$$
$$= \frac{\pi^{(3n-1)/2}}{2}\int_0^\infty \frac{d\beta}{|C_{kl}+\beta^2 J_{ij}|^{3/2}}\Big(\left[\boldsymbol{v}_k^\dagger(\boldsymbol{C}_{kl}+\beta^2\boldsymbol{J}_{ij})^{-1}\boldsymbol{A}(\boldsymbol{C}_{kl}+\beta^2\boldsymbol{J}_{ij})^{-1}\boldsymbol{v}_l\right]\left[\boldsymbol{w}_k^\dagger(\boldsymbol{C}_{kl}+\beta^2\boldsymbol{J}_{ij})^{-1}\boldsymbol{w}_l\right]+$$
$$+\{\boldsymbol{v}\leftrightarrow\boldsymbol{w}\}\Big), \quad (5.95)$$

where, as previously, $\boldsymbol{A} = A\otimes\boldsymbol{K}$ is a traceless symmetric matrix, and $\{\boldsymbol{v}\leftrightarrow\boldsymbol{w}\}$ denotes the additional term obtained by swapping $\boldsymbol{v}_l(\boldsymbol{v}_k)$ with $\boldsymbol{w}_l(\boldsymbol{w}_k)$. In the above expressions, we left only the terms that do not vanish after expanding Kronecker products (i.e. terms that contain the following vector-matrix-vector products: $\boldsymbol{\epsilon}_+^\dagger\boldsymbol{K}\boldsymbol{\epsilon}_+ = i$, $\boldsymbol{\epsilon}_+^\dagger\boldsymbol{\epsilon}_+ = 1$, and $\boldsymbol{\epsilon}_z'\boldsymbol{\epsilon}_z = 1$). Note that only the first term from the overlap matrix element $S_{kl}$ (Eq. (5.81)) contributes to the matrix elements. Evaluation of the integrals yields:

$$\frac{\partial}{\partial\alpha_k}\frac{\partial}{\partial\alpha_l}\left\langle\varphi_k\left|\frac{1}{r_{ij}}\right|\varphi_l\right\rangle_0 = \frac{\pi^{(3n-1)/2}}{|C_{kl}|^{3/2}}\left\{\gamma_{ij}[v_k'C_{kl}^{-1}v_l] - \frac{1}{3}\gamma_{ij}^3[v_k'C_{kl}^{-1}J_{ij}C_{kl}^{-1}v_l]\right\}\boldsymbol{\epsilon}_+^\dagger\boldsymbol{\epsilon}_+, \quad (5.96)$$

$$\left\langle k\left|\frac{1}{r_{ij}}\right|l\right\rangle = \frac{\pi^{(3n-1)/2}}{2\,|C_{kl}|^{3/2}}\Big\{\gamma_{ij}[\boldsymbol{v}_k^\dagger\boldsymbol{C}_{kl}^{-1}\boldsymbol{v}_l][\boldsymbol{w}_k^\dagger\boldsymbol{C}_{kl}^{-1}\boldsymbol{w}_l] - \frac{1}{3}\gamma_{ij}^3\big([\boldsymbol{v}_k^\dagger\boldsymbol{C}_{kl}^{-1}\boldsymbol{J}_{ij}\boldsymbol{C}_{kl}^{-1}\boldsymbol{v}_l][\boldsymbol{w}_k^\dagger\boldsymbol{C}_{kl}^{-1}\boldsymbol{w}_l]+$$
$$+[\boldsymbol{v}_k^\dagger\boldsymbol{C}_{kl}^{-1}\boldsymbol{v}_l][\boldsymbol{w}_k^\dagger\boldsymbol{C}_{kl}^{-1}\boldsymbol{J}_{ij}\boldsymbol{C}_{kl}^{-1}\boldsymbol{w}_l]\big) + \frac{1}{5}\gamma_{ij}^5[\boldsymbol{v}_k^\dagger\boldsymbol{C}_{kl}^{-1}\boldsymbol{J}_{ij}\boldsymbol{C}_{kl}^{-1}\boldsymbol{v}_l][\boldsymbol{w}_k^\dagger\boldsymbol{C}_{kl}^{-1}\boldsymbol{J}_{ij}\boldsymbol{C}_{kl}^{-1}\boldsymbol{w}_l]\Big\}, \quad (5.97)$$

$$\left\langle k\left|\frac{1}{r_{ij}}\boldsymbol{r}'\boldsymbol{A}\boldsymbol{r}\right|l\right\rangle_{L=1} = \frac{\pi^{(3n-1)/2}}{2\,|C_{kl}|^{3/2}}\Big\{\gamma_{ij}[v_k'C_{kl}^{-1}AC_{kl}^{-1}v_l][w_k'C_{kl}^{-1}w_l]-$$
$$-\frac{1}{3}\gamma_{ij}^3\big([v_k'C_{kl}^{-1}J_{ij}C_{kl}^{-1}AC_{kl}^{-1}v_l][w_k'C_{kl}^{-1}w_l] + [v_k'C_{kl}^{-1}AC_{kl}^{-1}J_{ij}C_{kl}^{-1}v_l][w_k'C_{kl}^{-1}w_l]+$$
$$+[v_k'C_{kl}^{-1}AC_{kl}^{-1}v_l][w_k'C_{kl}^{-1}J_{ij}C_{kl}^{-1}w_l]\big)+$$
$$+\frac{1}{5}\gamma_{ij}^5\big([v_k'C_{kl}^{-1}J_{ij}C_{kl}^{-1}AC_{kl}^{-1}J_{ij}C_{kl}^{-1}v_l][w_k'C_{kl}^{-1}w_l] + [v_k'C_{kl}^{-1}J_{ij}C_{kl}^{-1}AC_{kl}^{-1}v_l][w_k'C_{kl}^{-1}J_{ij}C_{kl}^{-1}w_l]+$$
$$+[v_k'C_{kl}^{-1}AC_{kl}^{-1}J_{ij}C_{kl}^{-1}v_l][w_k'C_{kl}^{-1}J_{ij}C_{kl}^{-1}w_l]\big)-$$
$$-\frac{1}{7}\gamma_{ij}^7[v_k'C_{kl}^{-1}J_{ij}C_{kl}^{-1}AC_{kl}^{-1}J_{ij}C_{kl}^{-1}v_l][w_k'C_{kl}^{-1}J_{ij}C_{kl}^{-1}w_l]\Big\}(\boldsymbol{\epsilon}_+^\dagger\boldsymbol{K}\boldsymbol{\epsilon}_+)(\boldsymbol{\epsilon}_z'\boldsymbol{\epsilon}_z). \quad (5.98)$$

Using these auxiliary integrals, we may easily evaluate matrix elements (5.84) and (5.85). Note that the matrix elements of type (5.97) that contain substitutions of $\boldsymbol{w}_k$ or $\boldsymbol{w}_l$ vanish due to the identity $\boldsymbol{\epsilon}_z'\boldsymbol{K}\boldsymbol{\epsilon}_z = 0$.

After collecting all the terms and performing some simplifications, we obtain the fol-

lowing expression for $f^{10/10}$:

$$f^{10/10}[ij,ij] = i\frac{\pi^{(3n-1)/2}}{|C_{kl}|^{3/2}}\Bigg\{\frac{1}{3}\gamma_{ij}^3[v_k'C_{kl}^{-1}J_{ij}E_{ij}C_k^*C_{kl}^{-1}v_l + v_k'C_{kl}^{-1}C_lE_{ji}J_{ij}C_{kl}^{-1}v_l][w_k'C_{kl}^{-1}w_l]+$$
$$+\frac{1}{5}\gamma_{ij}^5\Bigg([v_k'C_{kl}^{-1}J_{ij}E_{ij}C_lC_{kl}^{-1}J_{ij}C_{kl}^{-1}v_l - v_k'C_{kl}^{-1}J_{ij}C_{kl}^{-1}C_lE_{ji}J_{ij}C_{kl}^{-1}v_l][w_k'C_{kl}^{-1}w_l]-$$
$$-[v_k'C_{kl}^{-1}J_{ij}E_{ij}C_k^*C_{kl}^{-1}v_l + v_k'C_{kl}^{-1}C_lE_{ji}J_{ij}C_{kl}^{-1}v_l][w_k'C_{kl}^{-1}J_{ij}C_{kl}^{-1}w_l]\Bigg)-$$
$$-\frac{1}{7}\gamma_{ij}^7[v_k'C_{kl}^{-1}J_{ij}E_{ij}C_lC_{kl}^{-1}J_{ij}C_{kl}^{-1}v_l - v_k'C_{kl}^{-1}J_{ij}C_{kl}^{-1}C_lE_{ji}J_{ij}C_{kl}^{-1}v_l][w_k'C_{kl}^{-1}J_{ij}C_{kl}^{-1}w_l]\Bigg\}. \tag{5.99}$$

For the spatial part of SO matrix element, we need $f[ii,ii]$, $f[ii,ij]$, $f[ij,jj]$, and $f[ij,ii]$ (see formula (5.32)). The expressions for them are the following:

$$f^{10/10}[ii,ii] = i\frac{\pi^{(3n-1)/2}}{|C_{kl}|^{3/2}}\Bigg\{\frac{1}{3}\gamma_{ii}^3[j^{i\prime}C_{kl}^{-1}v_k\cdot j^{i\prime}C_k^*C_{kl}^{-1}v_l + j^{i\prime}C_lC_{kl}^{-1}v_k\cdot j^{i\prime}C_{kl}^{-1}v_l][w_k'C_{kl}^{-1}w_l]-$$
$$-\frac{1}{5}\gamma_{ii}^5[j^{i\prime}C_{kl}^{-1}v_k\cdot j^{i\prime}C_k^*C_{kl}^{-1}v_l + j^{i\prime}C_lC_{kl}^{-1}v_k\cdot j^{i\prime}C_{kl}^{-1}v_l][j^{i\prime}C_{kl}^{-1}w_k\cdot j^{i\prime}C_{kl}^{-1}w_l]\Bigg\}, \tag{5.100}$$

$$f^{10/10}[ii,ij] = i\frac{\pi^{(3n-1)/2}}{|C_{kl}|^{3/2}}\Bigg\{\frac{1}{3}\gamma_{ii}^3[j^{i\prime}C_{kl}^{-1}v_k\cdot j^{j\prime}C_k^*C_{kl}^{-1}v_l + j^{j\prime}C_lC_{kl}^{-1}v_k\cdot j^{i\prime}C_{kl}^{-1}v_l][w_k'C_{kl}^{-1}w_l]-$$
$$-\frac{1}{5}\gamma_{ii}^5[j^{i\prime}C_{kl}^{-1}v_k\cdot j^{j\prime}C_k^*C_{kl}^{-1}v_l + j^{j\prime}C_lC_{kl}^{-1}v_k\cdot j^{i\prime}C_{kl}^{-1}v_l][j^{i\prime}C_{kl}^{-1}w_k\cdot j^{i\prime}C_{kl}^{-1}w_l]\Bigg\}, \tag{5.101}$$

$$f^{10/10}[ij,jj] = i\frac{\pi^{(3n-1)/2}}{|C_{kl}|^{3/2}}\Bigg\{\frac{1}{3}\gamma_{ij}^3[j^{j\prime}C_k^*C_{kl}^{-1}v_l\cdot(j^{j\prime}C_{kl}^{-1}v_k - j^{i\prime}C_{kl}^{-1}v_k)+$$
$$+j^{j\prime}C_lC_{kl}^{-1}v_k\cdot(j^{j\prime}C_{kl}^{-1}v_l - j^{i\prime}C_{kl}^{-1}v_l)][w_k'C_{kl}^{-1}w_l]-$$
$$-\frac{1}{5}\gamma_{ij}^5[j^{j\prime}C_k^*C_{kl}^{-1}v_l\cdot(j^{j\prime}C_{kl}^{-1}v_k - j^{i\prime}C_{kl}^{-1}v_k) + j^{j\prime}C_lC_{kl}^{-1}v_k\cdot(j^{j\prime}C_{kl}^{-1}v_l - j^{i\prime}C_{kl}^{-1}v_l)]\times$$
$$\times[j^{j\prime}C_{kl}^{-1}w_k\cdot j^{j\prime}C_{kl}^{-1}w_l - j^{i\prime}C_{kl}^{-1}w_k\cdot j^{j\prime}C_{kl}^{-1}w_l - j^{j\prime}C_{kl}^{-1}w_k\cdot j^{i\prime}C_{kl}^{-1}w_l + j^{i\prime}C_{kl}^{-1}w_k\cdot j^{i\prime}C_{kl}^{-1}w_l]\Bigg\}, \tag{5.102}$$

$$f^{10/10}[ij,ii] = f^{10/10}[ij,jj]\big|_{(i\leftrightarrow j)}. \tag{5.103}$$

All the other matrix elements $f^{\cdot\cdot/\cdot\cdot}$ can be expressed through $f^{10/10}$ by simple substi-

tutions of $n$-vectors $v$ and $w$:

$$\begin{aligned} f^{10/01} &= f^{10/10}\big|_{(v_l \leftrightarrow w_l)}\,, \\ f^{01/10} &= f^{10/10}\big|_{(v_k \leftrightarrow w_k)}\,, \\ f^{01/01} &= f^{10/10}\big|_{(v_l \leftrightarrow w_l, v_k \leftrightarrow w_k)}\,. \end{aligned} \tag{5.104}$$

*D-state*

For the case of a $D$-state, we have $\boldsymbol{\eta}_v^k = \boldsymbol{\eta}_v^l = \boldsymbol{\eta}_w^k = \boldsymbol{\eta}_w^l = \boldsymbol{\epsilon}_+$. Only the first and third terms from the overlap matrix element $S_{kl}$ (Eq. (5.81)) contribute to (5.94), (5.95) (second term vanishes due to an identity $\boldsymbol{\epsilon}_+' \boldsymbol{K} \boldsymbol{\epsilon}_+ = 0$). For the wave functions of a $D$-state, the auxiliary matrix elements read:

$$\left\langle k \middle| \frac{1}{r_{ij}} \middle| l \right\rangle_{L=2} = \frac{\pi^{(3n-1)/2}}{2} \int_0^\infty \frac{d\beta}{|C_{kl} + \beta^2 J_{ij}|^{3/2}} \Big( [\boldsymbol{v}_k^\dagger (\boldsymbol{C}_{kl} + \beta^2 \boldsymbol{J}_{ij})^{-1} \boldsymbol{v}_l]\, [\boldsymbol{w}_k^\dagger (\boldsymbol{C}_{kl} + \beta^2 \boldsymbol{J}_{ij})^{-1} \boldsymbol{w}_l] + \\ + [\boldsymbol{v}_k^\dagger (\boldsymbol{C}_{kl} + \beta^2 \boldsymbol{J}_{ij})^{-1} \boldsymbol{w}_l]\, [\boldsymbol{w}_k^\dagger (\boldsymbol{C}_{kl} + \beta^2 \boldsymbol{J}_{ij})^{-1} \boldsymbol{v}_l] \Big), \tag{5.105}$$

$$\left\langle k \middle| \frac{1}{r_{ij}} \boldsymbol{r}' \boldsymbol{A} \boldsymbol{r} \middle| l \right\rangle_{L=2} = -\frac{\partial}{\partial \gamma} \left\langle k \middle| \frac{2}{\sqrt{\pi}} \int_0^\infty d\beta \exp\left[ -\boldsymbol{r}' \left( \gamma \boldsymbol{A} + \beta^2 \boldsymbol{J}_{ij} \right) \boldsymbol{r} \right] \middle| l \right\rangle = \\ = \frac{\pi^{(3n-1)/2}}{2} \int_0^\infty \frac{d\beta}{|C_{kl} + \beta^2 J_{ij}|^{3/2}} \Big( [\boldsymbol{v}_k^\dagger (\boldsymbol{C}_{kl} + \beta^2 \boldsymbol{J}_{ij})^{-1} \boldsymbol{A} (\boldsymbol{C}_{kl} + \beta^2 \boldsymbol{J}_{ij})^{-1} \boldsymbol{v}_l]\, [\boldsymbol{w}_k^\dagger (\boldsymbol{C}_{kl} + \beta^2 \boldsymbol{J}_{ij})^{-1} \boldsymbol{w}_l] + \\ [\boldsymbol{v}_k^\dagger (\boldsymbol{C}_{kl} + \beta^2 \boldsymbol{J}_{ij})^{-1} \boldsymbol{A} (\boldsymbol{C}_{kl} + \beta^2 \boldsymbol{J}_{ij})^{-1} \boldsymbol{w}_l]\, [\boldsymbol{w}_k^\dagger (\boldsymbol{C}_{kl} + \beta^2 \boldsymbol{J}_{ij})^{-1} \boldsymbol{v}_l] + \{\boldsymbol{v} \leftrightarrow \boldsymbol{w}\} \Big). \tag{5.106}$$

Additional terms in (5.105) and (5.106) have the same structure as for the case of a $P$-state and we may directly write expression for $f$ through already known expression for $f^{10/10}$:

$$f = f^{10/10} + f^{10/10}\big|_{(v_l \leftrightarrow w_l)} + f^{10/10}\big|_{(v_k \leftrightarrow w_k)} + f^{10/10}\big|_{(v_l \leftrightarrow w_l, v_k \leftrightarrow w_k)}\,. \tag{5.107}$$

Or, alternatively,

$$f = f^{10/10} + f^{10/01} + f^{01/10} + f^{01/01}. \tag{5.108}$$

It is quite remarkable that the expression for $f$ for the case of $D$-state is just another linear combination of terms that appear in the expression for $f$ in the case of a $P$-state (cf. (5.91)).

### 5.3.3 Matrix element of non-contact spin–spin operator

The spatial part of the non-contact spin–spin operator $g$ is given in Eqs. (5.63) and (5.65).

The action of differential operators in (5.65) on the generating wave functions is as follows:

$$\boldsymbol{\nabla}'\boldsymbol{D}_{ij}\boldsymbol{\nabla}\varphi_l = (4\boldsymbol{r}'(\boldsymbol{C}_l\boldsymbol{D}_{ij}\boldsymbol{C}_l)\boldsymbol{r} - 4\alpha_l\boldsymbol{r}'\boldsymbol{C}_l\boldsymbol{D}_{ij}\boldsymbol{v}_l - 4\beta_l\boldsymbol{r}'\boldsymbol{C}_l\boldsymbol{D}_{ij}\boldsymbol{w}_l + \\ +2\alpha_l\beta_l\boldsymbol{v}_l'\boldsymbol{D}_{ij}\boldsymbol{w}_l + O(\alpha_l^2) + O(\beta_l^2))\,\varphi_l, \quad (5.109)$$

$$\boldsymbol{\nabla}'\boldsymbol{D}_{ij}\boldsymbol{\nabla}\varphi_k^* = \Big(4\boldsymbol{r}'(\boldsymbol{C}_k^*\boldsymbol{D}_{ij}\boldsymbol{C}_k^*)\boldsymbol{r} - 4\alpha_k\boldsymbol{v}_k^\dagger\boldsymbol{D}_{ij}\boldsymbol{C}_k^*\boldsymbol{r} - 4\beta_k\boldsymbol{w}_k^\dagger\boldsymbol{D}_{ij}\boldsymbol{C}_k^*\boldsymbol{r} + \\ +2\alpha_k\beta_k\boldsymbol{v}_k^\dagger\boldsymbol{D}_{ij}\boldsymbol{w}_k^* + O(\alpha_k^2) + O(\beta_k^2)\Big)\,\varphi_k^*, \quad (5.110)$$

$$(\boldsymbol{\nabla}'\varphi_k^*)\boldsymbol{D}_{ij}(\boldsymbol{\nabla}\varphi_l) = \Big(4\boldsymbol{r}'(\boldsymbol{C}_k^*\boldsymbol{D}_{ij}\boldsymbol{C}_l)\boldsymbol{r} - 2\alpha_l\boldsymbol{r}'\boldsymbol{C}_k^*\boldsymbol{D}_{ij}\boldsymbol{v}_l - 2\alpha_k\boldsymbol{v}_k^\dagger\boldsymbol{D}_{ij}\boldsymbol{C}_l\boldsymbol{r} - 2\beta_l\boldsymbol{r}'\boldsymbol{C}_k^*\boldsymbol{D}_{ij}\boldsymbol{w}_l - \\ -2\beta_k\boldsymbol{w}_k^\dagger\boldsymbol{D}_{ij}\boldsymbol{C}_l\boldsymbol{r} + \alpha_k\alpha_l\boldsymbol{v}_k^\dagger\boldsymbol{D}_{ij}\boldsymbol{v}_l + \beta_k\beta_l\boldsymbol{w}_k^\dagger\boldsymbol{D}_{ij}\boldsymbol{w}_l + \alpha_k\beta_l\boldsymbol{v}_k^\dagger\boldsymbol{D}_{ij}\boldsymbol{w}_l + \beta_k\alpha_l\boldsymbol{w}_k^\dagger\boldsymbol{D}_{ij}\boldsymbol{v}_l\Big)\,\varphi_k^*\varphi_l, \quad (5.111)$$

where we used that $\boldsymbol{D}_{ij} = \boldsymbol{D}_{ij}'$ and $\boldsymbol{D}_{ij} = \boldsymbol{D}_{ij}^*$.

The corresponding matrix elements are:

$$\left\langle k\left|\frac{1}{r_{ij}}\boldsymbol{\nabla}'\boldsymbol{D}_{ij}\boldsymbol{\nabla}\right|l\right\rangle = 4\left\langle k\left|\frac{1}{r_{ij}}\boldsymbol{r}'(\boldsymbol{C}_l\boldsymbol{D}_{ij}\boldsymbol{C}_l)\boldsymbol{r}\right|l\right\rangle - 4\left\langle k\left|\frac{1}{r_{ij}}\right|l\right\rangle_{\boldsymbol{v}_l\to\boldsymbol{C}_l\boldsymbol{D}_{ij}\boldsymbol{v}_l} - \\ - 4\left\langle k\left|\frac{1}{r_{ij}}\right|l\right\rangle_{\boldsymbol{w}_l\to\boldsymbol{C}_l\boldsymbol{G}_{ij}\boldsymbol{w}_l} + 2\boldsymbol{v}_l'\boldsymbol{D}_{ij}\boldsymbol{w}_l\frac{\partial}{\partial\alpha_k}\frac{\partial}{\partial\beta_k}\left\langle\varphi_k\left|\frac{1}{r_{ij}}\right|\varphi_l\right\rangle_0, \quad (5.112)$$

$$\left\langle\boldsymbol{\nabla}'\boldsymbol{D}_{ij}\boldsymbol{\nabla}k\left|\frac{1}{r_{ij}}\right|l\right\rangle = 4\left\langle k\left|\frac{1}{r_{ij}}\boldsymbol{r}'(\boldsymbol{C}_k^*\boldsymbol{D}_{ij}\boldsymbol{C}_k^*)\boldsymbol{r}\right|l\right\rangle - 4\left\langle k\left|\frac{1}{r_{ij}}\right|l\right\rangle_{\boldsymbol{v}_k\to\boldsymbol{C}_k\boldsymbol{D}_{ij}\boldsymbol{v}_k} - \\ - 4\left\langle k\left|\frac{1}{r_{ij}}\right|l\right\rangle_{\boldsymbol{w}_k\to\boldsymbol{C}_k\boldsymbol{D}_{ij}\boldsymbol{w}_k} + 2\boldsymbol{v}_k^\dagger\boldsymbol{D}_{ij}\boldsymbol{w}_k^*\frac{\partial}{\partial\alpha_l}\frac{\partial}{\partial\beta_l}\left\langle\varphi_k\left|\frac{1}{r_{ij}}\right|\varphi_l\right\rangle_0, \quad (5.113)$$

$$\left\langle \boldsymbol{\nabla}' k \left| \frac{1}{r_{ij}} \boldsymbol{D}_{ij} \right| \boldsymbol{\nabla} l \right\rangle = 4 \left\langle k \left| \frac{1}{r_{ij}} \boldsymbol{r}' (\boldsymbol{C}_k^* \boldsymbol{D}_{ij} \boldsymbol{C}_l) \boldsymbol{r} \right| l \right\rangle - 2 \left\langle k \left| \frac{1}{r_{ij}} \right| l \right\rangle_{\boldsymbol{v}_l \to \boldsymbol{C}_k^* \boldsymbol{D}_{ij} \boldsymbol{v}_l} -$$
$$- 2 \left\langle k \left| \frac{1}{r_{ij}} \right| l \right\rangle_{\boldsymbol{v}_k \to \boldsymbol{C}_l^* \boldsymbol{D}_{ij} \boldsymbol{v}_k} - 2 \left\langle k \left| \frac{1}{r_{ij}} \right| l \right\rangle_{\boldsymbol{w}_l \to \boldsymbol{C}_k^* \boldsymbol{D}_{ij} \boldsymbol{w}_l} - 2 \left\langle k \left| \frac{1}{r_{ij}} \right| l \right\rangle_{\boldsymbol{w}_k \to \boldsymbol{C}_l^* \boldsymbol{D}_{ij} \boldsymbol{w}_k} +$$
$$+ \boldsymbol{v}_k^\dagger \boldsymbol{D}_{ij} \boldsymbol{v}_l \frac{\partial}{\partial \beta_k} \frac{\partial}{\partial \beta_l} \left\langle \varphi_k \left| \frac{1}{r_{ij}} \right| \varphi_l \right\rangle_0 + \boldsymbol{w}_k^\dagger \boldsymbol{D}_{ij} \boldsymbol{w}_l \frac{\partial}{\partial \alpha_k} \frac{\partial}{\partial \alpha_l} \left\langle \varphi_k \left| \frac{1}{r_{ij}} \right| \varphi_l \right\rangle_0 +$$
$$+ \boldsymbol{v}_k^\dagger \boldsymbol{D}_{ij} \boldsymbol{w}_l \frac{\partial}{\partial \alpha_l} \frac{\partial}{\partial \beta_k} \left\langle \varphi_k \left| \frac{1}{r_{ij}} \right| \varphi_l \right\rangle_0 + \boldsymbol{w}_k^\dagger \boldsymbol{D}_{ij} \boldsymbol{v}_l \frac{\partial}{\partial \beta_l} \frac{\partial}{\partial \alpha_k} \left\langle \varphi_k \left| \frac{1}{r_{ij}} \right| \varphi_l \right\rangle_0 . \quad (5.114)$$

Note that the right-hand sides of the above expressions involve the same type of integrals as those encountered in the case of the spin–orbit operator. Now, we come to the cases of $P$- and $D$-states.

*$P$-state*

$$g^{10/10} \text{ (case } \langle (x_{i_k} + iy_{i_k}) z_{j_k} | (x_{i_l} + iy_{i_l}) z_{j_l} \rangle).$$

We choose $\boldsymbol{\eta}_v^k = \boldsymbol{\eta}_v^l = \boldsymbol{\epsilon}_+$ and $\boldsymbol{\eta}_w^k = \boldsymbol{\eta}_w^l = \boldsymbol{\epsilon}_z$. Only the first term in the overlap matrix element $S_{kl}$ (5.81) gives non-zero contribution to the desired matrix elements. The remaining terms vanish due to the presence of factors $\boldsymbol{\epsilon}'_+ \boldsymbol{\Upsilon} \boldsymbol{\epsilon}_z$ or $\boldsymbol{\epsilon}'_+ \boldsymbol{\epsilon}_z$, which are identically zero.

After collecting and simplifying the terms, one obtains the following expression for $g^{10/10}$:

$$g^{10/10} = -\frac{2\pi^{(3n-1)/2}}{\sqrt{6}\,|C_{kl}|^{3/2}} \left\{ \frac{1}{5} \gamma_{ij}^5 \left( [v'_k C_{kl}^{-1} J_{ij} D_{ij} J_{ij} C_{kl}^{-1} v_l][w'_k C_{kl}^{-1} w_l] - 2\{v \leftrightarrow w\} \right) \right.$$
$$\left. - \frac{1}{7} \gamma_{ij}^7 \left( [v'_k C_{kl}^{-1} J_{ij} D_{ij} J_{ij} C_{kl}^{-1} v_l][w'_k C_{kl}^{-1} J_{ij} C_{kl}^{-1} w_l] - 2\{v \leftrightarrow w\} \right) \right\}. \quad (5.115)$$

The factor of $-2$ in front of the terms $\{v \leftrightarrow w\}$ comes from the Cartesian part $\boldsymbol{\epsilon}'_z \boldsymbol{\Upsilon} \boldsymbol{\epsilon}_z = -2$. Using the identity $J_{ij} D_{ij} J_{ij} = -J_{ij}$, we rewrite $g^{10/10}$ as follows:

$$g^{10/10} = \frac{2\pi^{(3n-1)/2}}{\sqrt{6}\,|C_{kl}|^{3/2}} \left\{ \frac{1}{5} \gamma_{ij}^5 \left( [v'_k C_{kl}^{-1} J_{ij} C_{kl}^{-1} v_l][w'_k C_{kl}^{-1} w_l] - 2[v'_k C_{kl}^{-1} v_l][w'_k C_{kl}^{-1} J_{ij} C_{kl}^{-1} w_l] \right) + \right.$$
$$\left. + \frac{1}{7} \gamma_{ij}^7 [v'_k C_{kl}^{-1} J_{ij} C_{kl}^{-1} v_l][w'_k C_{kl}^{-1} J_{ij} C_{kl}^{-1} w_l] \right\}. \quad (5.116)$$

Or, expressed in terms of vectors $j^i$, $j^j$:

$$g^{10/10} = \frac{2\pi^{(3n-1)/2}}{\sqrt{6}\,|C_{kl}|^{3/2}}\Bigg\{\frac{1}{5}\gamma_{ij}^5\Bigg([j^{i\prime}C_{kl}^{-1}v_k\cdot j^{i\prime}C_{kl}^{-1}v_l + j^{j\prime}C_{kl}^{-1}v_k\cdot j^{j\prime}C_{kl}^{-1}v_l - j^{i\prime}C_{kl}^{-1}v_k\cdot j^{j\prime}C_{kl}^{-1}v_l -$$
$$- j^{j\prime}C_{kl}^{-1}v_k\cdot j^{i\prime}C_{kl}^{-1}v_l][w_k^\prime C_{kl}^{-1}w_l] - 2[v_k^\prime C_{kl}^{-1}v_l][j^{i\prime}C_{kl}^{-1}w_k\cdot j^{i\prime}C_{kl}^{-1}w_l + j^{j\prime}C_{kl}^{-1}w_k\cdot j^{j\prime}C_{kl}^{-1}w_l -$$
$$- j^{i\prime}C_{kl}^{-1}w_k\cdot j^{j\prime}C_{kl}^{-1}w_l - j^{j\prime}C_{kl}^{-1}v_k\cdot j^{i\prime}C_{kl}^{-1}w_l]\Bigg) +$$
$$+\frac{1}{7}\gamma_{ij}^7[j^{i\prime}C_{kl}^{-1}v_k\cdot j^{i\prime}C_{kl}^{-1}v_l + j^{j\prime}C_{kl}^{-1}v_k\cdot j^{j\prime}C_{kl}^{-1}v_l - j^{i\prime}C_{kl}^{-1}v_k\cdot j^{j\prime}C_{kl}^{-1}v_l - j^{j\prime}C_{kl}^{-1}v_k\cdot j^{i\prime}C_{kl}^{-1}v_l]\times$$
$$[j^{i\prime}C_{kl}^{-1}w_k\cdot j^{i\prime}C_{kl}^{-1}w_l + j^{j\prime}C_{kl}^{-1}w_k\cdot j^{j\prime}C_{kl}^{-1}w_l - j^{i\prime}C_{kl}^{-1}w_k\cdot j^{j\prime}C_{kl}^{-1}w_l - j^{j\prime}C_{kl}^{-1}v_k\cdot j^{i\prime}C_{kl}^{-1}w_l]\Bigg\}. \tag{5.117}$$

To write the full matrix element for the $P$-state we have to collect contributions from all combinations of prefactors according to (5.91), where the terms $g^{\cdot\cdot/\cdot\cdot}$ are related to $g^{10/10}$ in the same way as for the quantities $f$ in Eq. (5.104).

*D-state*

In this case $\boldsymbol{\eta}_v^k = \boldsymbol{\eta}_v^l = \boldsymbol{\eta}_w^k = \boldsymbol{\eta}_w^l = \boldsymbol{\epsilon}_+$. Only the first and third terms in $S_{kl}$ contribute to the matrix elements in (5.65).

We introduce the quantity $h$:

$$h = \frac{2\pi^{(3n-1)/2}}{\sqrt{6}\,|C_{kl}|^{3/2}}\Bigg\{\frac{1}{5}\gamma_{ij}^5[v_k^\prime C_{kl}^{-1}J_{ij}C_{kl}^{-1}v_l][w_k^\prime C_{kl}^{-1}w_l] - \frac{1}{7}\gamma_{ij}^7[v_k^\prime C_{kl}^{-1}J_{ij}C_{kl}^{-1}v_l][w_k^\prime C_{kl}^{-1}J_{ij}C_{kl}^{-1}w_l]\Bigg\}, \tag{5.118}$$

and express $g$ in terms of $h$ as follows:

$$g = h + h|_{(v_k\leftrightarrow w_k)} + h|_{(v_l\leftrightarrow w_l)} + h|_{(v_k\leftrightarrow w_k, v_l\leftrightarrow w_l)}\,. \tag{5.119}$$

.

# 6 Evaluation of off-diagonal matrix elements

## 6.1 General approach

To evaluate second-order ($\propto \alpha^4$) perturbation theory corrections to atomic fine structure in Eq. (4.6), it is necessary to compute off-diagonal matrix elements which appear in the perturbation theory summation. The scalar matrix element $\langle\phi|\mathcal{H}_{\rm SR}^{(2)}|\psi\rangle$ is nonzero only when both states, $\phi$ and $\psi$, have the same spin multiplicity and orbital angular momentum. As a consequence, the code implementation of such matrix elements is

straightforward and requires only minimal modifications to the existing ECG framework.

On the other hand, the evaluation of the off-diagonal matrix elements of fine-structure Hamiltonian $\langle\phi|\mathcal{H}^{(2)}_{\mathrm{FS}}|\psi\rangle$ requires some additional analytical work. This is due to the fact that the spin–orbit and non-contact spin–spin interactions are non-scalar (in a sense of SO(3) group tensors). As a result, the selection rules allow for differences in spin and orbital angular momentum quantum numbers between the states $\phi$ and $\psi$.

Let us consider an operator $\mathcal{O}$ that is factorized into the product of spin $\boldsymbol{T}$ and spatial $\boldsymbol{U}$ tensors of rank $k$:

$$\mathcal{O} = \boldsymbol{T}^{(k)} \cdot \boldsymbol{U}^{(k)}. \tag{6.1}$$

The wave functions $\psi$, $\phi$ in the matrix element $\langle\phi|\mathcal{O}|\psi\rangle$ are defined as follows:

$$|\phi\rangle = |SLJM_J\rangle\,, \tag{6.2}$$

$$|\psi\rangle = |S'L'JM_J\rangle\,. \tag{6.3}$$

Note that we consider the states with the same total orbital angular momentum $J$, since otherwise, the matrix element is zero. Moreover, the matrix element is independent of total angular momentum projection $M_J$ which gives us freedom to choose a convenient value. Expansion of the initial- and final-state wave functions in the $|SM_S\,LM_L\rangle$ basis set through Clebsch–Gordan coefficients yields:

$$\begin{aligned}\left\langle SLJM_J\middle|(\boldsymbol{T}^{(k)} \cdot \boldsymbol{U}^{(k)})\middle|S'L'JM_J\right\rangle = \sum_{\substack{M_S,M_L\\M'_S,M'_L}} C^{JM_J}_{SM_SLM_L} C^{JM_J}_{S'M'_SL'M'_L} \times \\ \times \left\langle SM_SLM_L\middle|(\boldsymbol{T}^{(k)} \cdot \boldsymbol{U}^{(k)})\middle|S'M'_SL'M'_L\right\rangle.\end{aligned} \tag{6.4}$$

As before, each of the matrix elements in the rhs is factorized into the product of spin and spatial parts as follows:

$$\begin{aligned}&\left\langle SM_SLM_L\middle|(\boldsymbol{T}^{(k)} \cdot \boldsymbol{U}^{(k)})\middle|S'M'_SL'M'_L\right\rangle = \\ &\qquad = \sum_{\mathcal{P}_i\in S_n} \epsilon_{\mathcal{P}_i} \sum_q (-1)^q \left\langle SM_S\middle|T^{(k)}_q \mathcal{P}^{\boldsymbol{\sigma}}\middle|S'M'_S\right\rangle \left\langle LM_L\middle|U^{(k)}_{-q}\mathcal{P}^{\boldsymbol{r}}\middle|L'M'_L\right\rangle,\end{aligned} \tag{6.5}$$

where the sum over $\mathcal{P}_i$ is taken over all particle permutations, and the sum over tensorial components $q$ comes from the expansion of the scalar product of tensor operators.

As in the diagonal case, the spin part of the matrix element (6.5) is trivial and can be reduced to a linear combination of operators composed of products of one-particle spin ladder and $z$-projecting operators. Therefore, we focus on the spatial part of transition matrix elements. Furthermore, we only consider off-diagonal matrix elements of spin–orbit and spin–spin operators relevant for the fine structure of carbon ground and first excited triplet $P$-states, as well as the lowest triplet $D$-state.

### 6.2 Matrix elements of spin–orbit operator

First, let us explicitly write the scalar product of tensor operators $\boldsymbol{T}^{(k)}$ and $\boldsymbol{U}^{(k)}$ for the case $k = 1$:

$$\boldsymbol{T}^{(1)} \cdot \boldsymbol{U}^{(1)} = T^1_0 U^1_0 - T^1_1 U^1_{-1} - T^1_{-1} U^1_1, \tag{6.6}$$

where tensorial components were defined in Eq. (5.2). From the selection rules for rank-one tensor, the allowed changes in quantum numbers for the spin and orbital angular momentum of initial and final states are: $\Delta L = 0, \pm 1$; $\Delta S = 0, \pm 1$; and $\Delta J = 0$.

The general expression for the basic quantity $f$ for the spatial part of transition matrix elements retains the form (5.33):

$$f = \left\langle k \middle| \frac{1}{r_{ij}} \boldsymbol{\nabla}' \boldsymbol{F}_{ij} \boldsymbol{\nabla} \middle| l \right\rangle + \left\langle \boldsymbol{\nabla}' k \middle| \frac{1}{r_{ij}} \boldsymbol{G}_{ij} \middle| \boldsymbol{\nabla} l \right\rangle . \tag{6.7}$$

However, matrices $\boldsymbol{F}_{ij}$ and $\boldsymbol{G}_{ij}$ will differ from those in Eqs. (5.34) and (5.35) — they retain the same pseudoparticle structure, but Cartesian parts will be different in the Kronecker product.

We denote the spin part of the SO operator as $\boldsymbol{T}_i \equiv (\mathcal{H}^{\sigma}_{\mathrm{SO}})_i$, and spatial — $\boldsymbol{U}_i \equiv (\mathcal{H}^{r}_{\mathrm{SO}})_i$. For brevity, in what follows, we omit the pseudoparticle index $i$ and indicate only tensor components in the subscripts of the operators.

We also note that for the considered transition matrix elements, the initial-state wave-function (a targeted state) is written on the left side (bra-vector), which is a non-standard convention. However, this does not lead to any inconveniences since the matrix elements with permuted states are the same, thanks to the Hermiticity of spin–orbit and spin–spin operators.

*Transition* $^3P_2 \to {}^1D_2$:

$$\left\langle {}^3P_2 \middle| \mathcal{H}_{\mathrm{SO}} \middle| {}^1D_2 \right\rangle . \tag{6.8}$$

The initial- and final-state wave functions corresponding to the maximum value of angular momentum projection in the uncoupled representation $|SM_S\, LM_L\rangle$ are:

$$\left| {}^3P_2 \right\rangle_{M_J=2} = |11\, 11\rangle , \tag{6.9}$$

$$\left| {}^1D_2 \right\rangle_{M_J=2} = |00\, 22\rangle . \tag{6.10}$$

The desired matrix element in the uncoupled representation is written as follows:

$$\left\langle {}^3P_2 \middle| \mathcal{H}_{\mathrm{SO}} \middle| {}^1D_2 \right\rangle = - \langle 11 | (\mathcal{H}^{\sigma}_{\mathrm{SO}})_1 | 00 \rangle \, \langle 11 | (\mathcal{H}^{r}_{\mathrm{SO}})_{-1} | 22 \rangle . \tag{6.11}$$

Spatial wave functions $|LM_L\rangle$ in the ECG basis set are:

$$
\begin{aligned}
|11\rangle &= \frac{1}{\sqrt{2}}\big(z_{i_l}(x_{j_l}+iy_{j_l}) - (x_{i_l}+iy_{i_l})z_{j_l}\big)\exp(-\boldsymbol{r}'\boldsymbol{C}_l\boldsymbol{r}),\\
|22\rangle &= \frac{1}{2}(x_{i_l}+iy_{i_l})(x_{j_l}+iy_{j_l})\exp(-\boldsymbol{r}'\boldsymbol{C}_l\boldsymbol{r}).
\end{aligned}
\tag{6.12}
$$

Matrices $\boldsymbol{F}_{ij}$, $\boldsymbol{G}_{ij}$ are defined as:

$$
\begin{aligned}
\boldsymbol{F}_{ij} &= (E_{ij}-E_{ji})\otimes\frac{1}{\sqrt{2}}(\boldsymbol{\epsilon}'_y\boldsymbol{\epsilon}_z + i\boldsymbol{\epsilon}'_x\boldsymbol{\epsilon}_z),\\
\boldsymbol{G}_{ij} &= E_{ij}\otimes\boldsymbol{K},\\
\boldsymbol{K} &= \frac{1}{\sqrt{2}}\begin{pmatrix} 0 & 0 & i\\ 0 & 0 & 1\\ -i & -1 & 0\end{pmatrix}.
\end{aligned}
\tag{6.13}
$$

The basic quantity $f$ in this case is just a linear combination of matrix elements that appear in the diagonal matrix elements of a $P$-state (see Eqs. (5.99), (5.104)):

$$
f = f^{01/01} + f^{01/10} - f^{10/01} - f^{10/10}. \tag{6.14}
$$

*Transition* ${}^3P_0 \to {}^1S_0$:

$$
\left\langle {}^3P_0\middle|\mathcal{H}_{\rm SO}\middle|{}^1S_0\right\rangle. \tag{6.15}
$$

As usual, we begin by writing out the wave functions in $|SM_S\,LM_L\rangle$ representation:

$$
\left|{}^3P_0\right\rangle = \frac{1}{\sqrt{3}}\left(|11\,1-1\rangle + |1-1\,11\rangle - |10\,10\rangle\right), \tag{6.16}
$$

$$
\left|{}^1S_0\right\rangle = |00\,00\rangle. \tag{6.17}
$$

Using the Wigner-Eckart theorem, we rewrite the above matrix element as:

$$
\left\langle {}^3P_0\middle|\mathcal{H}_{\rm SO}\middle|{}^1S_0\right\rangle = -\sqrt{3}\,\langle 11|(\mathcal{H}^{\sigma}_{\rm SO})_1|00\rangle\,\langle 1-1|(\mathcal{H}^{r}_{\rm SO})_{-1}|00\rangle. \tag{6.18}
$$

For the $S$-states of systems containing two $p$-electrons, we currently use basis functions without angular prefactors, i.e. corresponding to the case where all electrons are in $s$-states. Since the spatial parity of a wave function for the system with two $p$-electrons is the same as that for the system containing $s$-electrons only, such basis set can be used to construct a trial wave function. Although this basis is not natural for describing a system with two $p$-electrons, the wave function, and hence all expectation values, still converge to their true values with the increase in basis size, but with a slower rate. Thus, for the

basis wave function $|l\rangle$ of ${}^1S_0$ state, we take:

$$|l\rangle = |00\rangle = \exp(-\boldsymbol{r}'\boldsymbol{C}_l\boldsymbol{r}). \tag{6.19}$$

The matrix elements in the rhs of (6.7) are then expanded as follows:

$$\left\langle k\left|\frac{1}{r_{ij}}\boldsymbol{\nabla}'\boldsymbol{F}_{ij}\boldsymbol{\nabla}\right|l\right\rangle = 4\left\langle k\left|\frac{1}{r_{ij}}\boldsymbol{r}'(\boldsymbol{C}_l\boldsymbol{F}_{ij}\boldsymbol{C}_l)\boldsymbol{r}\right|k\right\rangle, \tag{6.20}$$

$$\left\langle \boldsymbol{\nabla}'k\left|\frac{1}{r_{ij}}\boldsymbol{G}_{ij}\right|\boldsymbol{\nabla}l\right\rangle = 4\left\langle k\left|\frac{1}{r_{ij}}\boldsymbol{r}'(\boldsymbol{C}_k^*\boldsymbol{G}_{ij}\boldsymbol{C}_l)\boldsymbol{r}\right|k\right\rangle - 2\left\langle k\left|\frac{1}{r_{ij}}\right|l\right\rangle_{\boldsymbol{w}_k\to\boldsymbol{C}_l^*\boldsymbol{G}_{ij}^\dagger\boldsymbol{w}_k} - \\ - 2\left\langle k\left|\frac{1}{r_{ij}}\right|l\right\rangle_{\boldsymbol{v}_k\to\boldsymbol{C}_l^*\boldsymbol{G}_{ij}^\dagger\boldsymbol{v}_k}, \tag{6.21}$$

where the matrices $\boldsymbol{F}_{ij}$, $\boldsymbol{G}_{ij}$ are defined in (6.13). The basic quantity $f$ for this transition is

$$f = 4i\frac{\pi^{(3n-1)/2}}{|C_{kl}|^{3/2}}\Big\{\frac{1}{3}\gamma_{ij}^3\big([v_k'C_{kl}^{-1}J_{ij}E_{ij}C_lC_{kl}^{-1}w_k] - [v_k'C_{kl}^{-1}C_lE_{ji}J_{ij}C_{kl}^{-1}w_k]\big) - \\ - \frac{1}{5}\gamma_{ij}^5\big([v_k'C_{kl}^{-1}J_{ij}E_{ij}C_lC_{kl}^{-1}J_{ij}C_{kl}^{-1}w_k] - [v_k'C_{kl}^{-1}J_{ij}C_{kl}^{-1}C_lE_{ji}J_{ij}C_{kl}^{-1}w_k]\Big\}. \tag{6.22}$$

In particular,

$$f[ii,ii] = i\frac{4}{3}\frac{\pi^{(3n-1)/2}}{|C_{kl}|^{3/2}}\gamma_{ii}^3\big[j^{i\prime}C_{kl}^{-1}v_k\ \cdot\ j^{i\prime}C_lC_{kl}^{-1}w_k\ -\ j^{i\prime}C_{kl}^{-1}w_k\ \cdot\ j^{i\prime}C_lC_{kl}^{-1}v_k\big], \tag{6.23}$$

$$f[ii,ij] = i\frac{4}{3}\frac{\pi^{(3n-1)/2}}{|C_{kl}|^{3/2}}\gamma_{ii}^3\big[j^{i\prime}C_{kl}^{-1}v_k\ \cdot\ j^{j\prime}C_lC_{kl}^{-1}w_k\ -\ j^{i\prime}C_{kl}^{-1}w_k\ \cdot\ j^{j\prime}C_lC_{kl}^{-1}v_k\big], \tag{6.24}$$

$$f[ij,jj] = i\frac{4}{3}\frac{\pi^{(3n-1)/2}}{|C_{kl}|^{3/2}}\gamma_{ij}^3\big[j^{j\prime}C_lC_{kl}^{-1}w_k\cdot(j^{j\prime}C_{kl}^{-1}v_k - j^{i\prime}C_{kl}^{-1}v_k) + \\ + j^{j\prime}C_lC_{kl}^{-1}v_k\cdot(j^{i\prime}C_{kl}^{-1}w_k - j^{j\prime}C_{kl}^{-1}w_k)\big]. \tag{6.25}$$

*Transition* ${}^3P_1 \to {}^1P_1$:

$$\left\langle {}^3P_1\middle|\mathcal{H}_{\rm SO}\middle|{}^1P_1\right\rangle. \tag{6.26}$$

The wave functions in the $|SM_S\, LM_L\rangle$ basis are:

$$\left|{}^3P_1\right\rangle_{M_J=1} = \frac{1}{\sqrt{2}}\left(|11\,10\rangle - |10\,11\rangle\right), \tag{6.27}$$

$$\left|{}^1P_1\right\rangle_{M_J=1} = |00\,11\rangle\,. \tag{6.28}$$

The matrix element $\langle {}^3P_1|\mathcal{H}_{\rm SO}|{}^1P_1\rangle$ is expanded as follows:

$$\left\langle {}^3P_1\middle|H_{\rm SO}\middle|{}^1P_1\right\rangle = \frac{1}{\sqrt{2}}\Bigg(\langle 11\,10|\mathcal{H}_{\rm SO}|00\,11\rangle - \langle 10\,11|H_{\rm SO}|00\,11\rangle\Bigg) =$$
$$= -\frac{1}{\sqrt{2}}\Bigg(\langle 11|(\mathcal{H}^{\sigma}_{\rm SO})_1|00\rangle\,\langle 10|(H^{r}_{\rm SO})_{-1}|11\rangle + \langle 10|(\mathcal{H}^{\sigma}_{\rm SO})_0|00\rangle\,\langle 11|(\mathcal{H}^{r}_{\rm SO})_0|11\rangle\Bigg). \tag{6.29}$$

Using the Wigner-Eckart theorem, one obtains:

$$\langle 11|(\mathcal{H}^{\sigma}_{\rm SO})_1|00\rangle\,\langle 10|(\mathcal{H}^{r}_{\rm SO})_{-1}|11\rangle = C^{11}_{00\,11}C^{10}_{11\,1-1}\,\langle 1||\mathcal{H}^{\sigma}_{\rm SO}||0\rangle\,\langle 1||\mathcal{H}^{r}_{\rm SO}||1\rangle =$$
$$= \frac{1}{\sqrt{2}}\,\langle 1||\mathcal{H}^{\sigma}_{\rm SO}||0\rangle\,\langle 1||\mathcal{H}^{r}_{\rm SO}||1\rangle\,, \tag{6.30}$$

$$\langle 10|(\mathcal{H}^{\sigma}_{\rm SO})_0|00\rangle\,\langle 11|(\mathcal{H}^{r}_{\rm SO})_0|11\rangle = C^{10}_{00\,10}C^{11}_{11\,10}\,\langle 1||\mathcal{H}^{\sigma}_{\rm SO}||0\rangle\,\langle 1||\mathcal{H}^{r}_{\rm SO}||1\rangle =$$
$$= \frac{1}{\sqrt{2}}\,\langle 1||H^{\sigma}_{\rm SO}||0\rangle\,\langle 1||\mathcal{H}^{r}_{\rm SO}||1\rangle\,. \tag{6.31}$$

Here the notation $\langle S||\mathcal{O}^{\sigma}||S'\rangle$ (respectively, $\langle L||\mathcal{O}^{r}||L'\rangle$) denotes the reduced matrix element of operator $\mathcal{O}^{\sigma}$(respectively, $\mathcal{O}^{r}$) between the states with the total spin $S$ and $S'$ (respectively, orbital angular momentum $L$ and $L'$).

Thus, the SO matrix element can be rewritten as:

$$\left\langle {}^3P_1\middle|\mathcal{H}_{\rm SO}\middle|{}^1P_1\right\rangle = -\,\langle 1||\mathcal{H}^{\sigma}_{\rm SO}||0\rangle\,\langle 1||\mathcal{H}^{r}_{\rm SO}||1\rangle = -\sqrt{2}\,\langle 11|(\mathcal{H}^{\sigma}_{\rm SO})_1|00\rangle\,\langle 11|(\mathcal{H}^{r}_{\rm SO})_0|11\rangle\,. \tag{6.32}$$

The spatial matrix element $\langle 11|(\mathcal{H}^{r}_{\rm SO})_0|11\rangle$ is a diagonal matrix element for a $P$-state and has been evaluated in section 5.3.2.

*Transition* ${}^3P_1 \to {}^3D_1$:

$$\left\langle {}^3P_1\middle|\mathcal{H}_{\rm SO}\middle|{}^3D_1\right\rangle. \tag{6.33}$$

The wave function for the ${}^3D_1$ in the $|SM_S\, LM_L\rangle$ basis is:

$$\left|{}^3D_1\right\rangle_{M_J=1} = \frac{1}{\sqrt{10}}\Bigg(\sqrt{6}\,|1-1\,22\rangle - \sqrt{3}\,|10\,21\rangle + |11\,20\rangle\Bigg). \tag{6.34}$$

Using the Wigner-Eckart theorem, one obtains the following expression for the desired

matrix element:

$$\left\langle {}^3P_1\middle|\mathcal{H}_{\rm SO}\middle|{}^3D_1\right\rangle = -\frac{1}{2}\left\langle 1||\mathcal{H}^{\sigma}_{\rm SO}||1\right\rangle \left\langle 1||\mathcal{H}^{r}_{\rm SO}||2\right\rangle = \\ = -\sqrt{\frac{5}{6}}\left\langle 11|(\mathcal{H}^{\sigma}_{\rm SO})_0|11\right\rangle \left\langle 11|(\mathcal{H}^{r}_{\rm SO})_{-1}|22\right\rangle . \quad (6.35)$$

The spatial matrix element $\langle 11|(H^r_{\rm SO})_{-1}|22\rangle$ has been calculated in (6.8).

*Transition* ${}^3P_2 \to {}^3D_2$:

$$\left\langle {}^3P_2\middle|\mathcal{H}_{\rm SO}\middle|{}^3D_2\right\rangle . \quad (6.36)$$

The wavefunction for the $|{}^3D_2\rangle$ state in the $|SM_S\, LM_L\rangle$ basis is:

$$\left|{}^3D_2\right\rangle_{M_J=2} = \frac{1}{\sqrt{3}}\Big(|11\,21\rangle - \sqrt{2}\,|10\,22\rangle\Big). \quad (6.37)$$

The transition matrix element in terms of the reduced ones is written as follows:

$$\left\langle {}^3P_2\middle|\mathcal{H}_{\rm SO}\middle|{}^3D_2\right\rangle = -\frac{3}{2\sqrt{5}}\left\langle 1||\mathcal{H}^{\sigma}_{\rm SO}||1\right\rangle \left\langle 1||\mathcal{H}^{r}_{\rm SO}||2\right\rangle = \frac{3}{\sqrt{5}}\left\langle {}^3P_1\middle|\mathcal{H}_{\rm SO}\middle|{}^3D_1\right\rangle . \quad (6.38)$$

Thus, we reduced the evaluation of the given matrix element to the previously considered case.

*Transition* ${}^3P_1 \to {}^3S_1$:

$$\left\langle {}^3P_1\middle|\mathcal{H}_{\rm SO}\middle|{}^3S_1\right\rangle . \quad (6.39)$$

The wavefunction for the $|{}^3S_1\rangle$ state in the $|SM_S\, LM_L\rangle$ basis is:

$$\left|{}^3S_1\right\rangle_{M_J=1} = |11\,00\rangle . \quad (6.40)$$

The transition matrix elements is written as follows:

$$\left\langle {}^3P_1\middle|H_{\rm SO}\middle|{}^3S_1\right\rangle = \left\langle 1||H^{\sigma}_{\rm SO}||1\right\rangle \left\langle 1||H^{r}_{\rm SO}||0\right\rangle = \sqrt{2}\left\langle 11|(H^{\sigma}_{\rm SO})_0|11\right\rangle \left\langle 1-1|(H^{r}_{\rm SO})_{-1}|00\right\rangle . \quad (6.41)$$

The spatial matrix element in the latter expression has been evaluated previously when we considered the transition ${}^3P_0 \to {}^1S_0$ in (6.15).

Now, we come to the transitions relevant for the carbon ${}^3D$ state.

*Transition* ${}^3D_1 \to {}^1P_1$:

$$\left\langle {}^3D_1\middle|\mathcal{H}_{\rm SO}\middle|{}^1P_1\right\rangle . \quad (6.42)$$

Application of the Wigner-Eckart theorem yields:

$$\left\langle {}^1P_1 \middle| \mathcal{H}_{\mathrm{SO}} \middle| {}^3D_1 \right\rangle = -\frac{1}{\sqrt{3}} \langle 0||\mathcal{H}^{\sigma}_{\mathrm{SO}}||1\rangle \langle 1||\mathcal{H}^{r}_{\mathrm{SO}}||2\rangle = -\sqrt{\frac{5}{3}} \langle 00|(\mathcal{H}^{\sigma}_{\mathrm{SO}})_{-1}|11\rangle \langle 11|(\mathcal{H}^{r}_{\mathrm{SO}})_{-1}|22\rangle . \tag{6.43}$$

The spatial matrix element $\langle 11|(\mathcal{H}^{r}_{\mathrm{SO}})_{-1}|22\rangle$ was evaluated previously for the transition ${}^3P_2 \to {}^1D_2$ in (6.8).

*Transition* ${}^3D_2 \to {}^1D_2$:

$$\left\langle {}^3D_2 \middle| \mathcal{H}_{\mathrm{SO}} \middle| {}^1D_2 \right\rangle . \tag{6.44}$$

The desired matrix element is rewritten as:

$$\left\langle {}^3D_2 \middle| \mathcal{H}_{\mathrm{SO}} \middle| {}^1D_2 \right\rangle = -\langle 1||\mathcal{H}_{\mathrm{SO}}||0\rangle \langle 2||\mathcal{H}_{\mathrm{SO}}||2\rangle = -\sqrt{\frac{3}{2}} \langle 11|(\mathcal{H}^{\sigma}_{\mathrm{SO}})_1|00\rangle \langle 22|(\mathcal{H}^{r}_{\mathrm{SO}})_0|22\rangle . \tag{6.45}$$

The spatial matrix element $\langle 22|(\mathcal{H}^{r}_{\mathrm{SO}})_0|22\rangle$ was evaluated for the case of a diagonal $D$-state in section 5.3.2.

### 6.3 Matrix elements of spin–spin operator

We denote the spin and spatial tensors from Eqs. (5.12) and (5.13) as $\boldsymbol{T}_{ij} \equiv (\mathcal{H}^{\sigma}_{\mathrm{SS}})_{ij}$, $\boldsymbol{U}_{ij} \equiv (\mathcal{H}^{r}_{\mathrm{SS}})_{ij}$. Then, the basic quantity $g_{ij}$ is related to $\mathcal{H}^{r}_{\mathrm{SS}}$ as follows:

$$(\mathcal{H}^{r}_{\mathrm{SS}})_{ij} = \frac{q_i q_j}{m_i m_j} g_{ij}. \tag{6.46}$$

In the following derivations, we will not write the pseudoparticle indices $i, j$, implicitly assuming them. The general expression for $g$ reads (cf. (5.63)):

$$g = \left\langle k \middle| \left( \left[ \boldsymbol{\nabla}^{(1)}_i \times \boldsymbol{\nabla}^{(1)}_j \right]^{(2)}_q \frac{1}{r_{ij}} \right) \middle| l \right\rangle . \tag{6.47}$$

The choice of tensor component $q$ in the matrix element depends on the specific transition being considered.

For the ground triplet $P$ state of carbon, only the matrix elements with the ${}^3D$ states do not vanish.

*Transition* ${}^3P_1 \to {}^3D_1$:

$$\left\langle {}^3P_1 \middle| \mathcal{H}_{\mathrm{SS}} \middle| {}^3D_1 \right\rangle . \tag{6.48}$$

The application of the Wigner-Eckart Theorem yields:

$$\left\langle {}^3P_1\middle|\mathcal{H}_{\rm SS}\middle|{}^3D_1\right\rangle = \frac{3}{2\sqrt{5}}\left\langle 1||\mathcal{H}^{\sigma}_{\rm SS}||1\right\rangle\left\langle 1||H^{r}_{\rm SS}||2\right\rangle = 3\sqrt{\frac{5}{2}}\left\langle 11|(\mathcal{H}^{\sigma}_{\rm SS})_0|11\right\rangle\left\langle 11|(\mathcal{H}^{r}_{\rm SS})_{-1}|22\right\rangle. \tag{6.49}$$

The component $(\mathcal{H}^r_{\rm SS})_{-1}$ can be written via (5.4) as:

$$(\mathcal{H}^r_{\rm SS})_{-1} = \frac{q_iq_j}{m_im_j}\left[\boldsymbol{\nabla}^{(1)}_i\times\boldsymbol{\nabla}^{(1)}_j\right]^{(2)}_{-1} = \frac{q_iq_j}{m_im_j}\frac{1}{\sqrt{2}}\left(\frac{\boldsymbol{\nabla}_{i,x}-i\boldsymbol{\nabla}_{i,y}}{\sqrt{2}}\boldsymbol{\nabla}_{j,z}+\boldsymbol{\nabla}_{i,z}\frac{\boldsymbol{\nabla}_{j,x}-i\boldsymbol{\nabla}_{j,y}}{\sqrt{2}}\right). \tag{6.50}$$

Then the basic matrix element $g$ is expanded as follows:

$$g = \frac{1}{\sqrt{2}}\left(\left\langle\boldsymbol{\nabla}'\boldsymbol{D_{ij}}\boldsymbol{\nabla}k\middle|\frac{1}{r_{ij}}\middle|l\right\rangle+\left\langle k\middle|\frac{1}{r_{ij}}\middle|\boldsymbol{\nabla}'\boldsymbol{D_{ij}}\boldsymbol{\nabla}l\right\rangle+2\left\langle\boldsymbol{\nabla}'k\middle|\frac{1}{r_{ij}}\boldsymbol{D_{ij}}\middle|\boldsymbol{\nabla}l\right\rangle\right)\equiv$$
$$\equiv\frac{1}{\sqrt{2}}\left(g^{(2,0)}+g^{(0,2)}+2g^{(1,1)}\right), \tag{6.51}$$

where the matrix $\boldsymbol{D}_{ij}$ is defined as:

$$\begin{aligned}\boldsymbol{D}_{ij} &= D_{ij}\otimes\boldsymbol{\Upsilon}, \text{ where}\\ D_{ij} &= \frac{1}{2}(E_{ij}+E_{ji}),\\ \boldsymbol{\Upsilon} &= \frac{1}{\sqrt{2}}\begin{pmatrix}0&0&1\\0&0&-i\\1&-i&0\end{pmatrix}.\end{aligned} \tag{6.52}$$

Note that matrix $\boldsymbol{D}$ is symmetric and traceless. However, it is not real, as was in the diagonal case.

If we introduce quantity $h$ (note that up to a common factor it is the same as in the case with the diagonal $D$-state (5.118)):

$$h = \sqrt{2}\frac{\pi^{(3n-1)/2}}{|C_{kl}|^{3/2}}\left(\frac{1}{5}\gamma^5_{ij}[v'_kC^{-1}_{kl}J_{ij}C^{-1}_{kl}v_l][w'_kC^{-1}_{kl}w_l]-\frac{1}{7}\gamma^7_{ij}[v'_kC^{-1}_{kl}J_{ij}C^{-1}_{kl}v_l][w'_kC^{-1}_{kl}J_{ij}C^{-1}_{kl}w_l]\right), \tag{6.53}$$

we may write the expression for $g$ as follows:

$$g = -\big(h+h|_{v_l\leftrightarrow w_l}-h|_{v_k\leftrightarrow w_k}-h|_{v_k\leftrightarrow w_k,v_l\leftrightarrow w_l}\big). \tag{6.54}$$

*Transition* ${}^3P_2\to{}^3D_2$:

$$\left\langle {}^3P_2\middle|\mathcal{H}_{\rm SS}\middle|{}^3D_2\right\rangle. \tag{6.55}$$

We rewrite the matrix element as:

$$\left\langle {}^3P_2\middle|H_{\rm SS}\middle|{}^3D_2\right\rangle = -\frac{3}{10}\left\langle 1||H^{\sigma}_{\rm SS}||1\right\rangle\left\langle 1||H^{r}_{\rm SS}||2\right\rangle = -\frac{1}{\sqrt{5}}\left\langle {}^3P_1\middle|\mathcal{H}_{\rm SS}\middle|{}^3D_1\right\rangle, \tag{6.56}$$

where we expressed it through the matrix element considered previously.

*Transition* $^3D_1 \to {}^3S_1$:

$$\left\langle {}^3D_1 \middle| \mathcal{H}_{\rm SS} \middle| {}^3S_1 \right\rangle . \tag{6.57}$$

Applying the Wigner-Eckart theorem, we get:

$$\left\langle {}^3D_1 \middle| \mathcal{H}_{\rm SS} \middle| {}^3S_1 \right\rangle = \langle 1||\mathcal{H}^{\sigma}_{\rm SS}||1\rangle \, \langle 2||\mathcal{H}^{r}_{\rm SS}||0\rangle = \sqrt{10}\, \langle 11|(\mathcal{H}^{\sigma}_{\rm SS})_0|11\rangle \, \langle 22|(\mathcal{H}^{r}_{\rm SS})_2|00\rangle . \tag{6.58}$$

For this transition we need to evaluate the spatial matrix element $\langle 22|(\mathcal{H}^{r}_{\rm SS})_2|00\rangle$ with the ECG wave function $|l\rangle = |00\rangle$ given by (6.19). The operator $(\mathcal{H}^{r}_{\rm SS})_2$ is written as:

$$(\mathcal{H}^{r}_{\rm SS})_2 = \frac{1}{2}\frac{q_i q_j}{m_i m_j} \left(\boldsymbol{\nabla}_{i,x} + i\boldsymbol{\nabla}_{i,y}\right)\left(\boldsymbol{\nabla}_{j,x} + i\boldsymbol{\nabla}_{j,y}\right). \tag{6.59}$$

The basic matrix element $g$ is then expanded as follows:

$$\begin{aligned} g = \left\langle k \middle| \left( \left[ \boldsymbol{\nabla}_i^{(1)} \times \boldsymbol{\nabla}_j^{(1)} \right]^{(2)}_2 \frac{1}{r_{ij}} \right) \middle| l \right\rangle &= 4 \left\langle k \middle| \frac{1}{r_{ij}} \boldsymbol{r}'(\boldsymbol{C}_k^* \boldsymbol{D}_{ij} \boldsymbol{C}_k^*) \boldsymbol{r} \middle| l \right\rangle + \\ &+ 4 \left\langle k \middle| \frac{1}{r_{ij}} \boldsymbol{r}'(\boldsymbol{C}_l \boldsymbol{D}_{ij} \boldsymbol{C}_l) \boldsymbol{r} \middle| l \right\rangle + \left\langle k \middle| \frac{1}{r_{ij}} \boldsymbol{r}'(\boldsymbol{C}_k^* \boldsymbol{D}_{ij} \boldsymbol{C}_l + \boldsymbol{C}_l \boldsymbol{D}_{ij} \boldsymbol{C}_k^*) \boldsymbol{r} \middle| l \right\rangle - \\ - 4 \left\langle k \middle| \frac{1}{r_{ij}} \middle| l \right\rangle_{\boldsymbol{v}_k \to \boldsymbol{C}_{kl}^* \boldsymbol{D}_{ij}^\dagger \boldsymbol{v}_k} &- 4 \left\langle k \middle| \frac{1}{r_{ij}} \middle| l \right\rangle_{\boldsymbol{w}_k \to \boldsymbol{C}_{kl}^* \boldsymbol{D}_{ij}^\dagger \boldsymbol{w}_k} + 2 \boldsymbol{v}_k^\dagger \boldsymbol{D}_{ij} \boldsymbol{w}_k^* \left\langle \phi_k \middle| \frac{1}{r_{ij}} \middle| 00 \right\rangle_{\alpha_k = \beta_k = 0}, \end{aligned} \tag{6.60}$$

where the matrix $\boldsymbol{D}_{ij} = D_{ij} \otimes \boldsymbol{\Upsilon}$ with $D_{ij}$ defined in Eq. (6.52), and the matrix $\boldsymbol{\Upsilon}$ is:

$$\boldsymbol{\Upsilon} = \frac{1}{2} \begin{pmatrix} 1 & i & 0 \\ i & -1 & 0 \\ 0 & 0 & 0 \end{pmatrix}. \tag{6.61}$$

Evaluation of expression (6.60) yields:

$$g = -\frac{4\pi^{(3n-1)/2}}{5\,|C_{kl}|^{3/2}} \gamma^5_{ij} [v'_k C^{-1}_{kl} J_{ij} C^{-1}_{kl} w_k]. \tag{6.62}$$

# 7 Applications

The introduced algorithm for spin-dependent calculations for atoms with one and two $p$-electrons was successfully applied to calculate relativistic corrections in the positronic beryllium and study the fine structure of carbon. The first work was recently published in *Physical Review A* (Ref. [26]), while the second one is currently under review in *Physical Review Letters*.

## 7.1 Relativistic correction in positronic beryllium

### 7.1.1 Motivation and Background

A positron can bind to neutral atoms forming the positron–atom complexes. The first work verifying the stability of such systems was done for the ground state of positronic lithium [52, 53]. Later, the existence of bound states with positron was predicted for larger atoms [54–69]. Studying the stability of positron–atom complexes in excited states is especially important, as it would enable a comparison between experimental and theoretical spectroscopy of positronic atoms. However, an experimental realization of a positronic atom has not been achieved so far.

The binding energy of a positronic system is calculated as the difference between the energy of a parent (decoupled) system and a bound system. The positron–atom complex $e^+[A]$ can decay into an electron and a neutral atom — $e^+[A] \to e^+ + A$, or a positronium Ps (a bound state of electron and positron) and a positive ion — $e^+[A] \to A^+ + \mathrm{Ps}$. Depending on the decay channel, the binding energy is calculated in two different ways [26]:

$$\epsilon = E(A) - E(e^+[A]), \tag{7.1}$$

$$\epsilon = E(A^+) - 0.25 - E(e^+[A]), \tag{7.2}$$

corresponding to decay channels in positron and positronium, respectively. The value of $-0.25$ in (7.2) corresponds to the non-relativistic energy of positronium. It is worth noting, as pointed out in Ref. [62], that usually a neutral atom is capable of binding a positron when its ionization potential lies close to the ionization potential of a positronium (0.25 hartree).

Positronic atoms can be considered as a mixture of two configurations — a positron orbiting a slightly polarized nucleus, and a positronium interacting with an atomic ion. The prevalence of a particular state can be established by e.g. comparing the expectation values of interparticle distances (electron–electron, and electron–nucleus) in a parent atom and in an atom–positron complex.

With regard to positronic beryllium, the existence of bound ground $S$ and excited $P$ states was confirmed in Ref. [62]. However, the authors evaluated only the non-relativistic binding energies and estimated the influence of relativistic corrections on binding energies by evaluating the largest terms — Darwin and mass–velocity contributions. In our work [26], we evaluated all leading-order ($\propto \alpha^2$) relativistic corrections in positronic beryllium to study its influence on the dynamic stability in the ground singlet $S$ and excited triplet $S$ and $P$ states. My part of the work was to calculate the contribution coming from the non-contact spin–spin interaction.

### 7.1.2 Methods and Results

The relativistic corrections to the ground singlet $S$ and excited triplet $S$ and $P$ states were evaluated using the Dirac–Breit Hamiltonian presented in Section 4.2, extended to account for the presence of a positron. Specifically, the leading-order relativistic Hamiltonian included an additional annihilation term $\mathcal{H}_{\rm A}$:

$$\mathcal{H}_{\rm A} = -2\pi \sum_{\substack{i=1 \\ \text{over } e^+e^- \text{ pairs only}}}^{n} \sum_{j=1, j\neq i}^{n} \frac{q_i q_j}{m_i m_j} \left(\frac{3}{4} + \boldsymbol{s}_i' \boldsymbol{s}_j\right) \delta(\boldsymbol{r}_{ij}). \tag{7.3}$$

The non-relativistic wave functions were expanded through the thoroughly optimized ECG basis sets, corresponding to configurations when all particles are in $s$-states [70] (ground and excited $S$ states of positronic beryllium), or a single particle in a $p$-state [50] (excited $P$ state).

We considered the ground singlet $S$ state ($^{2;1}S$) and excited triplet $S$ ($^{2,4;3}S$) and $P$ states ($^{2,4;3}P$) of positronic beryllium. Here we denote an atomic term symbol as $^{2S+1;2S_e+1}L$, where $S$ is the total spin of a positronic atom, $S_e$ is the total spin of electrons only, $L$ is orbital angular momentum. The values separated by comma refer to different states — e.g. $^{2,4;3}S$ denotes two states $^{2;3}S$ and $^{4;3}S$. The ground state decays through the channel with a free positron in the final state, while the decays of excited states produce a positronium in the products.

In Table 1, we present the non-relativistic and relativistic binding energies of the mentioned states for the isotope $^9$Be and for the infinite nuclear mass limit (denoted as $^\infty$Be). These values were extrapolated to the infinite basis set limit and the numbers in parentheses represent the uncertainty due to basis set truncation. For all states, we used the maximum basis set of 6000 ECG functions. We found that the inclusion of relativistic corrections only slightly changes the binding energies of the considered states, by 2.2% or less.

The values of relativistic corrections for the parent atom/ion and positron–atom complex individually are each about $-2.3$ $m$hartree (see Ref. [26] for the contributions from each relativistic correction), which is comparable to the binding energies from Table 1. However, their difference, which enters the expressions for binding energy (7.1) or (7.2), is largely canceled out. This is because the dominant relativistic effects arise from the inner core electrons, whose configuration remains nearly unperturbed between the parent atom/ion and positron–atom complex. However, for the triplet $P$-state of positronic beryllium, this cancellation is less pronounced since $P$-states possess non-vanishing spin–spin and spin–orbit contributions which are absent in the parent $Be^+$ ion. Therefore, it is essential to account for spin-dependent relativistic corrections to binding energy. In Table 2, we present the expectation values of the spin–orbit and non-contact spin–spin Hamiltonians (without the factor of $\alpha^2$) for $P$-state of positronic beryllium. Note that the values are given for several different basis set sizes to demonstrate the convergence of

**Table 1:** Non-relativistic ($\epsilon_{\rm NR}$) and relativistic ($\epsilon_{\rm REL}$) positron binding energies (in $m$hartree) for different states of positronic beryllium. All values are extrapolated to the infinite basis set.

| $e^+$[A](state) | $\epsilon_{\rm NR}$ | $\epsilon_{\rm REL}$ |
|---|---|---|
| $e^+[^9\mathrm{Be}](^{2;1}S)$ | 3.256(1) | 3.250(1) |
| $e^+[^\infty\mathrm{Be}](^{2;1}S)$ | 3.254(1) | 3.247(1) |
| $e^+[^9\mathrm{Be}](^{2;3}S)$ | 3.137(5) | 3.136(5) |
| $e^+[^\infty\mathrm{Be}](^{2;3}S)$ | 3.138(5) | 3.138(5) |
| $e^+[^9\mathrm{Be}](^{4;3}S)$ | 3.137(5) | 3.120(5) |
| $e^+[^\infty\mathrm{Be}](^{4;3}S)$ | 3.138(5) | 3.121(5) |
| $e^+[^9\mathrm{Be}](^{2;3}P_{1/2})$ | 1.130(9) | 1.123(9) |
| $e^+[^\infty\mathrm{Be}](^{2;3}P_{1/2})$ | 1.132(9) | 1.125(9) |
| $e^+[^9\mathrm{Be}](^{2;3}P_{3/2})$ | 1.130(9) | 1.119(9) |
| $e^+[^\infty\mathrm{Be}](^{2;3}P_{3/2})$ | 1.132(9) | 1.120(9) |
| $e^+[^9\mathrm{Be}](^{4;3}P_{1/2})$ | 1.130(9) | 1.112(9) |
| $e^+[^\infty\mathrm{Be}](^{4;3}P_{1/2})$ | 1.132(9) | 1.113(9) |
| $e^+[^9\mathrm{Be}](^{4;3}P_{3/2})$ | 1.130(9) | 1.110(9) |
| $e^+[^\infty\mathrm{Be}](^{4;3}P_{3/2})$ | 1.132(9) | 1.111(9) |
| $e^+[^9\mathrm{Be}](^{4;3}P_{5/2})$ | 1.130(9) | 1.106(9) |
| $e^+[^\infty\mathrm{Be}](^{4;3}P_{5/2})$ | 1.132(9) | 1.107(9) |

our calculations.

The fine-structure splitting diagram is presented in Fig. 3. Notice that the characteristic value of fine-structure splitting is of the order of several $\mu$hartrees — three orders of magnitude smaller than the total relativistic corrections for a positron–atom complex, or a parent ion, which is about $-2.3$ $m$hartree. Nevertheless, due to the absence of cancellation of non-scalar spin-dependent terms, the influence of the latter on binding energies is not negligible, as clearly seen from the Table 1. It is also worth noting that the magnitude of spin–spin non-contact interaction is much smaller than that of spin–orbit. Finally, note that all fine-structure components of the quartet $^{4;3}P$ state still remain higher than those of a doublet $^{2;3}P$ state.

**Table 2:** Convergence of the spin–orbit and non-contact spin–spin operators' mean values $\langle \mathcal{H}_{\mathrm{SO(SSNC)}} \rangle_J / C_J^{\mathrm{SO(SSNC)}}$ (without the factor of $\alpha^2$) with the number of basis functions $\mathcal{K}$ for $e^+[^9\mathrm{Be}](^{2,4;3}P)$. Labels "high" and "low" stand for the states $e^+[^9\mathrm{Be}](^{4;3}P)$ and $e^+[^9\mathrm{Be}](^{2;3}P)$, respectively. Coefficients $C_J^{\mathrm{SO(SSNC)}}$ are calculated by formula (5.9). All values are given in a.u.

| $\mathcal{K}$ | $\langle \mathcal{H}_{\mathrm{SO1}} \rangle_{\mathrm{high}}$ | $\langle \mathcal{H}_{\mathrm{SO2}} \rangle_{\mathrm{high}}$ | $\langle \mathcal{H}_{\mathrm{SO1}} \rangle_{\mathrm{low}}$ | $\langle \mathcal{H}_{\mathrm{SO2}} \rangle_{\mathrm{low}}$ | $\langle \mathcal{H}_{\mathrm{SSNC}} \rangle_{\mathrm{high}}$ |
|---|---|---|---|---|---|
| | | | $^9$Be | | |
| 500 | 0.155 00 | −0.108 93 | 0.104 06 | −0.073 36 | 0.001 32 |
| 1000 | 0.147 82 | −0.103 05 | 0.099 29 | −0.069 46 | 0.001 22 |
| 2000 | 0.144 05 | −0.100 13 | 0.096 77 | −0.067 51 | 0.001 17 |
| 3000 | 0.143 14 | −0.099 39 | 0.096 16 | −0.067 02 | 0.001 16 |
| 4000 | 0.142 76 | −0.099 10 | 0.095 91 | −0.066 83 | 0.001 15 |
| 5000 | 0.142 56 | −0.098 94 | 0.095 77 | −0.066 72 | 0.001 15 |
| 6000 | 0.142 45 | −0.098 85 | 0.095 70 | −0.066 66 | 0.001 15 |
| | | | $^\infty$Be | | |
| 6000 | 0.142 45 | −0.098 84 | 0.095 70 | −0.066 66 | 0.001 15 |

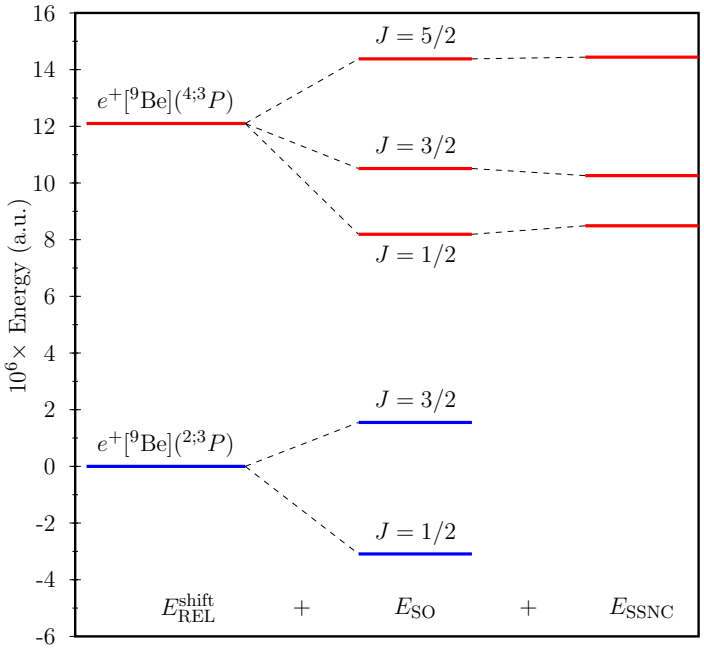


**Figure 3:** Fine-structure splitting of the $e^+[^9\mathrm{Be}](^{2;3}P)$ and $e^+[^9\mathrm{Be}](^{4;3}P)$ states. $E_{\mathrm{REL}}^{\mathrm{shift}}$ corresponds to the total relativistic energy without the spin–orbit and non-contact spin–spin corrections. The vertical axis in this figure is shifted so that $E_{\mathrm{REL}}^{\mathrm{shift}}$ is zero for the doublet state. The difference in $E_{\mathrm{REL}}^{\mathrm{shift}}$ between the doublet and quartet states comes from the Fermi contact and annihilation channel interactions. The non-contact spin–spin term for the doublet state vanishes due to the rotational symmetry.

## 7.2 Fine-structure calculations of neutral carbon

### 7.2.1 Motivation and Background

Carbon, the fourth most abundant element in the universe, exists in a wide range of environments — from interstellar clouds to complex chemical compounds on Earth. It forms the foundation of organic life on our planet and plays a key role in the chemical and thermal evolution of the interstellar medium (ISM) [71]. Due to its relatively low ionization energy of 11.26 eV [72, 73], carbon is primarily found in its ionized form (C II) throughout the ISM, while neutral carbon (C I) is prevalent in dense, UV-shielded regions. Inelastic collisions with electrons, protons, hydrogen atoms, and other particles, can excite the fine-structure levels of neutral and ionized carbon. These excitations are subsequently relaxed through the emission of far-infrared photons, effectively radiating away thermal energy and contributing to the cooling of the interstellar medium [74].

For carbon cation C II, high-precision calculations of the fine-structure splittings for the eight lowest Rydberg $^2P^o$ states have recently been reported in Ref. [9], achieving higher accuracy than that of the best available experimental data. In contrast, the fine-structure splittings of neutral carbon (C I) are still best determined from experimental measurements, with the most accurate values provided in the compilation by Haris and Kramida in the NIST Atomic Spectra Database (ASD) [72, 73]. Theoretical studies of C I remain scarce and have mostly concentrated on the ground state. A notable early attempt was made by Veseth in 1988, who employed many-body perturbation theory and included corrections for the electron's anomalous magnetic moment as well as approximate coupling with isoconfigurational $^1D$ and $^1S$ states [75]. However, the dominant off-diagonal spin–orbit matrix elements in his work were estimated from the experiment [76], making the results semi-empirical. The calculated fine-structure transition frequencies agreed with experiment at the level of 0.1–0.2 cm$^{-1}$. Since then, modest improvements have been made for the ground state; however, accurate theoretical predictions for excited states of neutral carbon are still absent. The most accurate theoretical calculations to date were carried out by Carette and Godefroid [77], who applied multiconfiguration Hartree–Fock (MCHF) method. Their calculated $J = 1 \to 0$ and $J = 2 \to 1$ transition frequencies deviate from experimental values by 0.03 cm$^{-1}$ and 0.08 cm$^{-1}$, respectively.

In this thesis, we present high-precision calculations of the fine-structure splittings for the ground and first excited triplet $P^e$ states, as well as the lowest triplet $D^e$ state of neutral carbon, using highly optimized explicitly correlated Gaussian (ECG) basis sets. We include the contribution from the electron's magnetic moment anomaly ($\propto \alpha^3$), along with the dominant second-order contributions ($\propto \alpha^4$) obtained through direct evaluation of the most significant off-diagonal spin–orbit and spin–spin interaction terms. We do not assume the Born–Oppenheimer approximation. Instead, nuclei and electrons are treated on equal footing, which enables automatic inclusion of nuclear recoil effects and enables for accurate determination of isotopic shifts for all three naturally occurring carbon iso-

topes. The resulting fine-structure intervals represent the most accurate theoretical values reported to date which agree with the experimental values at the level of 0.0001–0.01 $\mathrm{cm}^{-1}$.

### 7.2.2 Methods

To calculate fine-structure intervals, we used the perturbation series approach presented in section 4.3. To evaluate the leading-order ($\propto \alpha^2$), anomalous magnetic moment ($\propto \alpha^3$), and second-order perturbation theory corrections ($\propto \alpha^4$), we used formula (4.6), which we rewrite here for convenience:

$$E_{nJ} = \langle\psi|\mathcal{H}^{(2)}_{\mathrm{FS}}|\psi\rangle + \sum_{\phi\neq\psi} \frac{\left|\langle\phi|\mathcal{H}^{(2)}_{\mathrm{FS}}|\psi\rangle\right|^2}{E_\psi - E_\phi} + 2\sum_{\phi\neq\psi} \frac{\langle\psi|\mathcal{H}^{(2)}_{\mathrm{SR}}|\phi\rangle\langle\phi|\mathcal{H}^{(2)}_{\mathrm{FS}}|\psi\rangle}{E_\psi - E_\phi} + \langle\psi|\mathcal{H}^{(4)}_{\mathrm{FS}}|\psi\rangle, \quad (7.4)$$

where $|\psi\rangle = |nLSJM_J\rangle$ is a targeted state.

The diagonal and off-diagonal matrix elements of the fine-structure Hamiltonian $\mathcal{H}^{(2)}_{\mathrm{FS}}$ were computed using non-relativistic wave functions expanded through highly optimized explicitly correlated Gaussian (ECG) basis sets [39, 70]. For all targeted states considered in this work, the dominant $\alpha^4$ contribution arises from the second term in Eq. (7.4). As will be shown below, the primary source of this contribution is the off-diagonal matrix elements between isoconfigurational states. Therefore, the perturbative sum in Eq. (7.4) can be truncated once the desired numerical convergence is achieved.

The third term in Eq. (7.4) involves off-diagonal couplings through the scalar relativistic Hamiltonian $\mathcal{H}^{(2)}_{\mathrm{SR}}$. Due to its rotational invariance, only matrix elements between the states with identical orbital angular momentum and spin survive. The Hamiltonian $\mathcal{H}^{(2)}_{\mathrm{SR}}$ comprises the mass–velocity, Darwin, Fermi contact spin–spin, and orbit–orbit interactions. Among these, the mass–velocity and Darwin terms provide the largest corrections, while the orbit–orbit contribution is expected to be about two orders of magnitude smaller [78–80], which is below the accuracy of our calculations. Thus, we did not include the contribution from the orbit–orbit interaction.

We also note that all off-diagonal matrix elements of $\mathcal{H}^{(2)}_{\mathrm{SR}}$ were evaluated directly, without applying regularization techniques to enhance numerical convergence. This approach is sufficient for our purposes, as the overall contribution of these terms to the fine-structure splittings is small, of the order of $10^{-4}$ $\mathrm{cm}^{-1}$.

The evaluation of the fourth term with $\mathcal{H}^{(4)}_{\mathrm{FS}}$ in Eq. (7.4) represents a more challenging computational task and we did not include it in the present calculations. However, we do provide a rough estimate of the numerical uncertainty that results from neglecting this contribution.

### 7.2.3 Results

We studied the fine-structure of the carbon atom in its ground $1\,^3P^e$ state as well as the first excited $2\,^3P^e$ state and the lowest $1\,^3D^e$ state. In the perturbative expansion

**Table 3:** Non-relativistic energies of even-parity states of most common carbon isotopes. $\mathcal{K}$ denotes the ECG basis size used in the calculations. Entries marked with $\infty$ correspond to the extrapolated energies when $\mathcal{K} \to \infty$. Figures in parentheses represent the numerical uncertainty of the extrapolation.

| Config. | State | $\mathcal{K}$ | Energy | | | |
|---|---|---|---|---|---|---|
| | | | $^{12}$C | $^{13}$C | $^{14}$C | $^{\infty}$C |
| $1s^22s^22p^2$ | $1\,^3P$ | 9000 | −37.843 182 | −37.843 314 | −37.843 427 | −37.844 894 |
| | | $\infty$ | −37.843 189(7) | −37.843 321(7) | −37.843 434(7) | −37.844 901(7) |
| | $1\,^1D$ | 6000 | −37.796 832 | −37.796 964 | −37.797 077 | −37.798 543 |
| | | $\infty$ | −37.796 850(19) | −37.796 983(19) | −37.797 095(19) | −37.798 562(19) |
| | $1\,^1S$ | 6000 | −37.744 670 | −37.744 802 | −37.744 915 | −37.746 380 |
| | | $\infty$ | −37.744 684(14) | −37.744 816(14) | −37.744 929(14) | −37.746 394(14) |
| $1s^22s^22p3p$ | $1\,^1P$ | 6000 | −37.529 425 | −37.529 558 | −37.529 670 | −37.531 139 |
| | | $\infty$ | −37.529 437(11) | −37.529 569(11) | −37.529 682(11) | −37.531 150(11) |
| | $1\,^3D$ | 9000 | −37.525 489 | −37.525 621 | −37.525 734 | −37.527 203 |
| | | $\infty$ | −37.525 497(8) | −37.525 629(8) | −37.525 742(8) | −37.527 211(8) |
| | $1\,^3S$ | 6000 | −37.520 789 | −37.520 921 | −37.521 034 | −37.522 502 |
| | | $\infty$ | −37.520 820(32) | −37.520 952(32) | −37.521 065(32) | −37.522 534(32) |
| | $2\,^3P$ | 9000 | −37.517 959 | −37.518 091 | −37.518 204 | −37.519 673 |
| | | $\infty$ | −37.517 970(12) | −37.518 103(12) | −37.518 216(12) | −37.519 684(12) |
| | $2\,^1D$ | 6000 | −37.512 299 | −37.512 431 | −37.512 544 | −37.514 013 |
| | | $\infty$ | −37.512 327(28) | −37.512 459(28) | −37.512 572(28) | −37.514 041(28) |
| | $2\,^1S$ | 6000 | −37.506 044 | −37.506 176 | −37.506 289 | −37.507 758 |
| | | $\infty$ | −37.506 091(47) | −37.506 223(47) | −37.506 336(47) | −37.507 805(47) |
| $1s^22s^22p4p$ | $2\,^1P$ | 6000 | −37.476 057 | −37.476 189 | −37.476 302 | −37.477 769 |
| | | $\infty$ | −37.476 079(22) | −37.476 211(22) | −37.476 324(22) | −37.477 791(22) |
| | $2\,^3D$ | 6000 | −37.474 919 | −37.475 051 | −37.475 164 | −37.476 631 |
| | | $\infty$ | −37.474 945(26) | −37.475 077(26) | −37.475 190(26) | −37.476 658(26) |
| | $2\,^3S$ | 6000 | −37.473 505 | −37.473 637 | −37.473 750 | −37.475 218 |
| | | $\infty$ | −37.473 574(69) | −37.473 706(69) | −37.473 819(69) | −37.475 286(69) |
| | $3\,^3P$ | 6000 | −37.472 535 | −37.472 667 | −37.472 780 | −37.474 247 |
| | | $\infty$ | −37.472 567(32) | −37.472 699(32) | −37.472 812(32) | −37.474 280(32) |
| | $3\,^1D$ | 6000 | −37.470 546 | −37.470 679 | −37.470 791 | −37.472 259 |
| | | $\infty$ | −37.470 583(36) | −37.470 715(36) | −37.470 828(36) | −37.472 295(36) |
| | $3\,^1S$ | 6000 | −37.468 255 | −37.468 387 | −37.468 500 | −37.469 967 |
| | | $\infty$ | −37.468 376(122) | −37.468 509(122) | −37.468 621(122) | −37.470 089(122) |

in Eq. (7.4), we included off-diagonal matrix elements involving other even-parity states. Matrix elements between the states of mixed parity vanish due to parity inversion symmetry. To obtain the estimate of the second-order perturbation series contribution, we restricted ourselves to the states corresponding to the electronic configurations $1s^22s^22p^2$, $1s^22s^22p3p$, and $1s^22s^22p4p$. These states are listed in Table 3.

For each state, we report the non-relativistic energy to demonstrate the convergence at the non-relativistic level of theory. In fact, the energies presented in Table 3 represent the most accurate non-relativistic energies for carbon reported to date. The three targeted states were computed using an extensive basis of 9000 ECG functions, while the remaining states — entering only through second-order perturbative corrections — were calculated with smaller basis sets comprising 6000 ECGs.

In addition to the non-relativistic energies obtained with the largest basis sets, Table 3 also includes values extrapolated to the infinite basis set limit.

Our ground-state energy for the $^{12}$C isotope, −37.843 182 304 hartree, obtained using

**Table 4:** The values of the spin–orbit matrix elements, $\langle\cdot|\mathcal{H}_{\mathrm{SO}}|\cdot\rangle$, for the three targeted triplet states in the case of $^{12}$C isotope. The presented matrix elements correspond to the largest possible value of the total angular momentum $J$. Note that certain matrix elements vanish due to the rotational symmetry. The numbers in parentheses represent the extrapolation uncertainty. All values are in a.u.

| $\langle\cdot\vert$ \ $\vert\cdot\rangle$ | $1\,^3P^e$ | $1\,^3D^e$ | $2\,^3P^e$ |
|---|---|---|---|
| $1\,^3P^e$ | 1.196 676(5) | 0.607 81(4) | −0.142 59(4) |
| $1\,^1D^e$ | 1.981 759(3) | −0.928 0(2) | −0.233 2(2) |
| $1\,^1S^e$ | −3.832 767(4) | 0 | 0.297 7(2) |
| $1\,^1P^e$ | 0.525 18(2) | 1.725 78(2) | 1.153 95(4) |
| $1\,^3D^e$ | 0.607 81(4) | 1.880 577(6) | 1.437 137(6) |
| $1\,^3S^e$ | 0.768 2(1) | 0 | 1.949 57(1) |
| $2\,^3P^e$ | −0.142 59(4) | 1.437 137(6) | 0.923 47(1) |
| $2\,^1D^e$ | −0.294 80(4) | −1.987 95(6) | 1.327 97(1) |
| $2\,^1S^e$ | 0.566 5(1) | 0 | −2.586 3(1) |
| $2\,^1P^e$ | −0.278 45(3) | 0.012 0(4) | 0.231 2(2) |
| $2\,^3D^e$ | 0.330 96(3) | 0.043 4(6) | −0.219 1(4) |
| $2\,^3S^e$ | 0.432 6(2) | 0 | −0.190 1(9) |
| $3\,^3P^e$ | 0.089 24(2) | −0.073 0(6) | −0.013 3(3) |
| $3\,^1D^e$ | 0.178 08(2) | 0.222 5(9) | −0.119 9(5) |
| $3\,^1S^e$ | 0.337 9(3) | 0 | −0.406 1(9) |

9000 ECG functions, is approximately 5 $\mu$hartree lower, and therefore more accurate, than the value of −37.843 177 408 hartree reported by Strasburger [81], who employed 5896 ECG lobe functions.

A comparable level of precision is achieved in our calculations of the excited states. However, direct comparison with other high-accuracy studies is challenging due to the scarcity of such calculations. For example, for the $1\,^1D$ state of $^\infty$C, Carette and Godefroid [77] reported an energy of −37.798 111 hartree using the MCHF method. This value is in reasonable agreement with our result of −37.798 543 hartree obtained with 6000 ECGs and the extrapolated value of −37.798 562(19) hartree.

The spin–orbit and spin–spin matrix elements for the targeted states are listed in Tables 4 and 5. One can notice that the matrix elements between states of the same electronic configuration are significantly larger than those involving states of different configurations. The contribution of states with distinct configurations to the fine structure splitting is further diminished by their larger energy separations. Another noteworthy point is that the spin–spin matrix elements are two to four orders of magnitude smaller than the corresponding spin–orbit terms. Nevertheless, the inclusion of the electron spin–spin non-contact interaction is essential for reaching the desired accuracy of our results.

**Table 5:** The values of the electron spin–spin matrix elements, $\langle\cdot|\mathcal{H}_{\rm SSNC}|\cdot\rangle \times 10^3$ a.u., for the the three targeted triplet states of $^{12}$C. We show the matrix elements that correspond to the largest possible value of the total angular momentum $J$. The numbers in parentheses represent the extrapolation uncertainty.

| $\langle\cdot\vert$ \ $\vert\cdot\rangle$ | $1\,^3P^e$ | $1\,^3D^e$ | $2\,^3P^e$ |
|---|---|---|---|
| $1\,^3P^e$ | −13.351 5(2) | −4.779 2(5) | 3.863 2(3) |
| $1\,^3D^e$ | −4.779 2(5) | 0.562 4(2) | −0.406 9(3) |
| $1\,^3S^e$ | 0 | 2.181 2(4) | 0 |
| $2\,^3P^e$ | 3.863 2(3) | −0.406 9(3) | −1.419 21(1) |
| $2\,^3D^e$ | −2.946(3) | 0.241 8(4) | 0.042(2) |
| $2\,^3S^e$ | 0 | 0.958 9(7) | 0 |
| $3\,^3P^e$ | −2.297 8(2) | 0.119 3(4) | 0.824 8(2) |

The primary result of this work — the calculated fine-structure splittings for $^{12}$C — are presented in Table 6. To illustrate the relative importance of each contribution, the splittings are also provided at different levels of theory ($\alpha^2$, $\alpha^3$, and $\alpha^4$). It is evident that the inclusion of second-order corrections plays a crucial role in bringing the calculated values closer to the experimental ones, achieving an accuracy of 0.01 cm$^{-1}$ or better. This is particularly significant for the $2\,^3P^e$ and $1\,^3D^e$ states with the $2p3p$ configuration, as neighboring states with the same electronic configuration are close to each other on the energy scale.

The data presented in Table 6 is visualized in Figure 4. Notably, for five out of the six fine-structure splittings examined in this study, the second-order $\alpha^4$ correction is considerably larger than the $\alpha^3$ correction due to the electron magnetic moment anomaly. An important observation is that, at the $\alpha^4$ level, the dominant contribution comes from the couplings with isoconfigurational states. For each fine-structure splitting, we also include the results from the most accurate previous theoretical calculations. The most accurate values for the ground state were reported by Carette and Godefroid [77] and Froese Fischer and Tachiev [82], who employed MCHF calculations within the Breit–Pauli approximation. For the excited triplet states, the only available result is from Stancalie [85], obtained using the general-purpose relativistic atomic structure package GRASP [86]. Overall, our calculations provide significantly more accurate fine-structure intervals, with an improvement of nearly three orders of magnitude, especially for the excited states.

For our final results, we report three sources of uncertainty that contribute to the total uncertainty of the calculated fine-structure splittings. These include: the uncertainty due to truncation of the ECG basis set, the uncertainty arising from the truncation of the second-order perturbation theory summation, and the estimated uncertainty associated with the neglected $\langle\mathcal{H}^{(4)}_{\rm FS}\rangle$ term and higher-order contributions in Eq. (7.4).

The basis set truncation uncertainty was estimated by analyzing the numerical convergence of the values with the increase of basis size. The uncertainty due to the truncated

second-order perturbation series was conservatively estimated as half the sum of the absolute contributions from the $1s^22s^22p4p$ states. To ensure the convergence of the perturbation sums in Eq. (7.4), we also included two additional excited states with $1s^22s^22p5p$ configurations and found their impact to be negligible for the level of precision pursued.

A rough estimate of the uncertainty from the omitted $\langle \mathcal{H}^{(4)}_{\rm FS} \rangle$ term was made based on the nuclear charge scaling of QED corrections. In hydrogen-like systems, the $\alpha^4$ QED correction to the fine-structure splitting scales as $Z^6$, implying that the dominant contribution in carbon stems from electron–nucleus interactions. Using Slater's rules [87], the effective nuclear charge experienced by $p$-electrons in the ground state of carbon is estimated to be $Z^{\rm C}_{\rm eff} = 3.25$. Multiplying the known hydrogenic $\alpha^4$ QED contribution ($\approx 2.55 \times 10^{-5}$ cm$^{-1}$) [88] by $(Z^{\rm C}_{\rm eff})^6$ yields a value of approximately 0.03 cm$^{-1}$.

Using the known values of the fine-structure QED contributions for lithium [22] and helium [89, 90], along with their effective nuclear charges, and applying the same $Z^6$ scaling argument, we arrive at estimates for carbon in the range of 0.02–0.05 cm$^{-1}$. This agreement supports the validity of our simple estimate. Based on this reasoning, we assign an uncertainty of 0.03 cm$^{-1}$ to all transitions in Table 6 to account for the omitted $\langle \mathcal{H}^{(4)}_{\rm FS} \rangle$ term and higher-order corrections.

It is interesting to compare our fine-structure splittings for neutral carbon with the recent ECG calculations for the five-electron carbon cation by Stanke *et al.* [9]. The ground state splitting of 63.37 cm$^{-1}$ in the $^2P$ state of $C^+$ is significantly larger. This can be attributed to the greater effective nuclear charge experienced by the $p$-electron, as well as the fact that the leading-order contribution to the fine structure splitting from the one-electron spin-orbit interaction scales as $Z^4_{\rm eff}$.

Since our calculations do not rely on the Born–Oppenheimer approximation and both the wave function and all operators account for nuclear mass dependence, we can determine the isotopic shifts $\Delta\nu$ in the fine structure splittings relative to $^{12}$C. These values are presented in Table 7. For the isotopic shift in the ground state of $^{13}$C, we also include the most accurate calculations, along with data from the NIST Atomic Spectra Database [72, 73].

Unlike $^{12}$C and $^{14}$C, the $^{13}$C isotope has a nonzero nuclear spin ($I = 1/2$), leading to hyperfine structure. Haris and Kramida [72] determined the fine structure splittings for $^{13}$C by calculating the center-of-gravity of hyperfine structure transitions.

As shown in Table 7, our calculated isotopic shifts are significantly larger than those from Ref. [72], with discrepancies of 5.0 and 5.5 $\sigma$ (here and further $\sigma$ refers to an estimated total uncertainty) for the $J = 1 \to 0$ and $J = 2 \to 1$ transitions, respectively. Notably, other theoretical calculations also report higher values. Kozlov *et al.* [91] employed all-electron configuration interaction method with the Dirac–Breit Hamiltonian and found values of $\Delta\nu_{01} = 9.27 \times 10^{-5}$ and $\Delta\nu_{12} = 20.1 \times 10^{-5}$ cm$^{-1}$ for the $J = 1 \to 0$ and $J = 2 \to 1$ transitions. Similarly, many-body perturbation theory calculations by Veseth [92] yielded $\Delta\nu_{01} = 10.3 \times 10^{-5}$ and $\Delta\nu_{12} = 15.0 \times 10^{-5}$ cm$^{-1}$. The MCHF calculations

by Carette and Godefroid [77], incorporating relativistic corrections from Veseth [92], reported $\Delta\nu_{12} = 14 \times 10^{-5}$ cm$^{-1}$, which is closer to the NIST value of $13.78 \times 10^{-5}$ cm$^{-1}$. However, the numerical uncertainties associated with all results in Refs. [77, 91, 92] are difficult to quantify and probably quite large, potentially ranging from 30% to 50% of the reported values.

To better understand the discrepancy between our theoretical isotopic shifts and the NIST ASD values, we performed further analysis. The fine-structure levels of $^{13}$C reported by the NIST ASD were obtained by averaging experimental hyperfine structure transition frequencies, with the weights corresponding to the relative theoretical intensities of the transitions [72]. However, this method is only accurate up to the order of $\alpha^3$. To achieve higher accuracy, it is necessary to include the dominant second-order perturbation contribution, specifically the coupling between states with different $J$ values but the same total angular momentum $\boldsymbol{F} = \boldsymbol{I} + \boldsymbol{J}$, where $I$ is the nuclear spin.

We performed calculations using the hyperfine structure Hamiltonian from Ref. [24] and obtained second-order shifts of $1.2 \times 10^{-6}$ and $2.5 \times 10^{-7}$ cm$^{-1}$ for the $F = 1/2$ and $F = 3/2$ levels. While the details of the hyperfine structure calculations are not the primary focus of our work, we note that our results for the second-order shifts are in good agreement with the calculations by Jönsson and Froese Fischer [93], who reported second-order corrections of $1.2 \times 10^{-6}$ and $2.7 \times 10^{-7}$ cm$^{-1}$ for $F = 1/2$ and $F = 3/2$ levels, which are close to our values. More details of evaluation of the matrix elements for hyperfine interaction and the results for the hyperfine splittings of the ground state of carbon $^{13}$C are provided in the appendices A and B.

After correcting the NIST ASD data for the dominant $\alpha^4$ contribution to the hyperfine structure components, we obtain isotopic shifts of $\Delta\nu_{01} = 7.52 \times 10^{-5}$ and $\Delta\nu_{12} = 13.66 \times 10^{-5}$ cm$^{-1}$. This reduces the discrepancy to 4.5 $\sigma$ for the $J = 1 \to 0$ transition, while the discrepancy increases to 6.5 $\sigma$ for the $J = 2 \to 1$ transition. Other contributions to the fine-structure isotopic shift, including finite nuclear size effects and $\alpha^4$ relativistic and QED corrections, are estimated to be smaller than the numerical uncertainties. It is possible that the remaining discrepancy arises from fine-hyperfine mixing or an inaccurate estimate of the QED contribution, but further in-depth studies would be required to investigate this.

Nevertheless, the isotopic shifts in the fine structure splittings reported in this work represent the most accurate theoretical values to date.

**Table 6:** Fine-structure splittings (in $\mathrm{cm}^{-1}$) for the ground and lowest excited triplet states of $^{12}$C. $\delta_{\mathrm{AMM}}$ stands for the $\alpha^3$ contribution due to the electron anomalous magnetic moment. $\delta_{\mathrm{offdiag}}$ are the $\alpha^4$ second-order perturbation theory corrections: $\delta^{\mathrm{isoconf}}_{\mathrm{offdiag}}$ denotes the contribution of the isoconfigurational states, while $\delta^{\mathrm{full}}_{\mathrm{offdiag}}$ stands for the contribution of all states. The final theoretical values are shown with three separate numerical uncertainties: the first represents the ECG basis truncation uncertainty, second – the uncertainty due to the finite number of states used in the second-order perturbation theory, and the last one is an uncertainty due to the omitted $\langle \mathcal{H}^{(4)}_{\mathrm{FS}} \rangle$ term in (7.4).

| Transition | Contribution | $^{12}$C |
|---|---|---|
| $1\,^3P^e_1 \to 1\,^3P^e_0$ | $\alpha^2$ | 16.2830(2) |
| | $\alpha^2 + \delta_{\mathrm{AMM}}$ | 16.3268(2) |
| | $\alpha^2 + \delta_{\mathrm{AMM}} + \delta^{\mathrm{isoconf}}_{\mathrm{offdiag}}$ | 16.4191(2) |
| | $\alpha^2 + \delta_{\mathrm{AMM}} + \delta^{\mathrm{full}}_{\mathrm{offdiag}}$ | 16.4167(2)(5)(300) |
| MCHF [77] | | 16.39 |
| MCHF [82] | | 16.33 |
| Experiment [83] | | 16.416712(2) |
| NIST ASD [73] | | 16.4167122(6) |
| $1\,^3P^e_2 \to 1\,^3P^e_1$ | $\alpha^2$ | 26.9610(2) |
| | $\alpha^2 + \delta_{\mathrm{AMM}}$ | 27.0355(2) |
| | $\alpha^2 + \delta_{\mathrm{AMM}} + \delta^{\mathrm{isoconf}}_{\mathrm{offdiag}}$ | 26.9831(2) |
| | $\alpha^2 + \delta_{\mathrm{AMM}} + \delta^{\mathrm{full}}_{\mathrm{offdiag}}$ | 26.9836(2)(5)(300) |
| MCHF [77] | | 26.92 |
| MCHF [82] | | 26.70 |
| Experiment [84] | | 26.996742(2) |
| NIST ASD [73] | | 26.9967422(6) |
| $1\,^3D^e_2 \to 1\,^3D^e_1$ | $\alpha^2$ | 21.8764(1) |
| | $\alpha^2 + \delta_{\mathrm{AMM}}$ | 21.9329(1) |
| | $\alpha^2 + \delta_{\mathrm{AMM}} + \delta^{\mathrm{isoconf}}_{\mathrm{offdiag}}$ | 21.2041(7) |
| | $\alpha^2 + \delta_{\mathrm{AMM}} + \delta^{\mathrm{full}}_{\mathrm{offdiag}}$ | 21.2059(7)(4)(300) |
| MCHF [85] | | 18.9 |
| NIST ASD [73] | | 21.19335(28) |
| $1\,^3D^e_3 \to 1\,^3D^e_2$ | $\alpha^2$ | 32.9129(1) |
| | $\alpha^2 + \delta_{\mathrm{AMM}}$ | 32.9979(1) |
| | $\alpha^2 + \delta_{\mathrm{AMM}} + \delta^{\mathrm{isoconf}}_{\mathrm{offdiag}}$ | 33.3534(3) |
| | $\alpha^2 + \delta_{\mathrm{AMM}} + \delta^{\mathrm{full}}_{\mathrm{offdiag}}$ | 33.3515(3)(4)(300) |
| MCHF [85] | | 29.1 |
| NIST ASD [73] | | 33.36485(23) |
| $2\,^3P^e_1 \to 2\,^3P^e_0$ | $\alpha^2$ | 11.0130(1) |
| | $\alpha^2 + \delta_{\mathrm{AMM}}$ | 11.0417(1) |
| | $\alpha^2 + \delta_{\mathrm{AMM}} + \delta^{\mathrm{isoconf}}_{\mathrm{offdiag}}$ | 12.3827(55) |
| | $\alpha^2 + \delta_{\mathrm{AMM}} + \delta^{\mathrm{full}}_{\mathrm{offdiag}}$ | 12.3833(55)(19)(300) |
| MCHF [85] | | 9.0 |
| NIST ASD [73] | | 12.39252(31) |
| $2\,^3P^e_2 \to 2\,^3P^e_1$ | $\alpha^2$ | 21.4304(3) |
| | $\alpha^2 + \delta_{\mathrm{AMM}}$ | 21.4863(3) |
| | $\alpha^2 + \delta_{\mathrm{AMM}} + \delta^{\mathrm{isoconf}}_{\mathrm{offdiag}}$ | 20.4701(55) |
| | $\alpha^2 + \delta_{\mathrm{AMM}} + \delta^{\mathrm{full}}_{\mathrm{offdiag}}$ | 20.4718(55)(9)(300) |
| MCHF [85] | | 16.3 |
| NIST ASD [73] | | 20.47396(19) |

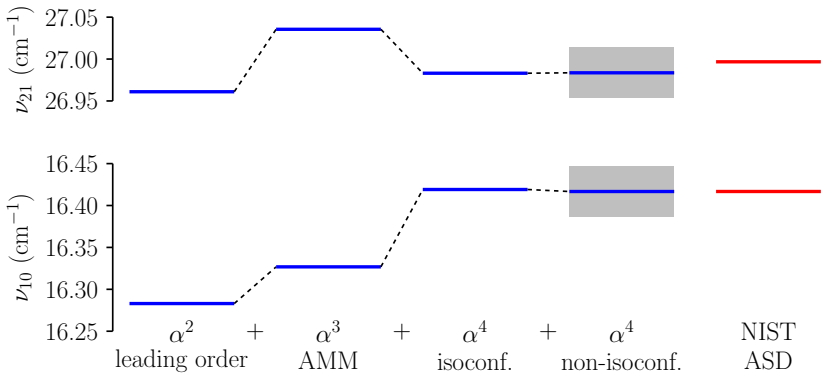


**(a)** $J = 2 \to 1$ and $J = 1 \to 0$ fine-structure splittings for the ground $1\,^3P^e$ state.

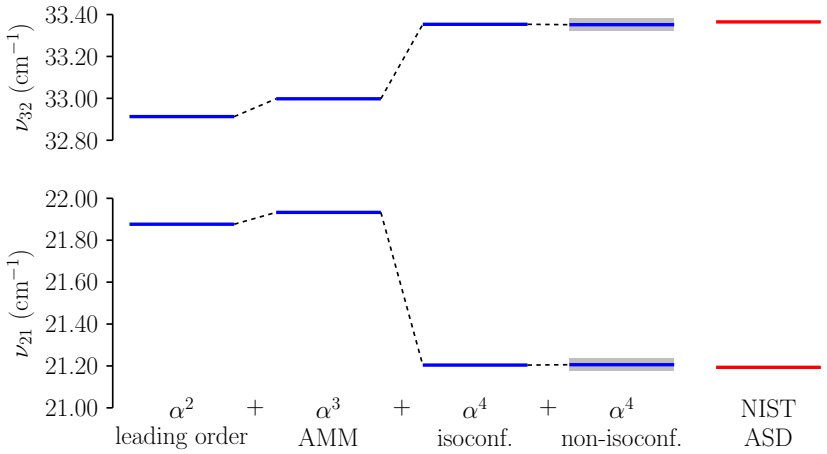


**(b)** $J = 3 \to 2$ and $J = 2 \to 1$ fine-structure splittings for the lowest $1\,^3D^e$ state.

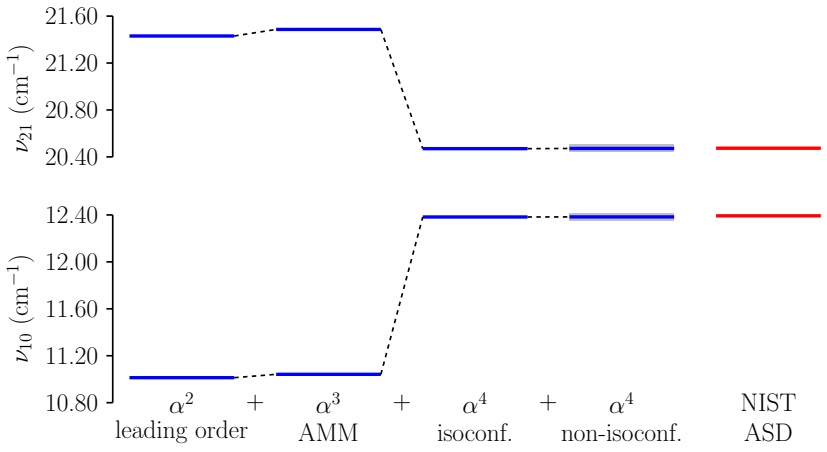


**(c)** $J = 3 \to 2$ and $J = 2 \to 1$ fine-structure splittings for the first excited $2\,^3P^e$ state.

**Figure 4:** Fine-structure splittings of carbon $^{12}$C for the ground $1^3P^e$ state (a), lowest $1^3D^e$ state (b), and first excited $2^3P^e$ state (c). The gray shade indicates the estimated uncertainty of theoretical calculations. In all diagrams, $\nu_{ab}$ denotes the energy difference between the levels with $J = a$ and $J = b$.

**Table 7:** Isotopic shifts of fine-structure intervals relative to $^{12}$C. For the calculated values, numbers in parentheses represent numerical uncertainties.

| Transition | $\Delta\nu \times 10^5$ (cm$^{-1}$) | | |
|---|---|---|---|
| | $^{13}$C | $^{14}$C | $^{\infty}$C |
| $1\,^3P_1 \to 1\,^3P_0$ | 7.91(4) | 14.70(7) | 102.5(5) |
| Veseth [92] | 10.3 | — | — |
| Kozlov *et al.* [91] | 9.27 | — | — |
| NIST ASD | 7.47(8) | — | — |
| $1\,^3P_2 \to 1\,^3P_1$ | 14.81(8) | 27.46(15) | 192.4(10) |
| Kozlov *et al.* [91] | 20.1 | — | — |
| Carette [77] + Veseth [92] | 14 | — | — |
| NIST ASD | 13.78(16) | — | — |
| $1\,^3D_2 \to 1\,^3D_1$ | 9.54(4) | 17.69(8) | 123.6(8) |
| $1\,^3D_3 \to 1\,^3D_2$ | 16.09(6) | 29.84(12) | 208.5(8) |
| $2\,^3P_1 \to 2\,^3P_0$ | 7.17(2) | 13.30(4) | 93.0(3) |
| $2\,^3P_2 \to 2\,^3P_1$ | 9.13(4) | 16.93(7) | 118.3(5) |

# 8 Conclusions

This thesis presents the theoretical framework, detailed derivation of matrix elements, and numerical results for the calculation of spin-dependent operators using explicitly correlated Gaussian (ECG) basis sets. Based on the methodology developed by our former group member D. Tumakov, I introduced the following key advancements:

1. Derived the matrix element of the spin–spin non-contact interaction in the ECG basis set corresponding to a single electron in a $p$-state.

2. Derived the matrix elements of the spin–orbit and non-contact spin–spin interactions in the ECG basis set corresponding to two electrons in $p$-states or a single electron in a $d$-state.

I implemented these matrix elements in the existing FORTRAN code for ECG variational calculations. The extended code was then applied to study relativistic corrections in positronic beryllium [26] and to investigate the fine structure of the carbon atom. The latter work is currently under review in *Physical Review Letters*.

For positronic beryllium, we considered the ground singlet $S$ state, and excited triplet $S$ and $P$ states. We found that the inclusion of the relativistic corrections does not affect the dynamic stability of any of these states, resulting in a change of less than 2.2% in binding energies. Although spin–orbit and spin–spin interactions for the $P$-states of positronic beryllium were much smaller than the largest relativistic corrections from Darwin and mass-velocity terms, their impact on the binding energies was found to be of comparable magnitude. This is because the binding energies involve the energy difference between the parent system and positron–atom complex; as a result, scalar relativistic corrections largely cancel out, while the spin–orbit and spin–spin interactions do not cancel out at all since they are absent in the $S$-state of the parent $Be^+$ ion.

In the project dedicated to the carbon fine-structure, we computed fine-structure splittings of the carbon ground and first excited $^3P^e$ states, as well as the lowest $^3D^e$ state. To obtain fine-structure intervals, we used a perturbation series approach and included the leading-order ($\propto \alpha^2$), anomalous magnetic moment ($\propto \alpha^3$), and the dominant part of the second-order perturbation theory contributions ($\propto \alpha^4$). Notably, at the $\alpha^4$ level of theory, no prior calculations have ever been performed for a system of comparable size. For all transitions, our results for the fine-structure showed an agreement with the experimental data at the level of 0.0001-0.01 $cm^{-1}$, representing the most accurate calculations of carbon to date. We estimate the largest uncertainty of our calculations to stem from the omitted higher-order QED terms, which may contribute as much as 0.03 $cm^{-1}$. Additionally, we obtained the most accurate values of the isotopic shifts of fine-structure levels. However, the disagreement between our calculated and experimental fine-structure isotopic shifts at the level of 4-6 $\sigma$ suggests that further investigation is needed.

# A Matrix elements of the hyperfine interaction for carbon $^{13}$C

*Leading-order correction*

To find the hyperfine structure splittings, one needs to build the eigenfunction of operators $\boldsymbol{J}^2$, $\boldsymbol{F}^2$ and $\boldsymbol{F}_z$, and evaluate the matrix elements of the Hamiltonian (4.7) in this basis.

The ground state of carbon has three fine-structure (FS) components. The components with $J = 1$ and $J = 2$ are split by the hyperfine interaction into two levels. The energies of the levels, expressed in terms of the hyperfine parameters $A_J$ according to (4.11), are:

$$E(J = 2, F = 5/2) = A_2, \tag{A.1}$$

$$E(J = 2, F = 3/2) = -\frac{3}{2}A_2, \tag{A.2}$$

$$E(J = 1, F = 3/2) = \frac{1}{2}A_1, \tag{A.3}$$

$$E(J = 1, F = 1/2) = -A_1. \tag{A.4}$$

To write the expressions for the energy levels of HFS components, we need the following basic matrix elements, evaluated in the uncoupled $|SM_SLM_LIM_I\rangle$ basis for the case of maximum projections:

$$\begin{aligned} M_{\rm c} &= \left\langle SSLLII\middle|\mathcal{H}^{\rm SSF}_{\rm HFS}\middle|SSLLII\right\rangle, \\ M_{\rm l} &= \left\langle SSLLII\middle|\mathcal{H}^{\rm SO}_{\rm HFS}\middle|SSLLII\right\rangle, \\ M_{\rm sd} &= \left\langle SSLLII\middle|\mathcal{H}^{\rm SSNC}_{\rm HFS}\middle|SSLLII\right\rangle, \end{aligned} \tag{A.5}$$

that we will refer to as contact, orbital, and spin–dipolar matrix elements and that are proportional to the corresponding coupling constants [47].

The evaluation of the matrix element of the HFS Hamiltonian (4.7) in the coupled basis $|JFM_F\rangle$ gives the following results for $A_J$ coefficients:

$$A_2 = \frac{1}{2}M_{\rm l} + M_{\rm sd} + \frac{1}{2}M_{\rm c}, \tag{A.6}$$

$$A_1 = \frac{1}{2}M_{\rm l} - 5M_{\rm sd} + \frac{1}{2}M_{\rm c}. \tag{A.7}$$

*Second-order perturbation correction*

The largest contribution in the second-order perturbation theory comes from the coupling between the HFS components of different $J$ within the same atomic term $^{2S+1}L$.

The corresponding energy correction to the state $|JF\rangle$ is:

$$E^{(4)}_{\rm HFS}(J,F) = \sum_{J'\neq J} \frac{|\langle JFM_F|\mathcal{H}_{\rm HFS}|J'FM_F\rangle|^2}{E_J - E_{J'}}. \tag{A.8}$$

The matrix elements in (A.8) are non-zero only when $J' = J\pm 1$ and are expressed through the basic matrix elements from (A.5) as follows:

$$\left\langle 2\frac{3}{2}\frac{3}{2}\middle|\mathcal{H}_{\rm HFS}\middle|1\frac{3}{2}\frac{3}{2}\right\rangle = \frac{\sqrt{5}}{2}M_{\rm l} + \sqrt{5}M_{\rm sd} - \frac{\sqrt{5}}{2}M_{\rm c}, \tag{A.9}$$

$$\left\langle 1\frac{1}{2}\frac{1}{2}\middle|\mathcal{H}_{\rm HFS}\middle|0\frac{1}{2}\frac{1}{2}\right\rangle = \sqrt{2}M_{\rm l} - \frac{5}{\sqrt{2}}M_{\rm sd} - \sqrt{2}M_{\rm c}. \tag{A.10}$$

*Spin–spin non-contact matrix element*

For a spin–dipolar term, we need to evaluate the matrix element with $\mathcal{H}^{\rm SSNC}_{\rm HFS}$. The operator can be represented as a scalar product of rank-two tensors:

$$\mathcal{H}^{\rm SSNC}_{\rm HFS} = -g_{\rm e}g_I\mu_{\rm B}\mu_{\rm N}\sum_i \left\{ \left[\boldsymbol{I}^{(1)}\times \boldsymbol{s}^{(1)}_i\right]^{(2)}\cdot\left[\boldsymbol{\nabla}^{(1)}_i\times\boldsymbol{\nabla}^{(1)}_i\right]^{(2)}\frac{1}{r_i}\right\}. \tag{A.11}$$

The spin part of the operator is the same as in the case of electron spin–spin operator in Eq. (5.11), except that the spin of one of electrons is replaced by the nuclear spin. The zeroth component of the spatial matrix element is:

$$-\left\langle 11\middle|\left[\nabla^{(1)}_i\times\nabla^{(1)}_i\right]^{(2)}_0\middle|11\right\rangle = f + f|_{v_l\leftrightarrow w_l} + f|_{v_k\leftrightarrow w_k} + f|_{v_k\leftrightarrow w_k, v_l\leftrightarrow w_l}, \tag{A.12}$$

where

$$f = \frac{2\pi^{(3n-1)/2}}{\sqrt{6}|C_{kl}|^{3/2}}\left\{\frac{1}{5}\gamma^5_{ii}\left([v'_kC^{-1}_{kl}E_{ii}C^{-1}_{kl}v_l][w'_kC^{-1}_{kl}w_l] - 2[w'_kC^{-1}_{kl}E_{ii}C^{-1}_{kl}w_l][v'_kC^{-1}_{kl}v_l]\right) + \right. \tag{A.13}$$

$$\left. + \frac{1}{7}\gamma^7_{ii}[v'_kC^{-1}_{kl}E_{ii}C^{-1}_{kl}v_l][w'_kC^{-1}_{kl}E_{ii}C^{-1}_{kl}w_l]\right\}. \tag{A.14}$$

# B Calculation of hyperfine structure levels of $^{13}$C

The weighting of experimentally measured transition frequencies between hyperfine structure components with the relative theoretical intensities gives the fine-structure splittings that account for $\alpha^3$ contributions (expectation value of the leading-order HFS Hamiltonian with the contribution from the electron magnetic moment anomaly). Let us denote

the transition frequencies between HFS components $J, F$ and $J', F'$ as $\nu(J, F \to J'F')$. Then, for the FS interval $E_{10}$ between levels with $J = 1$ and $J = 0$, we may write:

$$E_{10}^{(2)} = \frac{2}{3}\nu(1, \frac{3}{2} \to 0, \frac{1}{2}) + \frac{1}{3}\nu(1, \frac{1}{2} \to 0, \frac{1}{2}) \tag{B.1}$$

The non-zero off-diagonal matrix elements of $\mathcal{H}_{\rm HFS}$ between the levels with different $J$ and same $F$ lead to the $\alpha^4$ second-order shift of levels with $F = 3/2$ and $F = 1/2$ which does not comply with the weighting rule used above (see Fig. 5). Denoting the absolute value of the second-order shift of HFS levels with $F = 3/2$ and $F = 1/2$ as $\Delta E_{3/2}^{(4)}$ and $\Delta E_{1/2}^{(4)}$, we obtain for the FS splitting between $J = 1$ and $J = 0$ levels, corrected for the dominant part of second-order perturbation $\alpha^4$ contribution:

$$E_{10}^{\rm corr.} = E_{10}^{(2)} + \frac{2}{3}\Delta E_{3/2}^{(4)} - \frac{4}{3}\Delta E_{1/2}^{(4)}. \tag{B.2}$$

The same reasoning, applied to the FS splitting $E_{21}$ between the levels with $J = 2$ and $J = 1$, gives at the order of $\alpha^3$:

$$E_{21}^{(2)} = \frac{1}{3}\nu(2, \frac{3}{2} \to 1, \frac{1}{2}) + \frac{1}{15}\nu(2, \frac{3}{2} \to 1, \frac{3}{2}) + \frac{3}{5}\nu(2, \frac{5}{2} \to 1, \frac{3}{2}). \tag{B.3}$$

The inclusion of theoretically calculated values of the dominant second-order $\alpha^4$ contribution gives:

$$E_{21}^{\rm corr.} = E_{21}^{(2)} - \frac{1}{3}\Delta E_{1/2}^{(4)} + \frac{16}{15}\Delta E_{3/2}^{(4)}. \tag{B.4}$$

*Numerical results*

In Table 8, we present the hyperfine structure splittings of the ground $^3P^e$ state of $^{13}$C, computed at different levels of theory. For comparison, we also include values derived from the matrix elements $M_{\rm c}$, $M_{\rm l}$, and $M_{\rm sd}$ (see Eq. (A.5)), as calculated by Jönsson and Froese Fischer in Ref. [93].

Our computed value for the hyperfine splitting of the $J = 2$ level is significantly more accurate than that of Ref. [93], and is close to the experimental value. However, for the fine-structure component with $J = 1$, our result deviates notably from the NIST ASD value.

This discrepancy can be explained as follows. The hyperfine splitting for $J = 1$ is approximately two orders of magnitude smaller than that for $J = 2$, due to an effective cancellation between the contributions of the spin–orbit $\mathcal{H}_{\rm HFS}^{\rm SO}$ and spin–spin non-contact $\mathcal{H}_{\rm HFS}^{\rm SSNC}$ operators, which are close in magnitude but have opposite sign. As a result, the splitting between the $F = 1/2$ and $F = 3/2$ levels is predominantly determined by the contact Fermi spin–spin interaction $\mathcal{H}_{\rm HFS}^{\rm SSF}$ which involves a Dirac delta-function and is therefore singular, leading to slow convergence. Despite employing a regularization

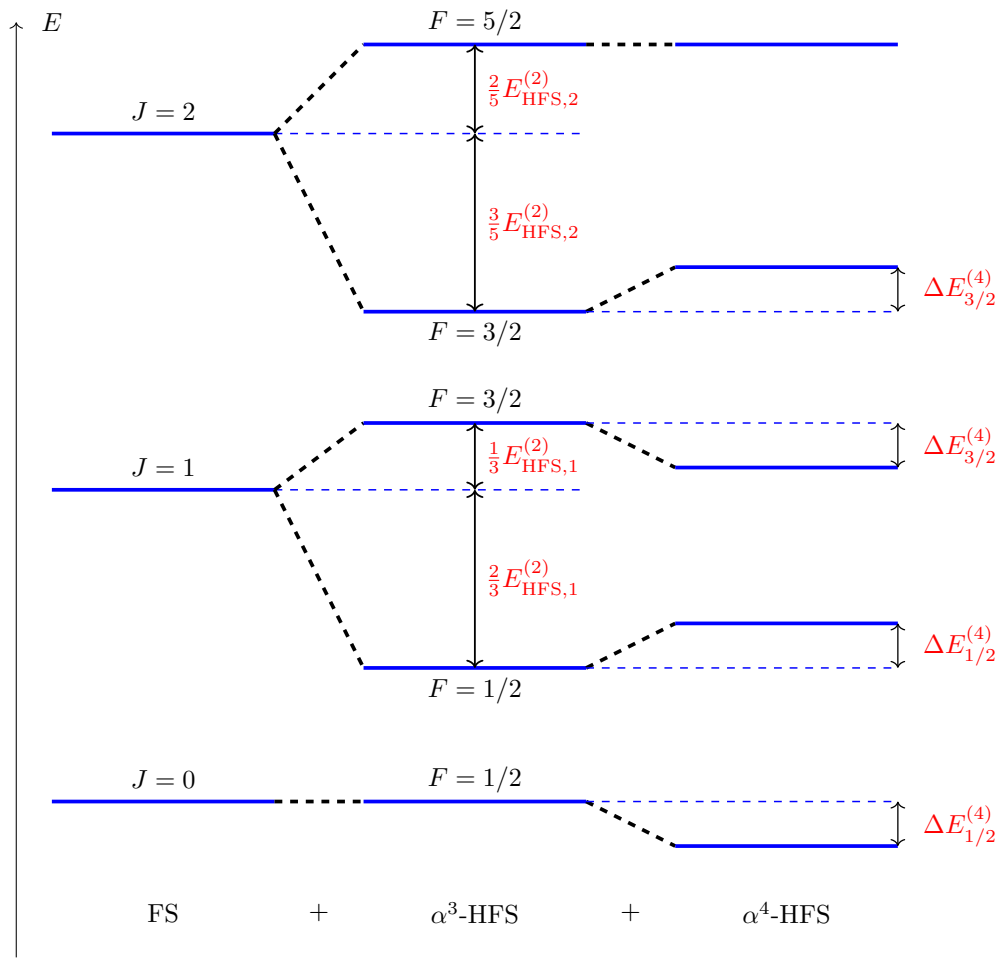


**Figure 5:** The scheme of fine-structure, $\alpha^3$ hyperfine structure, and second-order perturbation $\alpha^4$ hyperfine structure splittings for the ground $^3P^e$ state of $^{13}$C. The diagram is purely illustrative and does not reflect actual energy scales or relative level spacings.

technique [94] to improve the convergence of the contact term, its expectation value still converges more slowly than those of non-singular operators.

Another source of discrepancy may come from the effects of finite nuclear size and higher-order corrections ($\alpha^4$ and higher) which were not considered in this work. Interestingly, as shown in Ref. [24], most of the higher-order corrections are proportional to the Fermi contact term and thus can be approximately accounted for by including the additional factor of $(1 + \epsilon)$ in front of the corresponding expectation value.

Summing up, using a larger basis set for the calculation of the contact Fermi term, along with the inclusion of higher-order QED corrections and finite nuclear size effects, could improve agreement between the theoretical predictions and experimental results for the HFS splitting.

**Table 8:** Hyperfine structure splittings for the ground $^3P^e$ state of carbon $^{13}$C. $\delta_{\rm AMM}$ stands for the $\alpha^3$ contribution due to the electron anomalous magnetic moment. $\delta_{\rm offdiag}$ is the dominant $\alpha^4$ second-order perturbation theory correction due to coupling between the hyperfine structure components of different $J$ values. For the calculated values, the figures in parentheses represent the uncertainties due to basis set truncation. The uncertainty due to the omission of higher-order QED terms was not estimated.

| HFS splitting | Contribution | $\Delta E \times 10^4$, cm$^{-1}$ |
|---|---|---|
| $J = 2$ ($F = 5/2$–$3/2$) | $\alpha^2$ | 124.04(1) |
| | $\alpha^2 + \delta_{\rm AMM}$ | 124.07(1) |
| | $\alpha^2 + \delta_{\rm AMM} + \delta_{\rm offdiag}$ | 124.06(1) |
| MCHF [93] | | 123.06 |
| NIST ASD [73] | | 124.283(4) |
| $J = 1$ ($F = 3/2$–$1/2$) | $\alpha^2$ | 1.711(5) |
| | $\alpha^2 + \delta_{\rm AMM}$ | 1.642(5) |
| | $\alpha^2 + \delta_{\rm AMM} + \delta_{\rm offdiag}$ | 1.628(5) |
| MCHF [93] | | 1.249 |
| NIST ASD [73] | | 1.3993(8) |

# REFERENCES


[1] S. G. Karshenboim, "Precision physics of simple atoms: QED tests, nuclear structure and fundamental constants," Physics reports **422**, 1 (2005).

[2] R. Sánchez, W. Nörtershäuser, G. Ewald, D. Albers, J. Behr, P. Bricault, B. A. Bushaw, A. Dax, J. Dilling, M. Dombsky, G. W. F. Drake, S. Götte, R. Kirchner, H.-J. Kluge, T. Kühl, J. Lassen, C. D. P. Levy, M. R. Pearson, E. J. Prime, V. Ryjkov, A. Wojtaszek, Z.-C. Yan, and C. Zimmermann, "Nuclear Charge Radii of $^{9,11}$Li: The Influence of Halo Neutrons," Phys. Rev. Lett. **96**, 033002 (2006).

[3] P. Mueller, I. A. Sulai, A. C. C. Villari, J. A. Alcántara-Núñez, R. Alves-Condé, K. Bailey, G. W. F. Drake, M. Dubois, C. Eléon, G. Gaubert, R. J. Holt, R. V. F. Janssens, N. Lecesne, Z.-T. Lu, T. P. O'Connor, M.-G. Saint-Laurent, J.-C. Thomas, and L.-B. Wang, "Nuclear Charge Radius of $^{8}$He," Phys. Rev. Lett. **99**, 252501 (2007).

[4] R. Pohl, A. Antognini, F. Nez, F. D. Amaro, F. Biraben, J. M. R. Cardoso, D. S. Covita, A. Dax, S. Dhawan, L. M. P. Fernandes, A. Giesen, T. Graf, T. W. Hansch, P. Indelicato, L. Julien, C.-Y. Kao, P. Knowles, E.-O. Le Bigot, Y.-W. Liu, J. A. M. Lopes, L. Ludhova, C. M. B. Monteiro, F. Mulhauser, T. Nebel, P. Rabinowitz, J. M. F. dos Santos, L. A. Schaller, K. Schuhmann, C. Schwob, D. Taqqu, J. F. C. A. Veloso, and F. Kottmann, "The size of the proton," Nature (London) **466**, 213 (2010).

[5] X. Zheng, Y. R. Sun, J.-J. Chen, W. Jiang, K. Pachucki, and S.-M. Hu, "Laser Spectroscopy of the Fine-Structure Splitting in the $2^3P_J$ Levels of $^4$He," Phys. Rev. Lett. **118**, 063001 (2017).

[6] M. S. Safronova, D. Budker, D. DeMille, D. F. J. Kimball, A. Derevianko, and C. W. Clark, "Search for new physics with atoms and molecules," Rev. Mod. Phys. **90**, 025008 (2018).

[7] B. Maaß, T. Hüther, K. König, J. Krämer, J. Krause, A. Lovato, P. Müller, K. Pachucki, M. Puchalski, R. Roth, R. Sánchez, F. Sommer, R. B. Wiringa, and W. Nörtershäuser, "Nuclear Charge Radii of $^{10,11}$B," Phys. Rev. Lett. **122**, 182501 (2019).

[8] M. Puchalski, J. Komasa, and K. Pachucki, "Hyperfine structure of the $2^3P$ state in $^9$Be and the nuclear quadrupole moment," Phys. Rev. Research **3**, 013293 (2021).

[9] M. Stanke, A. Kędziorski, S. Nasiri, L. Adamowicz, and S. Bubin, "Fine structure of the $^2P$ energy levels of singly ionized carbon (C II)," Phys. Rev. A **108**, 012812 (2023).

[10] S. Nasiri, D. Tumakov, M. Stanke, A. Kedziorski, L. Adamowicz, and S. Bubin, "Fine structure of the doublet $P$ levels of boron," Phys. Rev. Research **6**, 043225 (2024).

[11] S. F. Boys, "The Integral Formulae for the Variational Solution of the Molecular Many-Electron Wave Equations in Terms of Gaussian Functions with Direct Electronic Correlation," Proc. R. Soc. London, Ser. A **258**, 402 (1960).

[12] T. Koga, "Hylleraas wave functions revisited," The Journal of Chemical Physics **96**, 1276 (1992).

[13] D. Ceperley and B. Alder, "Quantum Monte Carlo," Science **231**, 555 (1986).

[14] I. Shavitt, "The history and evolution of configuration interaction," Molecular Physics **94**, 3 (1998).

[15] C. F. Fischer and P. Jönsson, "MCHF calculations for atomic properties," Computer Physics Communications **84**, 37 (1994).

[16] K. A. Brueckner and C. A. Levinson, "Approximate Reduction of the Many-Body Problem for Strongly Interacting Particles to a Problem of Self-Consistent Fields," Phys. Rev. **97**, 1344 (1955).

[17] R. J. Bartlett and M. Musiał, "Coupled-cluster theory in quantum chemistry," Rev. Mod. Phys. **79**, 291 (2007).

[18] M. Orio, D. A. Pantazis, and F. Neese, "Density functional theory," Photosynthesis research **102**, 443 (2009).

[19] J. Mitroy, S. Bubin, W. Horiuchi, Y. Suzuki, L. Adamowicz, W. Cencek, K. Szalewicz, J. Komasa, D. Blume, and K. Varga, "Theory and application of explicitly correlated Gaussians," Rev. Mod. Phys. **85**, 693 (2013).

[20] T. Kato, "On the eigenfunctions of many-particle systems in quantum mechanics," Commun. Pure Appl. Math. **10**, 151 (1957).

[21] K. Pachucki and V. A. Yerokhin, "Fine structure of heliumlike ions and determination of the fine structure constant," Phys. Rev. Lett. **104**, 070403 (2010).

[22] M. Puchalski and K. Pachucki, "Quantum Electrodynamics Corrections to the $2P$ Fine Splitting in Li," Phys. Rev. Lett. **113**, 073004 (2014).

[23] C. Chen, "Energies, expectation values, fine structures and hyperfine structures of the ground state and excited states for boron," Eur. Phys. J. D **69**, 128 (2015).

[24] M. Puchalski, J. Komasa, and K. Pachucki, "Fine and hyperfine splitting of the low-lying states of $^9$Be," Phys. Rev. A **104**, 022824 (2021).

[25] M. Stanke, A. Kędziorski, and L. Adamowicz, "Fine structure of the beryllium $^3P$ states calculated with all-electron explicitly correlated Gaussian functions," Phys. Rev. A **105**, 012813 (2022).

[26] D. Tumakov, P. Rzhevskii, T. Shomenov, and S. Bubin, "Relativistic corrections in the ground and excited states of positronic beryllium," Phys. Rev. A **109**, 042826 (2024).

[27] J. R. Magnus and H. Neudecker, *Matrix-Differential Calculus with Applications in Statistics and Econometrics* (Wiley, Chichester, 1988).

[28] H. Yserentant, "A Short Theory of the Rayleigh–Ritz Method," Computational Methods in Applied Mathematics **13**, 495 (2013).

[29] E. A. Hylleraas, "Neue Berechnung der Energie des Heliums im Grundzustande, sowie des tiefsten Terms von Ortho-Helium," Z. Phys. **54**, 347 (1929).

[30] F. E. Harris, "Analytic evaluation of three-electron atomic integrals with Slater wave functions," Phys. Rev. A **55**, 1820 (1997).

[31] G. W. F. Drake, "Progress in helium fine-structure calculations and the fine-structure constant," Can. J. Phys. **89**, 1195 (2002).

[32] A. Wienczek, K. Pachucki, M. Puchalski, V. c. v. Patkóš, and V. A. Yerokhin, "Quantum-electrodynamic corrections to the $1s3d$ states of the helium atom," Phys. Rev. A **99**, 052505 (2019).

[33] M. Puchalski, D. Kędziera, and K. Pachucki, "Ground state of Li and $Be^+$ using explicitly correlated functions," Phys. Rev. A **80**, 032521 (2009).

[34] M. Puchalski, A. M. Moro, and K. Pachucki, "Isotope Shift of the $3^2S_{1/2} - 2^2S_{1/2}$ Transition in Lithium and the Nuclear Polarizability," Phys. Rev. Lett. **97**, 133001 (2006).

[35] Z.-C. Yan, W. Nörtershäuser, and G. W. F. Drake, "High Precision Atomic Theory for Li and $Be^+$: QED Shifts and Isotope Shifts," Phys. Rev. Lett. **100**, 243002 (2008).

[36] K. Singer, "The Use of Gaussian (Exponential Quadratic) Wave Functions in Molecular Problems. I. General Formulae for the Evaluation of Integrals," Proc. R. Soc. London, Ser. A **258**, 412 (1960).

[37] L. D. Landau and E. M. Lifshitz, *Quantum mechanics: non-relativistic theory*, Vol. 3 (Elsevier, 2013).

[38] C. Leforestier, R. Bisseling, C. Cerjan, M. Feit, R. Friesner, A. Guldberg, A. Hammerich, G. Jolicard, W. Karrlein, H.-D. Meyer, N. Lipkin, O. Roncero, and R. Kosloff, "A comparison of different propagation schemes for the time dependent Schrödinger equation," J. Comput. Phys. **94**, 59 (1991).

[39] T. Shomenov and S. Bubin, "Explicitly correlated Gaussians for high-precision variational calculations of $S^e$, $P^e$, and $D^e$ states of quantum systems: An efficient algorithm," Phys. Rev. E **108**, 065308 (2023).

[40] A. Edmonds, *Angular Momentum in Quantum Mechanics*, Princeton Landmarks in Mathematics and Physics (Princeton University Press, Princeton, 1996).

[41] W. E. Caswell and G. P. Lepage, "Effective lagrangians for bound state problems in QED, QCD, and other field theories," Phys. Lett. B **167**, 437 (1986).

[42] H. A. Bethe and E. E. Salpeter, *Quantum Mechanics of One- and Two-Electron Atoms* (Plenum, New York, 1977).

[43] A. I. Akhiezer and V. B. Berestetskii, *Quantum Electrodynamics* (John Wiley & Sons, New York, 1965).

[44] A. Kędziorski, M. Stanke, and L. Adamowicz, "Atomic fine-structure calculations performed with a finite-nuclear-mass approach and with all-electron explicitly correlated Gaussian functions," Chem. Phys. Lett. **751**, 137476 (2020).

[45] P. Mohr, D. Newell, B. Taylor, and E. Tiesinga, "CODATA Recommended Values of the Fundamental Physical Constants: 2022," (2024), arXiv:2409.03787 [hep-ph] .

[46] M. Puchalski and K. Pachucki, "Quantum electrodynamics $m\alpha^6$ and $m\alpha^6 \ln \alpha$ corrections to the fine splitting in Li and $Be^+$," Phys. Rev. A **92**, 012513 (2015).

[47] R. Glass and A. Hibbert, "The hyperfine structure of the ground states of first-row atoms," Journal of Physics B: Atomic and Molecular Physics **11**, 2257 (1978).

[48] G. P. Fisher, "The Thomas precession," American Journal of Physics **40**, 1772 (1972).

[49] B. R. Judd, *Operator Techniques in Atomic Spectroscopy*, Princeton Landmarks in Mathematics and Physics (Princeton University Press, 1998).

[50] S. Bubin and L. Adamowicz, "Energy and energy gradient matrix elements with $N$-particle explicitly correlated complex Gaussian basis functions with $L = 1$," J. Chem. Phys. **128**, 114107 (2008).

[51] K. L. Sharkey, S. Bubin, and L. Adamowicz, "An algorithm for calculating atomic $D$ states with explicitly correlated Gaussian functions," J. Chem. Phys. **134**, 044120 (2011).

[52] G. G. Ryzhikh and J. Mitroy, "Positronic Lithium, an Electronically Stable Li-$e^+$ Ground State," Phys. Rev. Lett. **79**, 4124 (1997).

[53] K. Strasburger and H. Chojnacki, "Quantum chemical study of simple positronic systems using explicitly correlated Gaussian functions – PsH and $PsLi^+$," J. Chem. Phys. **108**, 3218 (1998).

[54] D. M. Schrader, "Bound states of positrons with atoms and molecules: Theory," Nucl. Instrum. Methods Phys. Res. Sec. B **143**, 209 (1998).

[55] G. G. Ryzhikh, J. Mitroy, and K. Varga, "The structure of exotic atoms containing positrons and positronium," J. Phys. B **31**, 3965 (1998).

[56] J. Mitroy, M. W. J. Bromley, and G. G. Ryzhikh, "Positron and positronium binding to atoms," J. Phys. B **35**, R81 (2002).

[57] V. A. Dzuba, V. V. Flambaum, and G. F. Gribakin, "Detecting Positron-Atom Bound States through Resonant Annihilation," Phys. Rev. Lett. **105**, 203401 (2010).

[58] G. F. Gribakin, J. A. Young, and C. M. Surko, "Positron-molecule interactions: Resonant attachment, annihilation, and bound states," Rev. Mod. Phys. **82**, 2557 (2010).

[59] X. Cheng, D. Babikov, and D. M. Schrader, "Binding-energy predictions of positrons and atoms," Phys. Rev. A **83**, 032504 (2011).

[60] V. A. Dzuba, V. V. Flambaum, G. F. Gribakin, and C. Harabati, "Relativistic linearized coupled-cluster single-double calculations of positron-atom bound states," Phys. Rev. A **86**, 032503 (2012).

[61] D. Bressanini, "Positron Binding to Lithium Excited States," Phys. Rev. Lett. **109**, 223401 (2012).

[62] S. Bubin and O. V. Prezhdo, "Excited States of Positronic Lithium and Beryllium," Phys. Rev. Lett. **111**, 193401 (2013).

[63] C. Harabati, V. A. Dzuba, and V. V. Flambaum, "Identification of atoms that can bind positrons," Phys. Rev. A **89**, 022517 (2014).

[64] K. Strasburger, "Excited $S$-symmetry states of positronic lithium and beryllium," J. Chem. Phys. **144**, 144316 (2016).

[65] K. R. Brorsen, M. V. Pak, and S. Hammes-Schiffer, "Calculation of Positron Binding Energies and Electron–Positron Annihilation Rates for Atomic Systems with the Reduced Explicitly Correlated Hartree–Fock Method in the Nuclear–Electronic Orbital Framework," J. Phys. Chem. A **121**, 515 (2017).

[66] T. Yamashita, M. Umair, and Y. Kino, "Bound and resonance states of positronic copper atoms," J. Phys. B **50**, 205002 (2017).

[67] P. H. R. Amaral and J. R. Mohallem, "Descriptor for positron binding to atoms," Phys. Rev. A **104**, 042808 (2021).

[68] J. A. Charry Martinez, M. Barborini, and A. Tkatchenko, "Correlated Wave Functions for Electron–Positron Interactions in Atoms and Molecules," J. Chem. Theory Comput. **18**, 2267 (2022).

[69] J. Hofierka, B. Cunningham, C. M. Rawlins, C. H. Patterson, and D. G. Green, "Gaussian-basis many-body theory calculations of positron binding to negative ions and atoms," arXiv:2311.13066 [physics.atom-ph] .

[70] S. Bubin and L. Adamowicz, "Matrix elements of $N$-particle explicitly correlated Gaussian basis functions with complex exponential parameters," J. Chem. Phys. **124**, 224317 (2006).

[71] T. Henning and F. Salama, "Carbon in the Universe," Science **282**, 2204 (1998).

[72] K. Haris and A. Kramida, "Critically Evaluated Spectral Data for Neutral Carbon (C I)," Astrophys. J. Suppl. Ser. **233**, 16 (2017).

[73] A. E. Kramida, Yu. Ralchenko, J. Reader, and NIST ASD Team, *NIST Atomic Spectra Database (ver. 5.11) [Online]* (2023), available at http://physics.nist.gov/asd.

[74] A. Dalgarno and R. A. McCray, "Heating and Ionization of HI Regions," Annu. Rev. Astron. Astrophys. **10**, 375 (1972).

[75] L. Veseth, "Refined many-body calculations of atomic fine structure," J. Phys. B **21**, 1719 (1988).

[76] L. Veseth, "Spin-extended Hartree-Fock calculation of atomic fine structure," J. Phys. B **14**, 795 (1981).

[77] T. Carette and M. R. Godefroid, "Theoretical study of the $C^-$ $^4S^o_{3/2}$ and $^2D^o_{3/2,5/2}$ bound states and C ground configuration: Fine and hyperfine structures, isotope shifts, and transition probabilities," Phys. Rev. A **83**, 062505 (2011).

[78] I. Hornyák, S. Nasiri, S. Bubin, and L. Adamowicz, "$^2S$ Rydberg spectrum of the boron atom," Phys. Rev. A **104**, 032809 (2021).

[79] M. Stanke, E. Palikot, K. L. Sharkey, and L. Adamowicz, "Benchmark calculations of the $^2D$ Rydberg spectrum of lithium," Mol. Phys. **119**, e1925765 (2021).

[80] S. Nasiri, L. Adamowicz, and S. Bubin, "Benchmark Calculations of the Energy Spectra and Oscillator Strengths of the Beryllium Atom," J. Phys. Chem. Ref. Data **50**, 043107 (2021).

[81] K. Strasburger, "Explicitly correlated wave functions of the ground state and the lowest quintuplet state of the carbon atom," Phys. Rev. A **99**, 052512 (2019).

[82] C. Froese Fischer and G. Tachiev, "Breit–Pauli energy levels, lifetimes, and transition probabilities for the beryllium-like to neon-like sequences," At. Data Nucl. Data Tables **87**, 1 (2004).

[83] S. Yamamoto and S. Saito, "Laboratory observation of the $^3P_1 - ^3P_0$ transition of the neutral carbon atom by submillimeter-wave absorption spectroscopy," Astrophys. J. **370**, L103 (1991).

[84] H. Klein, F. Lewen, R. Schieder, J. Stutzki, and G. Winnewisser, "Precise Laboratory Observation of the $^3P_2 \leftarrow ^3P_1$ Fine-Structure Transitions of $^{12}$C and $^{13}$C," Astrophys. J. **494**, L125 (1998).

[85] V. Stancalie, "Contribution to the theoretical investigation of electron and photon interaction with carbon atom and its ions," J. Phys. Conf. Ser. **576**, 012010 (2015).

[86] P. Jönsson, G. Gaigalas, J. Bieroń, C. Froese Fischer, and I. Grant, "New version: Grasp2K relativistic atomic structure package," Comput. Phys. Commun. **184**, 2197 (2013).

[87] J. C. Slater, "Atomic shielding constants," Phys. Rev. **36**, 57 (1930).

[88] M. Haidar, Z.-X. Zhong, V. I. Korobov, and J.-P. Karr, "Nonrelativistic QED approach to the fine- and hyperfine-structure corrections of order $m\alpha^6$ and $m\alpha^6(m/M)$: Application to the hydrogen atom," Phys. Rev. A **101**, 022501 (2020).

[89] K. Pachucki and V. A. Yerokhin, "Reexamination of the helium fine structure," Phys. Rev. A **79**, 062516 (2009).

[90] K. Pachucki and V. A. Yerokhin, "Publisher's Note: Reexamination of the helium fine structure [Phys. Rev. A 79, 062516 (2009)]," Phys. Rev. A **80**, 019902 (2009).

[91] M. G. Kozlov, I. I. Tupitsyn, and D. Reimers, "Coefficients for sensitivity of fine-structure transitions in carbonlike ions to $\alpha$ variation," Phys. Rev. A **79**, 022117 (2009).

[92] L. Veseth, "Isotopic shift in atomic fine structure," Phys. Rev. A **32**, 1328 (1985).

[93] P. Jönsson and C. Froese Fischer, "Large-scale multiconfiguration Hartree-Fock calculations of hyperfine-interaction constants for low-lying states in beryllium, boron, and carbon," Phys. Rev. A **48**, 4113 (1993).

[94] R. J. Drachman, "A new global operator for two-particle delta functions," J. Phys. B **14**, 2733 (1981).